From the Biochemischen Institut

(Leader of the institution: Prof. Dr. Stefan Rose-John)

at Christian-Albrechts-Universität zu Kiel - Kiel University

Application of Recombinant Human Pro-Cathepsin B as a Therapeutic Approach in Neuronal Ceroid Lipofuscinosis

Dissertation

to acquire the doctoral degree (Dr. med.)

at the Faculty of Medicine

at Christian-Albrechts-Universität zu Kiel - Kiel University

presented by

NIKLAS THIEßEN

from Kiel

Kiel 2022

1st Reviewer: Prof. Dr. Paul Josef Saftig, Biochemisches Institut

2nd Reviewer: Prof. Dr. Dieter Adam, Institut für Immunologie

Date of oral examination: 29.09.2023

Approved for printing, Kiel, 16.06.2023

Signed: Prof. Dr. Paul Josef Saftig (Chairman of the Examination Committee)

“Men ought to know that from the brain, and from the brain only, arise our pleasures, joys, laughter and jests, as well as sorrows, pains, griefs and tears."

- Hippocrates

Table of contents

List of Abbreviations

aa	Amino acids
APS	Ammonium persulfate
BBB	Blood brain barrier
BCA	Bicinchoninic acid
BSA	Bovine serum albumin
cDNA	Complementary DNA
CTSB	Cathepsin B
$CTSB^{-/-}$	Cathepsin B deficient
CTSD	Cathepsin D
$CTSD^{-/-}$	Cathepsin D deficient
DABCO	1,4-diaza-bicyclo-2,2,2-octane
DAPI	4-,6-diamidino-2-phenylindole
DMSO	Dimethylsulfoxid
DNA	Deoxyribonucleic acid
dNTP	Deoxyribonucleoside triphosphate
E. coli	Escherichia coli
FCS	Fetal calf serum
GAPDH	Glyceraldehyde 3-phosphate dehydrogenase
HEK	Human embryonic kidney
HEK-EBNA	HEK cells stably expressing Epstein Barr Virus Nuclear Antigen 1
i.c.v.	intracerebroventricular
i.p.	intraperitoneal
i.v.	intravenous
kDa	Kilo Dalton
LAMP1/2	Lysosomal associated protein 1/2
LRP	Lipoprotein-related protein
LSD	Lysosomal storage disease

M6P	Mannose-6-phosphate
Man	Mannose
MEF	Mouse embryonic fibroblast
NCL	Neuronal Ceroid Lipofuscinosis
P	Postnatal day
PAGE	Polyacrylamide gel electrophoresis
PB	Phosphate buffer
PBS	Phosphate buffered saline
PCR	Polymerase chain reaction
PEI	Polyethylenimine
PFA	Paraformaldehyde
P/S	Penicillin-Streptomycin
RAP	Receptor-associated protein
rhCTSB	Recombinant human proCathepsin B
SDS	Sodium dodecyl sulfate
TAE	Tris-acetate-EDTA
TBS	Tris-buffered saline
TEMED	Tetramethylethylenediamine
TPP1	Tripeptidyl peptidase 1
WT	Wild-type

1 INTRODUCTION

1.1 Neurodegenerative diseases

Neurodegenerative diseases are characterized by the progressive decay of neuronal cells of the central nervous system, leading to a decline of various cognitive functions and eventually the complete loss of autonomy and death. They pose a major threat to our health and society as a whole.

In 2018, a total number of about 1.6 million people in Germany was estimated to be suffering from a form of dementia, with Alzheimer's disease being the most abundant form. Without any major breakthrough in the prevention and therapy of these diseases, this number is expected to reach 2.7 million by 2050 (Georges et al., 2020).

Neurodegenerative diseases already constitute an enormous burden for our society, which will further aggravate due to the continuous demographic change. Due to the incremental number of patients and costs it is necessary to gain further insight into the underlying pathological mechanisms and develop causal therapies.

Today, we still lack such therapies against neurodegenerative diseases such as Alzheimer's disease (AD), Parkinson's disease (PD) or dementia in children.

Even though individual diseases show rather different clinical manifestations over the course of their progression, they have perturbance of common cellular pathways, begging the question of mutual therapeutic approaches (Armstrong et al., 2005).

Most of these disorders exhibit an impairment of a highly conserved process called "autophagy" (Tanaka and Matsuda, 2014).

1.2 Autophagy

The main requirement of cellular homeostasis is the equilibrium between the anabolic processes of biosynthesis and the continuous degradation of macromolecules. Hereby produced monomers, can be used for the synthesis of macromolecules. This turnover ensures the operation of all vital processes and protects the organism from aged and potentially toxic macromolecules (Dikic and Elazar, 2018).

The complex interplay relies on the routing of cellular components to lysosomes in a process termed autophagy. There are different forms of autophagy at play: via Microautophagy small

vesicles filled with cytosolic cargo fuse with the lysosomes, where the engulfed cytosolic constituents are degraded. Chaperone mediated autophagy relies on specific sequence motifs and receptors to selectively route targets into lysosomes. Most extensively studied is the third form, macroautophagy, hereafter referred to as "autophagy" (Shen and Mizushima, 2014). It is a highly conserved process, present in all eukaryotic organisms (Levine and Klionsky, 2004) and it consists of several steps starting with the formation of elongating double membranes. These phagophores start engulfing cellular constituents and are upon closure termed autophagosomes. Fusion of the latter with lysosomes introduces the sequestered cargo to the hydrolase-rich environment of the lysosome, thus leading to the formation of an autolysosome where the degradation takes place at an acidic pH (**figure 1**) (Kaur and Debnath, 2015, Glick et al., 2010).

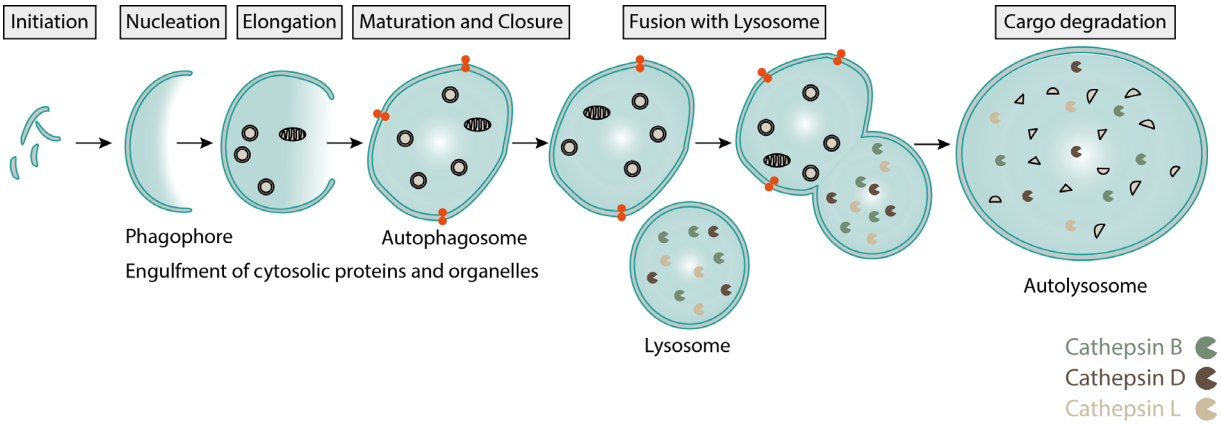

figure 1 Schematic overview of the process of autophagy. The initiation is characterized by formation of phospholipid double layers, which fuse into a so-called phagophore in the process of nucleation. Following this step, the double membrane further extents in the elongation step, and successfully sequesters cellular components upon closure of the membrane. At this point LC3-II can be detected within the membrane (orange). The fusion of this autophagosome with a lysosome leads to the formation of an autolysosome and due to the release of lysosomal hydrolases (exemplarily shown here CTSB, CTSD, CTSL) the degradation of the cargo (modified after Marques et al., 2019).

Autophagy is kept at a basal level at the cellular steady state, but certain circumstances can affect the turnover rate. For instance, nutrient deprivation (Russell et al., 2014) or inflammatory processes induce the autophagic flow (Shi et al., 2012).

Degradation via autophagy has been described for many characteristic storage aggregates found in neurodegenerative diseases (Cuervo et al., 2004, Sarkar and Rubinsztein, 2008, Wang et al., 2009).

Consequently, autophagy impairment and accumulation of autophagic vacuoles is characteristic for AD (Yu et al., 2005), PD (Stefanis et al., 2001), HD (Ravikumar et al., 2004) and lysosomal storage disorders, e.g. the neuronal ceroid lipofuscinoses.

On the other hand, neurodegeneration can be induced through inhibition of autophagy (Hara et al., 2006, Komatsu et al., 2006). The interplay of neuronal survival and regulation of autophagy has been studied in various models (Kuma et al., 2017). For example, Loss of *Atg7* in mice leads to progressive cerebral and cerebellar neuronal loss and early death (Komatsu et al., 2006). Similarly, otherwise neonatally lethal $Atg5^{-/-}$ mice were rescued by neural re-expression (Yoshii et al., 2016). The findings stress the dependence of the nervous system on intact autophagy and lysosomal degradation, as the lysosome constitutes the endpoint of this vital mechanism.

1.3 The lysosome

Lysosomes are organelles found in all mammalian cells, except in erythrocytes. The complex degradation and recycling of both endo- or phagocytosed and intracellular components is orchestrated by a set of more than 60 hydrolytic enzymes (Saftig, 2006). Most are synthesised as inactive zymogens and routed to their destination via multiple transport mechanisms, for instance by addition of mannose-6-phosphate in the Golgi apparatus and subsequent mannose-6-phosphate-receptor-dependent transport (Appelqvist et al., 2013). Their activation and functionality are ensured by the acidic environment (pH 4.5-5) inside the organelle's phospholipid double layer, attained by the vacuolar H^+-ATPase.

In addition, the organelle's phospholipid double layer contains over a hundred integral lysosomal membrane proteins (Schwake et al., 2013) acting as transporters for the import and export of molecules, initiating membrane fusion with other cellular compartments and forming the glycocalyx (Saftig and Klumperman, 2009).

Beside the pivotal role in degradation, the lysosome acts as a nexus of various metabolic and signalling pathways, like controlling the cytosolic supply of metabolites (Abu-Remaileh et al., 2017). Even nutrient sensing and subsequently cell growth and cell division itself are under lysosomal control via lysosomal serine/threonine kinase mechanistic target of rapamycin 1 (mTORC1) (Rabanal-Ruiz and Korolchuk, 2018).

Furthermore, lysosomes play a crucial role in immune response; in antigen presentation via MHC-II in dendritic cells and execution by natural killer cells and T-lymphocytes (Marques and Saftig, 2019), regulating inflammation by affecting glucocorticoid signalling (He et al., 2011), and in executing apoptosis (Aits and Jaattela, 2013).

Lysosomal biogenesis and degradative activity are carried out among others by genes of the coordinated lysosomal expression and regulation (CLEAR) network, which is under the control

of transcription factor EB (TFEB). Phosphorylation of TFEB by mTORC1 inhibits nuclear translocation and transcription of CLEAR-genes. In times of starvation, mTORC1 inhibition allows TFEB activity to thrive (Parenti et al., 2015). Besides TFEB other members of the MiT-TFE family are involved in the regulation of autophagy and lysosomal biogenesis (Puertollano et al., 2018).

Different subpopulations of lysosomes, fulfilling distinct functions within the cell, have been identified, differing in pH and degradative activity with perinuclear lysosomes representing the metabolic nexus and peripheral acting as reservoir, e.g. for acid hydrolases (Marques and Saftig, 2019).

1.3.1 Cathepsin B

Lysosomal degradation relies on acid hydrolases among which the cathepsins constitute a major group.

A variety of cathepsins has been identified, while they exhibit different catalytic properties, their commonality lies in the predominantly lysosomal localization and their role in lysosomal degradation (Yadati et al., 2020).

Cathepsin B (CTSB) is the first described highly abundant cysteine protease. It belongs to the papain like superfamily and is expressed ubiquitously showing a very broad substrate specificity (Mort, 2013, Biniossek et al., 2011). In human it is coded by the *CTSB* gene, located on chromosome 8p22 (Fong et al., 1992).

The human preproform of CTSB contains 339 amino acids (aa) and while the prepeptide is cleaved off cotranslationally (figure 2A,B step 1), the proform (322 aa) undergoes further processing as it passes through the endoplasmic reticulum and the Golgi-apparatus (figure 2A,B step 2-3). In the latter, two sites are N-glycosylated. Through routing via the Mannose-6-phosphate receptor or secretion and recapture mechanisms the proform reaches the endolysosomal compartment, where the activation takes place (figure 2A,B step 4). Hydrolytic cleavage leads to the single chain form of CTSB (254 aa) before the final processing leads to the so-called two-chain-form (47 aa + 205 aa) bound together by a disulfide bond (Biniossek et al., 2011) (figure 2A,B step 5).

CTSB differs from other cysteine cathepsins functionally as it is the only member expressing both endopeptidase activity and dipeptidyl carboxypeptidase activity. This duality is achieved through a structural feature composed of 20 aa and termed the “occluding loop” that can switch between the two functions by shifting the catalytic site (Musil et al., 1991, Illy et al., 1997).

However, the occluding loop seems to hinder the endopeptidase activity (Nägler et al., 1997). While the endopeptidase activity of CTSB increases with pH up to a maximum around pH 7, the exopeptidase activity shows an activity maximum around acidic pH (pH 4-6) (Almeida et al., 2001, Koga et al., 1991, Nägler et al., 1997).

A

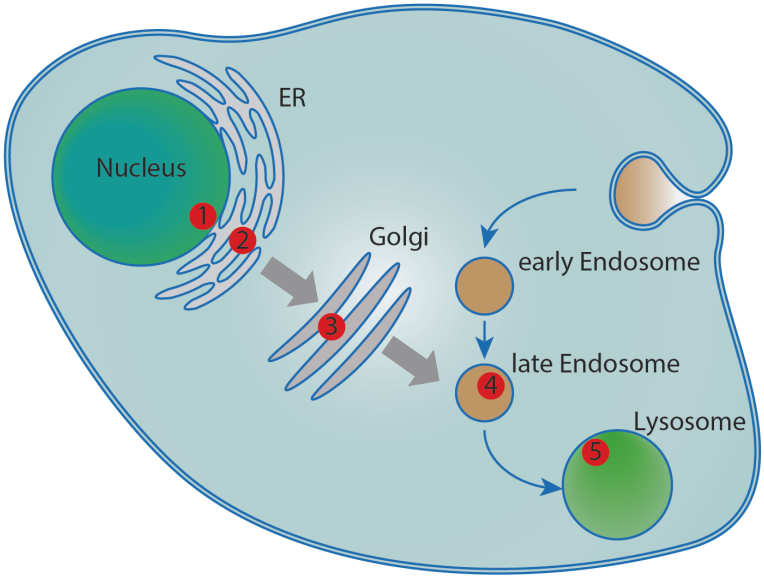

B

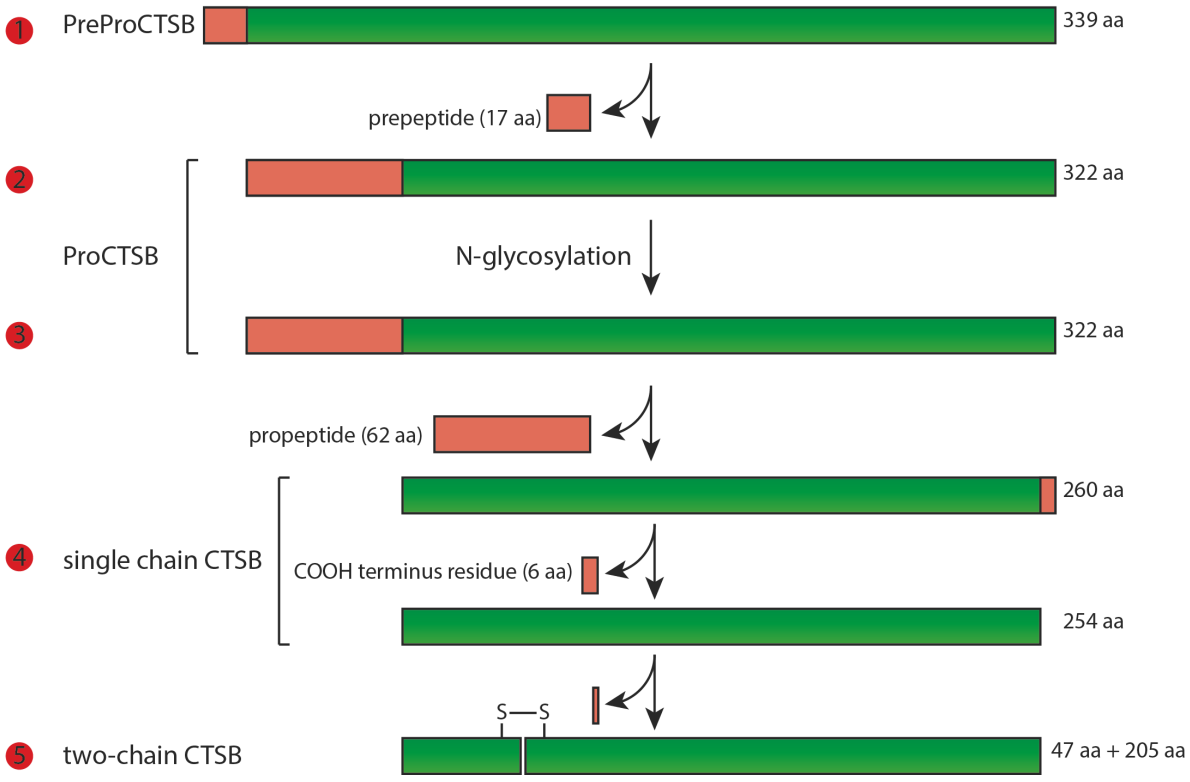

figure 2.A-B Schematic overview of the cellular location and organelles involved in the processing and activation of CTSB (**A**) as well as respective cleavage steps (**B**). Co-translational cleavage of the 17 aa prepeptide, leads to the transformation of PreProCTSB (1) to ProCTSB (2). After passing through the ER, ProCTSB is N-glycosylated in the Golgi (3). Endosomal cleavage of the 62 aa propeptide results in the active single chain form (4), which is further cleaved at the C-terminus. The final activation step takes place intralysosomally and results in the two-chain form of CTSB, with the two chains bound together by a disulfide-bond.

Beside its role in lysosomal degradative processes, CTSB has been associated with cancer progression and invasion (Sloane et al., 1990) as it shows the capability to degrade extracellular matrix components (Guinec et al., 1993).
Curiously, CTSB does not only not possess hydrolase abilities, but also acts as a ligase under certain conditions as recently shown (Lambeth et al., 2021).
Ctsb$^{-/-}$ mice do not exhibit a distinctive phenotype in comparison to *Ctsb*$^{+/+}$ mice, presumably due to compensation by other lysosomal cysteine proteases. However, mice deficient for both CTSB and CTSL, present a rapidly progressing brain atrophy, protein aggregates in neurons and the early demise after approximately 12 postnatal days (Felbor et al., 2002). This phenocopies the course of lysosomal storage disorder neuronal ceroid lipofuscinosis (1.6 Neuronal Ceroid Lipofuscinosis (NCL)). Further studies of such double-deficient mice found impairment of autophagy (Koike et al., 2005) and accumulation of a variety of lysosomal proteins in brain lysosomes (Stahl et al., 2007). Accordingly, lysosomal cysteine cathepsins seem to fulfil an essential role in the function of the postnatal nervous system.
The involvement of CTSB in various neurodegenerative diseases has been frequently described. Its role in AD is controversially discussed as on the one hand CTSB promotes the formation of β-amyloid plaques through the processing of the amyloid precursor protein (Hook et al., 2005). On the other hand, *in vivo* β-amyloid is degraded in part by CTSB (Mueller-Steiner et al., 2006, Embury et al., 2017). Even learning and memory impairment was ameliorated in an AD mouse model through viral transduction of CTSB (Embury et al., 2017).
In PD the degradation of cytosolic α-synuclein-aggregates is performed by the aspartyl protease Cathepsin D (CTSD) together with the cysteine proteases CTSL and CTSB (McGlinchey and Lee, 2015), while in HD models overexpression of CTSB protects cells from huntingtin accumulation (Liang et al., 2011). All these findings stress the role of CTSB in modulating the course of various entities of neurodegenerative disorders.

1.4 Lysosomal storage disorders (LSDs)

Perturbance of the lysosomal activity due to mutation of involved enzymes, membrane, transport or activator proteins gives rise to more than 70 distinct disorders. Collectively 1 in 5000 live births is affected by an LSD (Platt, 2018). The mutations cause either impaired functionality or deficiency of the translated protein, the commonality lies in the accumulation of disease specific substrate storage (Wraith, 2002).

Generally, LSDs can be divided into groups according to the accumulated storage material in: sphingolipidoses, mucopolysaccharidoses, glycogen storage diseases, glycoproteinoses, Lipid storage diseases, Post-translational modification defects, Integral membrane protein disorders, lysosome related organelles disorders and neuronal ceroid lipofuscinoses (Platt et al., 2018).

All cells contain lysosomes, but the clinical spectrum of these predominantly recessively inherited metabolic disorders varies greatly. For example, the mucopolysaccharidoses lead to prenatal dysmorphia due to affected extracellular matrix and bone formation, the sphingolipidoses show renal, hepatic and cardiac system failure, while others present primarily cognitive disability or psychiatric symptoms (Platt, 2018).

The relatively low incidence prevented pharmaceutic companies from investing intensively in the drug development for LSDs and rare diseases in general. Only after the European Government and the Council of the European Union passed the Regulation (EC) No 141/2000 on orphan medicinal products in 1999 and similar initiatives had been started in the US (Orphan drug Act 1983) and Japan (1993), that financial incentives, market exclusivity and simplified approval procedures were set into place for the development of so-called “orphan drugs”. Companies set their primary focus on these orphan diseases, leading to the development of many expensive and profitable therapies to a degree not anticipated by legislators (Platt, 2018).

While all LSD patients profit from symptomatic and supportive therapies, over the last decades a variety of causal therapeutic approaches has become available.

One of the first approaches was the hematopoietic stem cell transplantation (HSCT)(Hobbs et al., 1981), intended to repopulate tissues and secrete lysosomal enzymes to rescue other cells. However, HSCT has proven effective for only some LSDs and only in a restricted therapeutic window (Parenti et al., 2015).

A different approach is followed by the substrate reduction therapy (SRT). Inhibition of biosynthesis of macromolecules in order to slow down the accumulation of storage material. Such therapies are approved for Gaucher disease type I and Niemann-Pick type C with further clinical trials ongoing (Platt et al., 2018).

Small molecule pharmacological chaperones (PC) are used to stabilize proteins prone to being misfolded (Marques and Saftig, 2019). Their major drawback is the limitation to missense mutations affecting stability (Mohamed et al., 2017).

Recently, gene therapy has gained a lot of interest, as it has the ability to actually cure an LSD. So far two main ways are used: direct viral transduction using adeno-associated viruses or lentiviruses and the *ex vivo* application of such viruses to hematopoietic stem cells followed by autologous transplantation. Promising results have been achieved in metachromatic

leukodystrophy (Biffi et al., 2013) and many other clinical trials are currently in progress (Platt et al., 2018, Nagree et al., 2019).

Today however, the standard of care for many LSDs is the enzyme replacement therapy.

1.4.1 Enzyme replacement therapy (ERT)

Already in 1961 after previously coining the term "lysosome" (De Duve et al., 1955), Christian de Duve, set the foundation of ERT principles for LSDs, by noting that almost all endocytosed substances eventually find their way to the lysosome (De Duve, 1964). This intriguing mechanism can be exploited by ERT. In ERT the defective or missing enzyme is recombinantly produced externally in a host organism, secreted and purified, before it is administered to the patient in order to compensate for the lack of enzyme activity intralysosomally.

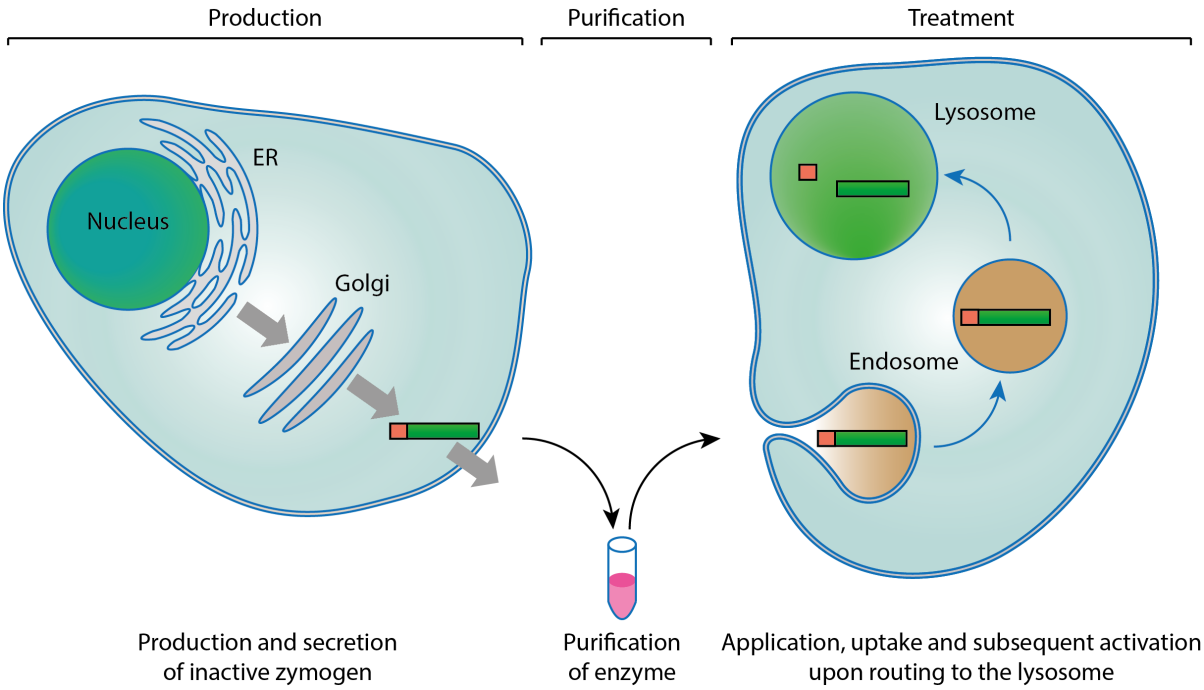

figure 3 Schematic overview of the principle of ERT. Production: The recombinant enzyme undergoes processing as the endogenous counterpart (**figure 2**), however use of a secretion peptide ensures the secretion of inactive zymogens. Purification: Tagged propeptide (red) enables purification of enzyme. Treatment: Application of proform leads to endocytosis. Final activation within the endolysosomal system leads to cleavage of the tagged propeptide and leaves the active enzyme undistinguishable from the endogenous enzyme.

Nowadays, ERT presents an approved causal treatment option for many LSDs with many more in pre-/clinical trials (Parenti et al., 2015).

Disease	Replaced Enzyme	Year of approval
Type 1 Gaucher Disease	Glucocerebrosidase	1991
Fabry Disease	α-Galactosidase	2003
MPS 1	α -L-Iduronidase	2003
MPS VI	N-acetylgalactosamine-4-sulfatase	2005
MPS II	Iduronate sulfatase	2006
Pompe	α-Glucosidase	2006
MPS IVa	N-acetylgalactosamine-6-sulfatase	2014
CLN2	Tripetidyl peptidase	2017
Mannosidosis	α -Mannosidase	2018

Table 1 List of selected ERTs for LSDs and respective year of approval (Platt, 2018, Markham, 2017) It should be noted that except from CLN2 all listed ERTs are administered intravenously, whereas Tripeptidyl peptidase is delivered intracerebroventricularly.

Weekly i.v. application of recombinant enzyme ensures adequate effective levels. Upon systemic distribution and cellular endocytosis, the enzyme is routed to the lysosome, where it successfully carries out the defective enzyme's function and prevents the progression of the disease (Desnick and Schuchman, 2012).

While ERT has proven effective in the treatment of peripheral pathologies in many cases, the highly selective permeability of the blood-brain-barrier (BBB) poses a considerable obstacle (Begley et al., 2008). Hence, ERT often fails in treating the neurological symptoms, exhibited by approximately 70 % of LSD patients (Das et al., 2017).

The production of recombinant enzymes requires the use of mammalian cells, accepting the lower production yield in comparison to prokaryotic cells on behalf of the complex posttranslational modifications performed in mammalian cells. The elaborate production and frequent application make ERT a very expensive therapy with costs of several hundred thousand Euros per patient and year of treatment (Das et al., 2017).

Unfortunately, over time the risk of generating endogenous antibodies against the recombinant enzyme can jeopardize the ERT (Broomfield et al., 2016). A second drawback is the limitation to enzymatic disorders.

1.5 Neuronal ceroid lipofuscinosis (NCL)

A group of rare recessive LSDs are the neuronal ceroid lipofuscinoses (NCLs). With an incidence of 1 in 30.000 live births they constitute the most common cause of neurodegeneration in children. Caused by mutations in 14 genes, the different forms (CLN1-CLN14) lead to blindness and neurodegeneration (Schulz et al., 2013). The affected gene products show a high heterogeneity, coding for lysosomal proteases, transporters, and proteins of so far unknown functions. Furthermore, the age of onset ranges from congenital to adult forms.

Designation of diseases	Reported form of onset	Gene	Protein	Characterization	Therapeutic approaches	Approved Therapies
CLN1	**Infantile** Late infantile Juvenile Adult	*CLN1 (PPT1)*	Palmitoyl protein thioesterase 1 (PPT1)	Soluble lysosomal protein	ERT, SCT, GT, PT	
CLN2	**Late infantile** Juvenile	*CLN2 (TPP1)*	Tripeptidyl peptidase (TPP1)	Soluble lysosomal protein	SCT, GT, PT	ERT
CLN3	**Juvenile**	*CLN3*	CLN3 (Battenin)	Lysosomal membrane protein	GT, PT	
CLN4	**Adult** (autosomal dominant)	*CLN4 (DNAJC5)*	Cysteine string protein α (CSP α)	Cytosolic, associated with vesicular membranes		
CLN5	**Late infantile** Juvenile Adult	*CLN5*	CLN5	Soluble lysosomal protein	GT	
CLN6	**Late infantile** Adult	*CLN6*	CLN6	ER membrane protein	GT, PT	
CLN7	**Late infantile** Juvenile	*CLN7 (MFSD8)*	CLN7	Lysosomal membrane protein	GT	
CLN8	**Late infantile** Juvenile	*CLN8*	CLN8	ER membrane protein	SCT	
CLN9	**Juvenile**	*CLN9*	CLN9	Unknown		
CLN10	**Congenital** Juvenile Adult	*CLN10 (CTSD)*	Cathepsin D (CTSD)	Soluble lysosomal protein	ERT	
CLN11	**Adult**	*CLN11 (GRN)*	Progranulin	Soluble lysosomal protein	GT	
CLN12	**Juvenile**	*CLN12 (ATP13A2)*	ATP 13A2	Lysosomal membrane protein		
CLN13	**Adult**	*CLN13 (CTSF)*	Cathepsin F	Soluble lysosomal		

				protein	
CLN14	**Infantile** Late infantile	*CLN14 (KCTD7)*	Potassium channel tetramerization domain-containing protein type 7	Cytosolic, partially associated with membranes	

Table 2 List of Neuronal Ceroid Lipofuscinoses with respective therapeutic approaches (adapted from (Specchio et al., 2021, Kohlschütter et al., 2019))Therapeutic approaches range from Enzyme replacement therapy (ERT), to Stem cell therapy (SCT), gene therapy (GT) and pharmacological therapies (PT).

What most forms have in common is an impairment of the autophagic flux, causing accumulation of storage material, in particular but not limited to lipofuscin (Brandenstein et al., 2016, Cao et al., 2006, Koike et al., 2005, Thelen et al., 2012, Seranova et al., 2017). Lipofuscin is an autofluorescent aggregate of oxidized proteins, fats, carbohydrates and traces of metals (Porta, 1991). It is considered a marker for cellular aging, is thought to develop upon impairment of proteolytic degradation and its formation can be induced via inhibition of lysosomal cysteine proteases (Ivy et al., 1984, Ivy et al., 1989, Nunomura and Miyagishi, 1993). Furthermore, accumulation of subunit C of the mitochondrial ATP synthase (SCMAS) and saposins have been observed (Anderson et al., 2013, Jalanko and Braulke, 2009, Tyynelä et al., 1993, Palmer et al., 1989).

The clinical features include blindness, seizures and the progressive cognitive decline paired with loss of motor functions, ultimately leading to a premature death (Schulz and Nickel, 2018). Except for the congenital form CLN10, the affected children develop normally until the point of sudden neuronal decline.

The therapeutic options are very limited. For most forms only a palliative treatment, mitigating the symptoms, is available. The medicinal therapy of the epilepsy poses a major obstacle as the neurodegeneration constantly changes the dose dependent efficacy and toxicity (Schulz et al., 2013).

While there are clinical trials currently ongoing for gene therapy in CLN2, CLN3 and CLN6 the only approved causal therapy available for any NCL is an ERT (Liu et al., 2020). In 2017 a very successful ERT for CLN2 was approved (Markham, 2017, Schulz et al., 2017). The affected protease tripeptidyl-peptidase 1 (TPP1) is recombinantly produced and administered intracerebroventricularly via a port canula, performed at the UKE Hamburg a renowned center for CLN2 patients from all over the world.

1.5.1 CLN10

One form of NCL is CLN10, caused by mutations in the *CTSD*-gene resulting in a loss of function of the lysosomal aspartyl protease Cathepsin D (CTSD).

CLN10 is the only NCL form that classically manifests as a congenital disease (Mole et al., 2019). Patients suffering from congenital NCL typically show microcephaly at birth, exhibit general motor seizures and only live up to a few days (Barohn et al., 1992). Later, mutations of the *CTSD*-gene were found to be responsible for congenital NCL (Siintola et al., 2006, Steinfeld et al., 2006). To this day a variety of homozygous mutations and compound heterozygous mutations have been identified as cause of CLN10 (Fritchie et al., 2009, Varvagiannis et al., 2018). However, depending on the degree of enzymatic impairment, not only congenital but also later childhood onset has been described (Steinfeld et al., 2006). Even juvenile forms with an onset at 15 years of age were found (Hersheson et al., 2014).

The pathology was first observed in mice deficient for CTSD. Such mice were found to exhibit intestinal atrophy in their third postnatal week, loss of lymphoid cells and eventually death at postnatal day 26±1 (Saftig et al., 1995). Later, their neurological phenotype and accumulation of storage material within neurons were detected (Koike et al., 2000). Even heterozygous mice were shown to exhibit behavioural abnormalities (Zhou et al., 2015). Viral re-expression of *Ctsd* in the central nervous system was in contrast to visceral re-expression capable of prolonging the life-span of $Ctsd^{(-/-)}$ mice to 63±3 days and even ameliorating peripheral effects of CTSD deficiency (Shevtsova et al., 2010). Accordingly, mice with conditional neuroectoderm-specific knock-out of CTSD only lived 5.5 days longer than mice ubiquitously deficient for CTSD, stressing the criticality of central CTSD-expression (Ketscher et al., 2016). Curiously, in this model peripheral effects of CTSD deficiency like intestinal atrophy were observed in this model as well even though the enzyme was present in these tissues, indicating a necessary draining mechanism of CTSD from CNS to the periphery.

So far, there is no causal therapy available for patients. However, ERT with recombinant human CTSD has proven to be effective, preclinically, in $Ctsd^{-/-}$ mice (Marques et al., 2019) paving the way for future clinical trials. As with many ERTs, not all aspects of the disease are fully addressed, stressing the need to further elucidate the pathologies and address them all.

2 AIM

The aim of our project is to analyse whether the application of recombinant human pro-cathepsin B (hereafter referred to as rhCTSB) can lead to a correction of the biochemical storage material in a preclinical model of CLN10 and hence ameliorate the clinical outcome. It is envisaged that such a protease replacement therapy may also be applied to other types of neuronal ceroid lipofuscinoses.

In our previous work, a *Ctsd*$^{-/-}$ mouse strain served as a suitable animal model for CLN10, a rapidly progressive, congenital form of NCL (Marques et al., 2019). *In vivo* application of recombinant human pro-cathepsin D (rhCTSD) led to a reduction of characteristic storage markers, normalization of the autophagic flux and a reduction of lysosomal hypertrophy. Addressing all three pathological hallmarks constitutes the major challenge for any new therapeutic approach.

The goal of our project is to assess, if rhCTSB can be used in a therapeutic approach in order to tackle the three hallmarks mentioned above and assess how it compares to the benchmark rhCTSD. By boosting bulk degradation via application of rhCTSB, we aim to restore cellular homeostasis and mitigate the progression of the disease.
The project was divided into different sections:

- The stable transfection of a cell line as expression system of rhCTSB
- The establishment of a production pipeline for highly purified rhCTSB
- The analysis of the uptake mechanisms and kinetics *in cellula*
- The proper uptake and processing upon application *in vivo*.

Ultimately, we try to analyse if in our CLN10 murine model rhCTSB can:

- Normalize the autophagic flux in the affected cells;
- Reduce the lysosomal hypertrophy reflecting the perturbance of the degradative cellular machinery;
- Reduce the accumulation of specific storage material within the cells.

3 MATERIAL AND METHODS

3.1 Material

3.1.1 Chemicals

Unless stated otherwise, all chemicals were purchased from Sigma-Aldrich, Carl Roth, AppliChem or Merck with the purity grade pro analysi (p. a.).

3.1.2 Frequently used buffers

Table 3 List of frequently used buffers

Buffer		Composition
LB medium	1 %	(w/v) Trypton/ Pepton
	0.5 %	(w/v) Yeast extract
	1 %	(w/v) NaCl
		pH 7.0
LB agar	1.5 %	(w/v) Agar-agar
		In LB medium
Phosphate-buffer saline (PBS) (10x)	100 mM	Na_2HPO_4
	18 mM	KH_2PO_4
	1,37 M	NaCl
	27 mM	KCl
		pH 6.8

3.1.3 Cell culture media and additives

Table 4 List of used cell culture media and additives

Chemical	Reference
Bafilomycin A1	Calbiochem
Dulbecco's Modified Eagle Medium (DMEM)	Gibco
Fetal calf serum (FCS)	Biochrom

Leupeptin	Enzo Life Sciences
Pepstatin A	Enzo Life Sciences
Mannose (Man)	Serva
Mannose-6-phosphate (M6P)	Sigma
Penicillin-Streptomycin (P/S)	Sigma Aldrich
Polyethylenimin Max MW 40,000 (PEI)	Polysciences
Puromycin	Invivo Gen
RAP	Kindly provided by Prof. Thomas Braulke
Trypsin/EDTA	Sigma Aldrich
Zeocin	InvivoGen

3.1.4 Devices

Table 5 List of used devices

Device	Reference
Aekta Purifier system	GE Healthcare
Agarose gel chamber, subcell GT	Biorad
Centrifuge 5425 R	Eppendorf
FV1000 confocal laser microscope	Olympus
Image Quant LAS800	GE Healthcare
Heracell 150 CO_2 incubator	Thermo Fisher Scientific
Multiple Tecan Reader	BioTek
Power Pac 200	Biorad
Precellys homogeniser	Bertin instruments
SDS-PAGE gel chamber	Biorad
Thermomixer comfort	Eppendorf

3.1.5 Cell lines

All lines were kept in a sterile incubator at 5 % CO_2. Mouse embryonic fibroblasts (MEF WT, MEF CTSB KO), all human embryonic kidney cells (HEK-293T WT, HEK EBNA, HEK

CTSB Crispr KO), HeLa cells, and human neuroblastoma cell line (SH-SY5Y) were cultured at 37 °C in Dulbecco´s Modified Eagle Medium (DMEM) with 4 mM L-glutamine and 4.5 g/l D-glucose (Thermo Fisher Scientific), supplemented with 10 % of fetal calf serum (FCS) and 1 % Penicillin Streptomycin (Life-Technologies). Chinese hamster ovary cells (CHO-K1) were cultured in Roswell Park Memorial Institute medium (RPMI).

Upon transfection with the respective vector selection pressure was applied, HEK-293T and HEK-EBNA cells were selected utilizing Pyromycin at a concentration of 1 µg/ mL, in the case of CHO-K1 cells Zeocin at 500 µg/mL was used.

Table 6 List of used cell lines

Cell line	Description	Reference
CHO-K1	Chinese hamster ovary cells	Kindly provided by J. Grötzinger
HEK-EBNA	Human embryonic kidney cells transfected with Epstein-Barr virus nuclear antigen 1	Kindly provided by J. Grötzinger
HEK-293T WT	Human embryonic kidney cells	Kindly provided by André Marques, PhD
HEK CTSB Crispr KO	Human embryonic kidney cells deficient for cathepsin B	Generated and kindly provided by H. Aerts
MEF WT	Wild-type murine embryonic fibroblasts	Kindly provided by André Marques, PhD
CTSB KO MEF	Murine embryonic fibroblasts deficient for cathepsin B	Kindly provided by Thomas Reinheckel
HeLa	Cervical carcinoma cells (Henrietta Lacks)	CCL-2™ (ATCC)
SH-SY5Y	Human neuroblastoma cell line	CRL-2266™ (ATCC)

3.1.6 Mouse strains

3.1.6.1 CTSD deficient mice

Cathepsin-D knockout mice were first established and described in 1990 by Saftig et al. These mice exhibit an Exon deletion of the *Ctsd* gene, leading to a complete deficiency of this lysosomal aspartyl-protease. Cathepsin-D knockout mice undergo normal development during the first two weeks, however, start to gain less weight than wild-type mice, progressively develop motor deficits and usually die around P25, thus mimicking the progression of CLN10, the congenital form of NCL and serving as a preclinical model of the disease for assessment of potential therapeutics. All experiments were performed according to ethical standards and the German animal welfare law in accordance with the guidelines of the Christian-Albrechts-University of Kiel and approved by the Ministry of Energy, Agriculture, the Environment and Rural Areas Schleswig-Holstein under the reference number V242–40536/2016(81–6/16).

3.1.6.2 CTSB deficient mice

Cathepsin-B knockout mice were kindly provided by T. Reinheckel and used for more precise studies of the recombinant enzyme's distribution within a living organism.

3.1.7 Antibodies

3.1.7.1 Primary antibodies

Table 7 List of primary antibodies

Antigen	Host	Relevant dilution			Reference
		WB	IF	IHC	
β-Actin	Mouse	1:1000			Sigma-Aldrich #A2066
CTSB	Goat	1:1000	1:250		R&D AF953
CTSB	Rabbit	1:1000	1:250		CST (D1C7Y)
CTSD	Rabbit	1:1000			Provided by Prof. Andrej Hasilik
CTSD	Goat	1:1000			Santa Cruz Biotechnology sc-6486
CTSL	Goat	1:1000			R&D (AF952)
GAPDH	Rabbit	1:1000			Santa Cruz Biotechnology #sc-25778
GFP	Rabbit	1:1000			Merck SAB4301138
His-Tag	Mouse	1:4000			R&D MAB050

LAMP1	Rat	1:1000	1:500	DSHB #1D4B
LAMP2	Mouse	1:1000	1:500	DSHB #H4B4
LC-3	Rabbit	1:2000		MBL #PM036
Limp2	Rabbit	1:1000		Pineda # L2T2
p62	Rabbit	1:1000		Enzo Life Sciences #BHL-PW-9860
SapC	Rabbit	1:1000		Provided by G. Grabowski
SapD	Rabbit	1:000		Provided by G. Grabowski
SCMAS	Rabbit	1:3000		Provided by E. Neufeld
A-Tubulin	Mouse	1:1000		DSHB #E7

3.1.7.2 Secondary antibodies

Table 8 List of secondary antibodies

Antibody	Coupled to	Host	Relevant dilution	Reference
α-goat	Horseradish-peroxidase	Rabbit	1:5000	Dianova
α-mouse		Sheep	1:5000	
α-rabbit		Goat	1:5000	
α-rat		Goat	1:5000	
α-goat	AlexaFluor® 488, 594, 647, 680	Donkey	1:300	Cell Signalling Technology
α-mouse		Goat/Donkey	1:300	
α-rabbit		Goat/Donkey	1:300	
α-rat		Goat	1:300	

3.1.8 Plasmids

Table 9 List of used plasmids

Plasmid	Resistence	Reference
pcDNA3.1 Zeo (-)	Ampicillin/ zeocin™	
pcDNA3.1 Tn hEF SB9 cl 1 real	Ampicillin/Puromycin	

pCEP-Pu with BM40 leader peptide and His-tag	Ampicillin/Puromycin	(Kohfeldt et al., 1997)

3.1.9 Constructs

Table 10 List of used constructs

Construct	Encoded protein	Tag	Source
Recombinant human Pro-Cathepsin B	rhCTSB for CHO	Hexa-Histidin	Life Technologies GmbH
	rhCTSB for HEK 293T	Hexa-Histidin	Life Technologies GmbH
	rhCTSB for HEK EBNA	Hexa-Histidin	Life Technologies GmbH
	eGFP		Provided by Dr. Manfred Gossen
	pSB-100x		Provided by Dr. Manfred Gossen
	pSB-SM		Provided by Dr. Manfred Gossen

3.1.10 Oligonucleotides

Table 11 List of used oligonucleotides

Oligonucleotide name	Sequence 5' – 3'
CHO_T7 forward	TAATACGACTCACTATAGGG
CHO_BGH reverse	TAGAAGGCACAGTCGAGG
EBNA_CMV forward	CGCAAATGGGCGGTAGGCGTG
EBNA_SV40 reverse	GAAATTTGTGATGCTATTGC
HEK_EF1 forward	TCAAGCCTCAGACAGTGGTTC
HEK_BGH reverse	TAGAAGGCACAGTCGAGG
HEK_SV40 reverse	GAAATTTGTGATGCTATTGC
CTSB_NT1 forward	GAGGACCTGCTCACATGCT
CTSB_NT2 forward	ACGTCACCGGAGATGATG

CTSB_NT3 reverse	GGCCTTTTCTTGTCCAGAAGT
CTSB_NT4 reverse	AGTTGGCAACCAGCCAGTAG
CHO_CTSB_NT5 forward	AGAGATCAGGGCTCCTGCGG
CHO_CTSB_NT6 forward	TCCGAGAAGGACATCATGGCTGA
CHO_CTSB_NT7 reverse	CGGACACGTGAGCATTGGTGT
CHO_CTSB_NT8 reverse	CGCCGGACTTGTACAGCAGGA

3.2 Methods

3.2.1 Molecular biological methods

3.2.1.1 Polymerase chain reaction (PCR)

PCR was utilized to amplify specific DNA sequences. Oligonucleotides, so-called primers, complementary to a sequence of the template DNA were added and bind to their specific region, hereby determining the starting point for the following synthesis of DNA performed by DNA taq-polymerase. These enzymes synthetize a complementary DNA strand in 5' → 3' direction at an optimal temperature of 72 ° C. Utilization of both a forward and a reverse primer bordering a given target sequence allows the precise the amplification of DNA, which was established by repeating three steps multiple times (**Table 10**).

Table 12 Standard PCR procedure and protocol

Step	Temperature	Time	Cycles
Denaturation	95 °C	5 min.	
Denaturation	96 °C	15 sec.	30x
Annealing	58 °C	30 sec.	
Extension	72 °C	2 min.	
Final Extension	72 °C	3 min.	
End	10 °C	∞	

3.2.1.2 Restriction enzyme digestion and DNA ligation

Constructs for secreted recombinant human Pro-Cathepsin B in corresponding plasmids were synthesized by Life Technologies GmbH (Darmstadt, Germany) with the cDNA sequence

based on the UniProt accession number AAC37547.1. The plasmids were digested using respective restriction endonucleases. These enzymes cleave dsDNA upon recognition of specific palindromic sequence motifs, hereby generating an overlap of the strands. Such so-called “sticky ends” can be reconnected to other dsDNA molecules digested by the same restriction endonuclease in a process termed “Ligation”, as was performed in this work.
In case of the construct destined for the HEK-EBNA expression system, the chosen vector pCEP-Pu already contained the BM40 leader peptide for secretion of the following construct, the information coding for the Hexahistidin-tag as well as the EBV origin of replication (oriP) and puromycin resistance. The vector was incubated with the cDNA and the restriction enzymes Nhel and Notl for one hour at 37 °C.
The restriction enzymes were heat inactivated at 65 °C for 20 minutes. The cleaved DNA fragments were separated via 0.8 % gel electrophoresis and the bands of interest isolated for ligation (s. 3.2.1.6). The obtained DNA was ligated in a ratio of 3:1 (construct to vector) overnight at 16 °C before the ligase was heat inactivated at 65 °C for 10 minutes.

3.2.1.3 Amplification of plasmid DNA

XL1-Blue Escherichia coli (E. coli) were transformed with plasmid DNA by heat shock. Frozen cells were slowly thawed on ice. After addition of 2-5 µL of plasmid solution, cells were left on ice for another 30 min. and then heated to 42 °C for 45 seconds. Afterwards cells were cooled down on ice for 3-5 minutes.
300 µL of LB-medium were added to the suspension and cells put shaking at 37 °C for 30 min. before being transferred to 10 cm LB agar dishes with ampicillin for overnight incubation at 37 °C. Afterwards, single colonies were picked and transferred to Erlenmeyer flasks containing 150 mL and 150µL Ampicillin. These were incubated overnight at 37 °C while shaking before purifying the amplified plasmid DNA.

3.2.1.4 Purification of plasmid DNA

Plasmid DNA purification was performed following the manufacturers’ protocol for GeneJet Plasmid Miniprep kits (Thermo Fisher Scientific) or PureYield Plasmid Midiprep Systems (Promega). For Midipreps Erlenmeyer flasks containing transformed E. coli were successively decanted into 50 mL Falcon tubes and centrifuged until the formation of a pellet. Subsequently the supernatant was discarded, further Erlenmeyer content was added and previous steps repeated.

The sequencing of the obtained DNA was performed by GATC with appropriate sequencing primers.

3.2.1.5 Measurement of DNA concentration

The DNA concentration was determined using a Synergy HT Microplate Reader (BioTec). The maximum absorbance of DNA at a wavelength of 280 nm was measured and compared to the absorbance at 260 nm for the purpose of evaluating the purity of the sample and determining possible protein contaminations. A ratio of A_{260}/A_{280} between 1.7 and 2.0 is considered sufficient for pure DNA.

3.2.1.6 Agarose gel electrophoresis

Agarose gel electrophoresis was used to separate nucleic acid samples according to their molecular weight. 0.8% agarose (1.2 g) in 1x TAE buffer (150 mL) were heated in a microwave and 15 µL of SYBR safe DNA gel stain (Thermo Fisher Scientific) were added for later visualization of bands under UV- light.

50x Tris-Acetate-EDTA (TAE) buffer	2 M	Tris/ HCl pH 8.0
	5.5 % (v/v)	Acetic acid
	50 mM	EDTA

Nucleic acid samples were supplemented with 6* Loading buffer (Thermo Fisher Scientific), loaded onto gel wells and a voltage of 120 mV was applied. The migration of the samples through the gel was compared to a DNA ladder (Thermo Fisher Scientific) as size reference. Bands of interest were cut out and purified according to the manual of the kit (High Pure PCR-Purification Kit, Roche).

3.2.2 Cell biological methods

3.2.2.1 Maintenance of cell lines

Cells were kept in a sterile incubator in a humidified 5% CO_2 environment under the respective condition (see 3.1.4). Sterile handling of the cells was performed under a laminar air flow cabinet. Cells were grown on 6-10 cm dishes and passaged when maintained over extended time periods using 0.5-1 mL of Trypsin/EDTA after being rinsed with PBS. Upon detachment cells were resuspended in respective media and seeded at the desired concentration.

3.2.2.2 Cryo-preservation of cells

All cell lines were cryo-preserved in liquid nitrogen. Cells were trypsinized as described above, resuspended in media and transferred to a 15 mL falcon tube. After centrifugation at 220 × g for 5 min. the supernatant was discarded and the cell pellet dissolved in freezing solution.

Freezing solution	1.12 mL	DMEM
(per 10cm dish)	0.32 mL	FCS
	0.16 mL	DMSO

This was then transferred to a 1.6 mL CryoPure tube (Sarstedt) and frozen at -80 °C before being cryo-preserved in liquid nitrogen.

3.2.2.3 Thawing of cells

Liquid nitrogen stored cells were thawed in a waterbath at 37 °C and transferred into 15 mL falcon tubes (Sarstedt) containing 10 mL of respective medium. After 5 min. of centrifugation at 220 × g the supernatant was discarded and the cells, now cleansed from the DMSO from the freezing solution, were resuspended in new medium and seeded on 10 cm dishes.

3.2.2.4 Indirect immunofluorescence labelling of cells

Intracellular structures were stained using antibodies against characteristic marker-proteins of respective compartments.

Cells were grown on cover slips to semi-confluency, before being rinsed twice with PBS and fixed in either 4 % paraformaldehyde (PFA) in PBS at room temperature for 20 min. or in methanol at -20 °C for 20 min. In both cases fixed cells were then washed thrice with PBS and permeabilized in 0.2 % (w/v) saponin in PBS for 5 minutes. The fixative was quenched with quenching solution for 10 min. before being blocked with blocking solution for 30 min. in order to prevent unspecific antibody binding in the following procedure.

Quenching solution:	1x	PBS pH 7.6
	0.2 % (w/v)	Saponin
	0.12 % (w/v)	Glycine
Blocking solution:	1x	PBS pH 7.6
	0.2 % (w/v)	Saponin

10 % (v/v)	FCS

The fixative was incubated with the desired primary antibody in blocking solution ON at 4 °C. On the following day, cover slips were rinsed 5x with 0.2 % (w/v) saponin in PBS before the secondary antibody was applied. After an incubation at RT for 60 min., the cover slips were washed thrice in
0.2 % (w/v) saponin in PBS and twice in dH_2O before they were mounted onto microscope slides with mounting solution and left for at least three hours to polymerize.

Mounting solution:	
1x	PBS pH 7.6
17 % (w/v)	Mowiol 4-88
33 % (v/v)	Glycerol
20 mg/mL	1,4-diaza-bicyclo-2,2,2-octane (DABCO)

The acquisition of images was performed with a FV1000 confocal laser scanning microscope using a U Plan S Apo 100x oil immersion objective (NA = 1.40) and the software Olympus FluoView™.

3.2.2.5 Generation of neural stem cell-derived astrocytes

Neural stem cells were isolated according to protocol (Stahl et al., 2007). Cerebral cortices of 14-day-old *Ctsd*$^{+/+}$ and *Ctsd*$^{-/-}$ mice were used to generate neurospheres, from which neural stem cells were obtained upon passage (Conti et al., 2005). Approximately 3×10^5 cells were seeded on 13 mm coverslips coated with 0.1% matrigel matrix (Corning) in a 12 well plate for cultivation in Dulbecco's modified Eagle's medium/F12 (DMEM/ F12) supplemented with 1% B27, 1% N2 (both from Life Technologies), 10 ng/mL fibroblast growth factor-2 (FGF-2) and 10 ng/mL epidermal growth factor (EGF) (both from Immunotools). The medium was changed after 24 hours to DMEM/F12 supplemented with 1% fetal bovine serum and 2% B27, and cells were further cultivated for 2 weeks during which the neural stem cells differentiated into astrocytes. Cells were treated with recombinant human Cathepsin B, D and L (rhCTSB, rhCTSD and rhCTSL), respectively at a concentration of 40 µg/mL for 1 week.

3.2.2.6 Generation of a stable expression cell line

For the production of recombinant human Pro-Cathepsin B different expression systems were utilized. Mammalian cells were transfected using Polyethylenimine (PEI). Due to the permeabilization of the plasma membrane the plasmid DNA was incorporated into the cells. Transfected eGFP was used as a reporter gene for the positive control as well as dishes with PEI without any plasmid DNA as negative control. To 10µg of DNA and 25 µL of PEI DMEM was added to a total volume of 500 µL, thoroughly mixed and added drop by drop to the cells' media.

After three hours of incubation the media of the transfected cells was changed. In order to induce a stable integration of the plasmid DNA into the genome, the cells were kept under antibiotic selection.

Different expression systems were utilized:

CHO K1 cells were expressed the plasmid episomally. In the course of time plasmid DNA can be integrated into the genome of the cells randomly.

HEK EBNA cells have been optimized for episomal replication by inserting the EBV nuclear antigen 1 (EBNA).

HEK cells were transfected using the sleeping beauty transposon system. By cotransfecting a Transposase, the integration of the construct into a region of the host DNA that is cleaved by the Transposase could be achieved, which leads to a direct stable transfection (Holstein et al., 2018).

3.2.2.7 Serial dilution for single clone selection

For the selection of a single high producing clone cells were trypsinized and seeded on 96-well plates, followed by a serial of dilution steps in order to obtain single clones. The procedure followed a protocol by John A. Ryan, Ph.D. from Corning Incorporated Life Sciences. Promising wells were successively cultured to grow on larger wells and analysed regarding their enzyme production properties via immunoblot (see 3.2.3.6) and pulldown assay (3.2.3.13).

3.2.2.8 Collection, Filtration and Concentration of transfected cells' conditioned media

The process of protein purification required several preparative steps beforehand. Transfected HEK-EBNA cells were cultured in five T175 producer flasks (Sarstedt) in 35 mL medium each. After seeding, cells were grown to confluency under normal selection conditions. Approximately one week later at approximately 80 % confluency, the medium was exchanged with 100 mL production medium without Puromycin and reduced FCS concentration (2.5 %).

Production Medium	DMEM
	1.0% (v/v) Penicillin/Streptomycin
	2.5% (v/v) FCS

After another week the medium was transferred successively into 50 mL falcon tubes and detached cells spun down by centrifugation for 5 min. at 300 × g. After decantation of the supernatant into a new 50 mL falcon tube the centrifugation was repeated and the supernatant media filtered through a fluted filter (Rotilabo® type 600P, Roth) and a vacuum driven filtration device (Stericup® and Steritop™, Merck).
The filtered media was concentrated to a final volume of 50 mL in an Amicon Stirred cell system using an ultrafiltration disk (Millipore, PLGC07610) and thereafter filtered once again using a 0,2 µm Filtropur S filter (Sarstedt).

3.2.3 Protein biochemical methods

3.2.3.1 Purification of recombinant His-tagged enzyme

Hexa-Histidin-tagged rhCTSB was purified using an ÄKTApurifier 10 system (GE Healthcare). All Buffer solutions used in the purification process were filtered and degassed prior to usage. Before starting the purification procedure, the entire system was washed with ddH_2O and PBS successively. For extended periods in between purification runs the system was left in ddH_2O with 20% Ethanol.
In a first step the media was injected into a 50 mL chromatography column (GE Healthcare). In the first run the medium was passed through a HisTrap™ Nickel-column (GE Healthcare) in order to perform an affinity chromatography, capture the His-tagged protein and isolate it from the other components of the medium.
After passage of the medium through the Nickel-column, the Nickel-bound protein fraction was exposed to an increasing Imidazole gradient, which first led to the elution of unspecifically bound proteins and eventually to the elution of the His-tagged protein 250 mM imidazole. Structurally, the aa histidine contains the basic imidazole ring.

1x PBS + 500 mM Imidazole	50 mL	10x PBS
	17g	Imidazole
	pH 7,4	with HCl

ad 500 mL with ddH_2O

The eluted protein was fractionated and collected in 13 mm diameter test tubes (Sarstedt). Measurement of the UV-spectra indicated in which fractions the His-tagged protein resided. These fractions were then pooled and injected into the 50 mL column of the ÄKTApurifier, after it had been washed with PBS.

The Nickel-column was replaced with a Superdex 75 column (GE Healthcare) in order to perform a size-exclusion chromatography and cleanse the sample from the toxic Imidazole. The gel matrix of the Superdex allows smaller proteins to immerse deeply into the pores and thus travel slowly, whereas bigger molecules do not penetrate the matrix as deeply and pass through the column faster. This allows a size-dependent fractionation of the molecules upon injection of the pooled sample into the Superdex. Again UV-spectra were used to determine the protein fractions.

After running and staining a Coomassie gel (see 3.2.3.8) to clarify that there was only protein in the anticipated fractions at the molecular weight corresponding to rhCTSB, the fractions were filtered through a 0,2 µm Filtropur S filter (Sarstedt)and concentrated by centrifugation in a Vivaspin® 20 tube (Sartorius) and stored at -20 °C.

3.2.3.2 Generation of protein cell lysates

Cells obtained from cell culture were lysed via the addition of RIPA lysis buffer and subsequent shaking at 4 °C for approximately 45 minutes.

RIPA lysis buffer	50 mM	HEPES/ NaOH pH 7.4
	150 mM	NaCl
	1 mM	EDTA
	0.5 mM	Sodium deoxycholate
	1 % (v/v)	Nonidet™ P-40
	1 pill	c0mplete protease inhibitor (Roche 11836145001)
	1 mM	Na_3VO_4

Afterwards cells were centrifuged at 17000 × g and 4 °C for 10 minutes. The supernatant was transferred to a new 1,5 mL micro tube and the pellet composed of cell debris tossed.

3.2.3.3 Preparation of tissue homogenates

Murine tissues were thawed and tissue lysis buffer was added according to the samples' weight. 9x the sample's weight in microgram was added in microliter to achieve a 10x dilution. Screw cap tubes were supplemented with three 1.4 mm diameter Precellys porcelain beads (Peqlab, VWR) and samples lysed and homogenized in a Precellys® 24 homogeniser (Peqlab, VWR) in two rounds of shaking at 6000 rpm for 20 sec. with cooling on ice in between rounds.

3.2.3.4 Determination of protein concentration

The protein concentration of the samples was determined prior to adequate dilution with MilliQ ® water (Millipore, Merck) in order to generate equal concentrations. For this purpose, the Pierce™ BCA Protein Assay Kit (Thermo Fisher Scientific) was utilised. It relies on proteins' peptide bonds' ability to reduce Cu^{2+} to Cu^{+}, which in a second step is chelated by bicinchoninic acid. The formation of this purple colored complex can be measured by the proportional increase in absorbance at a wavelength of 562 nm as was performed using a Synergy HT microplate reader (Biotek).

3.2.3.5 Sodium dodecyl sulfate polyacrylamide gel electrophoresis (SDS-PAGE)

SDS-PAGE was used in order to separate proteins according to their molecular weight. Protein samples were supplemented with 5* Loading Buffer and boiled for 4 min. at 95 °C.

5* Loading Buffer	4 mL	Tris pH 6.8 1 M
	24 mL	99 % Glycerol
	4 g	SDS
	4 g	DTT
		Ad 40 mL with ddH_2O
		Addition of one drop Bromophenolblue

The SDS in the buffer gives proteins an overall negative charge and allows a strictly size dependent separation regardless of the molecules' initial charge.
Protein samples were loaded onto self-cast 12.5 % polyacrylamide gels or 4-12 % NuPAGE Bis-Tris gradient gels (Thermo Fisher Scientific) and a constant voltage of 80-90 V was applied and later increased to 120-150 V.

3.2.3.6 Immunoblotting

In order to visualize desired proteins with antibodies, separated protein fractions were transferred from the polyacrylamide gels onto 8.5 × 6.0 cm Amersham Protran 0.2 µm nitrocellulose membranes (GE Healthcare) in a semi-dry manner. The polyacrylamide gel and the respective membrane were washed with Transfer buffer (TB) and assembled to a stack flanked by two layers of 9.0 ×7.00 cm TB soaked Whatman paper (GE Healthcare) on both sides, facing towards either the anode or cathode.

1x Transfer buffer	25 mM	Tris pH 8.3
	0.2 M	Glycine
	20 % (v/v)	Methanol

The transfer was performed in a Trans-Blot® SD Semi-Dry Electrophoretic Transfer Cell (Bio-Rad) at a constant amperage of 65mA per stack for 120 min. in case of self-cast gels. In the case of NuPAGE gels a shorter transfer of 80 min. was chosen to prevent smaller molecules from trespassing the nitrocellulose membrane.

3.2.3.7 Incubation with antibodies and stripping of immunoblots

Blotted nitrocellulose membranes were incubated in rolling 50 mL falcon tubes overnight at 4 °C in 5% milk powder (Roth) in TBS/T buffer with addition of the desired antibody at the respective concentration (see 3.1.6.1).

TBS/T buffer	20 mM	Tris/HCl pH 7.0
	150 mM	NaCl
	0.1 % (w/v)	Tween® 20

Before secondary antibodies were applied, membranes were washed thrice by shaking for 10 min. in TBS/T to cleanse the membranes from excess antibody. Secondary Horse-Radish-Peroxidase (HRP) coupled antibodies were chosen according to the primary antibodies' host species, utilised at a dilution of 1:10 000 in TBS/T with 5 % milk powder and left rolling in a 50 mL falcon tube at room temperature (RT) for one hour.
After two repetitions of the washing steps mentioned above, membranes were developed in an Amersham Imager 680 (GE Healthcare) chemiluminescence imager. For the substrate of the

detected enzymatic reaction, enhanced chemiluminescence (ECL) solution A and B were mixed 1:1, 300 µL of combined substrate solution applied to the membrane and equally distributed.

Solution A	0.1 M	Tris/HCl pH 8.6
	0.025 % (w/v)	luminol
Solution B	0.11 % (w/v)	p-Coumaric acid
	in	DMSO

HRP degrades hydrogen peroxide leading to the emission of a charge-coupled device (CCD) detectable light signal.

For visualization of multiple proteins on single membranes, immunoblots were either stripped with mild Stripping buffer for approximately 30 min. at RT, in case of the following antibody being raised in a different host species than the previous one, or with 20 mL of harsh Stripping buffer and 70 µL of β-mercapto-ethanol for 30 minutes at approximately 90 °C.

In both cases membranes were washed in TBS/T buffer after stripping.

3.2.3.8 Coomassie staining

Protein fractions generated through the process of purification, were separated via SDS-PAGE and stained with Coomassie Brilliant Blue to validate the estimated protein. Gels were washed in MilliQ water, and stained with 20 mL of GelCode Blue Stain Reagent (Thermo Fisher Scientific) for approximately 6 hours at RT while shaking. Afterwards gels were destained by floating several days in MilliQ water with a tissue for absorption of the staining.

3.2.3.9 Cathepsin B activity assay

In order to assess the recombinant enzyme's catalytic activity, a fluorometric assay was used. The fluorogenic substrate ZZ-R-R-AMC (Enzo life science) is selectively cleaved by Cathepsin B as it exhibits two Arginine residues in a row (Barrett and Kirschke, 1981). Prior to assessing the activity, cell lysates had to be prepared by washing the dishes thrice with PBS, adding 100 µL of cathepsin activity buffer and leaving the dishes shaking at 4 °C for 1 hour.

Cathepsin activity buffer	50 mM Sodium acetate
	0.1 M NaCl
	1 mM EDTA
	0.2 % Triton X-100

Afterwards the lysed cells were scraped from the surface and transferred into 1.5 mL Eppendorf tubes. A centrifugation at 17 × g for 10 min. lead to the formation of a pellet of cell debris. The supernatant composed of the soluble cellular components was used to determine the activity of cathepsin B in cell lysates. In the case of tissue homogenates, a 10x dilution was acquired by adding cathepsin activity buffer according to the sample's weight, the tissue samples homogenized by shaking twice in a Precellys® 24 homogeniser (Peqlab, VWR) together with three Precellys porcelain beads (Peqlab, VWR) for 20 sec. at 6000 rpm and the supernatant used for the assay generated through a centrifugation at 4°C and 17 × g for 10 minutes.
A master mix of the specific substrate in cathepsin activity buffer at a concentration of 20 µM was prepared in advance and stored on ice. 100µL of this master mix were pipetted per well of a black 96 well plate (Thermo Fisher Scientific). 2µL of murine tissue lysates or 8µL of cell culture cell lysates were added to each well and the 96 well was incubated at 37 °C. Measurements were performed after 30, 60 and 120 minutes. The emitted fluorescence signal of the cleaved substrate was measured with a HT Synergy microplate reader (Biotek) at a wavelength of 440 nm using an excitation wavelength of 360 nm. Blanks, representing the background activity measured by the assay were subtracted from the values actually recorded.

3.2.3.10 β-Hexosaminodase activity assay

As β-Hexosaminodase (β-Hex) is a lysosomal enzyme, its activity was chosen as readout of lysosomal hypertrophy and thus lysosomal stress in murine tissues of WT and *Ctsd*$^{(-/-)}$ mice.
Tissue homogenates generated with tissue lysis buffer were prepared and prediluted to a mutual concentration of 4 µg/µL. 10 µL of sample were added to 100 µL of β-Hex substrate mix and incubated for 20 min at 37 °C.

β-Hex substrate mix:	
0.2 M	Citric acid
0.4 % (w/v)	BSA
0.08 % (w/v)	NaN_3
	pH adjusted to 6.8 with NaOH
10 mM	p-nitrophenyl-n-acetyl-β-D-glucosamid

After the incubation 1 mL of Stop buffer was added to the solution.

Stop-buffer:	0.4 M	Glycine pH adjusted to 10.4 with NaOH

Tubes were centrifuged for 10 min. at 17 × g to clear the liquid from floating particles and 161 µL of the supernatant pipetted onto a 96 well plate. The absorbance was measured at a wavelength of 405 nm.

3.2.3.11 Autocatalytic processing of Cathepsin B

The autocatalytic activation of rhCTSB was assessed using the established cathepsin B activity assay (see 3.2.3.9). 100 µL of 3.2 M rhCTSB in Processing buffer adjusted to the desired pH by addition of sodium acetate were incubated for either 20 or 60 min. at 37 °C. The tubes were vortexed and 5 µL of processed rhCTSB transferred into a new tube filled with 100 µL of cathepsin activity buffer. After mixing it thoroughly, 10 µL were added to 100 µL of master mix in a black 96 well micro plate and the activity assay performed as described above.

Processing buffer:	0.1 M	Tris-HCl pH 7.6
	3 mM	EDTA
	5 mM	Cysteine

3.2.3.12 Pulldown assay

160µL of Equilibration buffer were added to 40µL OF HisPur™ Ni-NTA Magnetic Beads (Thermofisher). Tubes were vortexed, beads collected on a magnetic stand and the supernatant discarded

Equilibration buffer (pH 8.0):	100 mM	Na_3PO_4
	600 mM	NaCl
	0.05 %	Tween-20 detergent solution
	30 mM	Imidazole

Washing steps were repeated with 400 µL of Equilibration buffer, before media samples (250 µL diluted with 250 µL of Equilibration buffer) were added to the beads, tubes were vortexed and afterwards placed in an end-over-end rotator for three hours. Supernatant was collected as "Flow-through". 400 µL of Wash buffer were added, tubes were inverted several times, beads

collected on the magnetic stand and the supernatant discarded. These washing steps were repeated.

Washing buffer (pH 8.0):		
	100 mM	Na_3PO_4
	600 mM	NaCl
	0.05 %	Tween-20 detergent solution
	50 mM	Imidazole

25 µL of Elution buffer were added to the beads, tubes were vortexed, centrifuged for one minute at 700 × g, placed on an end-over-end rotator for 30 minutes and the eluate was collected. Elution steps were repeated.

Elution buffer (pH 8.0):		
	100 mM	Na_3PO_4
	600 mM	NaCl
	250 mM	Imidazole

Input, flow-through and eluate were prepared for SDS-PAGE, separated and analysed via immunoblotting.

3.2.3.13 Deglycosylation of proteins

Glycoproteins can be characterized by the two enzymes endoglycosidase H (Endo H) and Peptide-N-Glycosidase F (PNGase F) that cleave N-linked glycosylations. While the core glycosylation (high mannose structures) occurs in the endoplasmic reticulum (ER) and is sensitive to digestion by endo H, later modifications occurring in the Golgi (complex glycan structures) make glycoproteins unsusceptible to digestion by endo H. However, PNGase F is capable of cleaving both types of posttranslational modification, hereby providing a positive control for the digestion of N-linked glycosylations.

For both digestions 0.5 µg of rhCTSB were utilized and completed to a final volume of 20 µL with ddH_2O. Upon the addition of 23 µL endoH buffer or 11.5 µL of PNGase F buffer 1, respectively, samples were boiled for 5 min. at 95 °C. Afterwards 2 µL of the respective enzyme were added to the mix and the tubes incubated at 37 °C ON. At the following day Loading buffer was added, the samples heated to 55 °C for 30 min. and then separated via SDS-PAGE together with undigested samples for comparison.

3.2.4 Animal experimentation

3.2.4.1 Animal handling

All animal experiments were performed in accordance with the German animal welfare law and the guidelines of the Christian-Albrechts-University of Kiel. Mice were housed in individually ventilated cage (IVC) under a 12 h light/12 h dark cycle with free access to food (pellets by Sniff Spezialdiäten, V1534) and water. Mice cages were maintained in a room with a temperature between 19 and 22 ◦C and humidity of 45–60%. CTSD deficient mice (NCL10 model) were obtained from heterozygotes matings.

3.2.4.2 Genotyping of mice

In order to determine the phenotype of new-born mice, tail biopsies were taken at P0 – P3 and the DNA was isolated. For this purpose, the biopsies were digested for 60 min. at 55 °C using 100µL of DirectPCR Lysis Reagent Tail (Peqlab) and 1.5 µL of proteinase K (stock at 20µg/µL). The digestion was stopped by inactivating proteinase K for 45 min. at 85 °C. The liberated DNA was amplified for by PCR according to **Table 10** and the pipetting scheme **Table 11**. In case of the CTSD $^{(-/-)}$ mice one set of primers was complementary to the NEO cassette that was integrated in the KO allele, the other one to the exon of the *Ctsd* gene. The amplified DNA was separated via agarose gel electrophoresis.

Table 13 Pipetting scheme of the PCR for genotyping of mice

Volume	Substance
1 µL	forward-Primer (stock 10 µM)
1 µL	reverse-Primer (stock 10 µM)
5 µL	10x Buffer (with $MgCl_2$)
5 µL	dNTP (stock 2 mM)
1.5 µL	DMSO
0.5 µL	dream Taq-polymerase
2 µL	template DNA (100 – 200 ng/µL)
33 µL	ddH_2O
50 µL	final volume

3.2.4.3 Application of recombinant enzyme

The rhCTSB was applied, peripherally, either via intraperitoneal (IP) or via intravenous (IV) injections.

For this purpose, the enzyme was applied with a Micro Fine + Demi 0.3 mL (Becton Dickinson) syringe. For IP injections, the maximum volume applicable was 20 µL/g bodyweight, for IV injections 10 µL/g bodyweight.

Application of rhCTSB to the central nervous system was performed via intracerebroventricular injection under anaesthesia on P1 and P19 before mice were sacrificed and tissues analysed on P23. On P1 10 µL containing 100 µg of the respective recombinant enzyme were injected into the region of the putamen of the right hemisphere. The P19 dose was injected slowly (3 min.) into the left hemisphere using a microsyringe (30 G) with a spacing device to ensure an injection depth of 1.15 mm.

3.2.4.4 Anesthetization of mice

Mice were anaesthetized with 168 mg/kg body weight ketamine (HFW Heinrich Fromme) and 22.4 mg/kg body weight xylazine (Rompun, Bayer) dissolved in PBS via IP injection. The depth of the anaesthesia was assessed by pressing the paws of the animals to test the reflexes.

3.2.4.5 Perfusion of mice

Anaesthetized mice were perfused with 10 mL 0.1 M phosphate buffer (PB) from the left ventricle utilizing a Model '11' Plus Syringe Pump (Harvard apparatus). Organ samples were collected and either immediately frozen in liquid nitrogen or left in 4 % PFA in PB for 4 hours before being transferred to PB only ON. The following day, samples were stored in 30% (w/v) Sucrose in PBS until used for histological analyses.

0.1 M Phosphate buffer (PB):	77.4 mL	1 M Na_2HPO_4
	22.6 mL	1 M NaH_2PO_4
		Ad 1000 mL with ddH_2O
		pH adjusted to 7.4

3.2.4.6 Blood extraction and serum preparation

Blood samples were obtained by puncturing the facial vein with a lancet. Drops were collected in a micro tube. Additionally, blood samples were also collected prior to perfusion by cutting

into the right auricle of the heart. Outflowing venous blood was collected with a pipette and transferred into a 1.5 mL tube. After leaving the sample at RT for 30 min. it was stored for 1 hour at 4 °C to let coagulation take place. The newly formed clod was spun down via centrifugation at 1900 × g and supernatant blood serum collected and diluted 1:10 with water for further analysis.

3.2.4.7 Generation of sagittal brain vibrosections

15-day-old mice were sacrificed and brains were fixed in 4% PFA for 4 hours before being washed at 4 °C in PB overnight, immersed in 30% sucrose in PB, and stored at 4 ◦C. Sagittal sections (35 μm) were cut using a Leica SM 2000R sliding microtome (Leica Microsystems) with dry-ice cooling. Samples were stored in PB containing 0.02% (w/v) sodium azide. Floating slides were washed thrice in PB, blocked and permeabilized using 0.5% Triton X-100, 4% normal goat serum (Gibco) and incubated overnight with respective primary antibodies. After three additional washing steps with 0.3% Triton X-100 in PB, sections were incubated with their respective secondary antibodies for three hours at room temperature, washed again 3 times in washing buffer, and fixed on a coverslip in Mowiol/DABCO.

3.2.5 Statistical analysis

Data are expressed as mean ± S.E.M. For statistical analysis unpaired t-tests were employed using GraphPad Prism 6. (Graph Pad Software, Inc., San Diego, USA): * $P < 0.05$; ** $P < 0.01$; *** $P < 0.001$; **** $P < 0.0001$)

4 RESULTS

4.1 Cloning of rhCTSB

Firstly, the generation of three different expression systems for the secretion of recombinant human pro-CTSB (rhCTSB) was devised. HEK-293T were transfected with the vector *pcDNA3.1*, HEK-EBNA with *pCEP-Pu* and CHO-K1 cells with *pcDNA3.1* using PEI (3.1.8 Plasmids). Stable transfection was established via continuous selection pressure by antibiotics in combination with the available resistance genes in the vectors. The proper secretion of the enzyme's proform was ensured through the use of either the IgK (HEK-293T, CHO-K1) or the BM40 (SPARC) leader peptide (HEK-EBNA) upstream of the pro-CTSB region. The addition of an N-terminal hexa-histidine extension allowed the purification later on in the process.

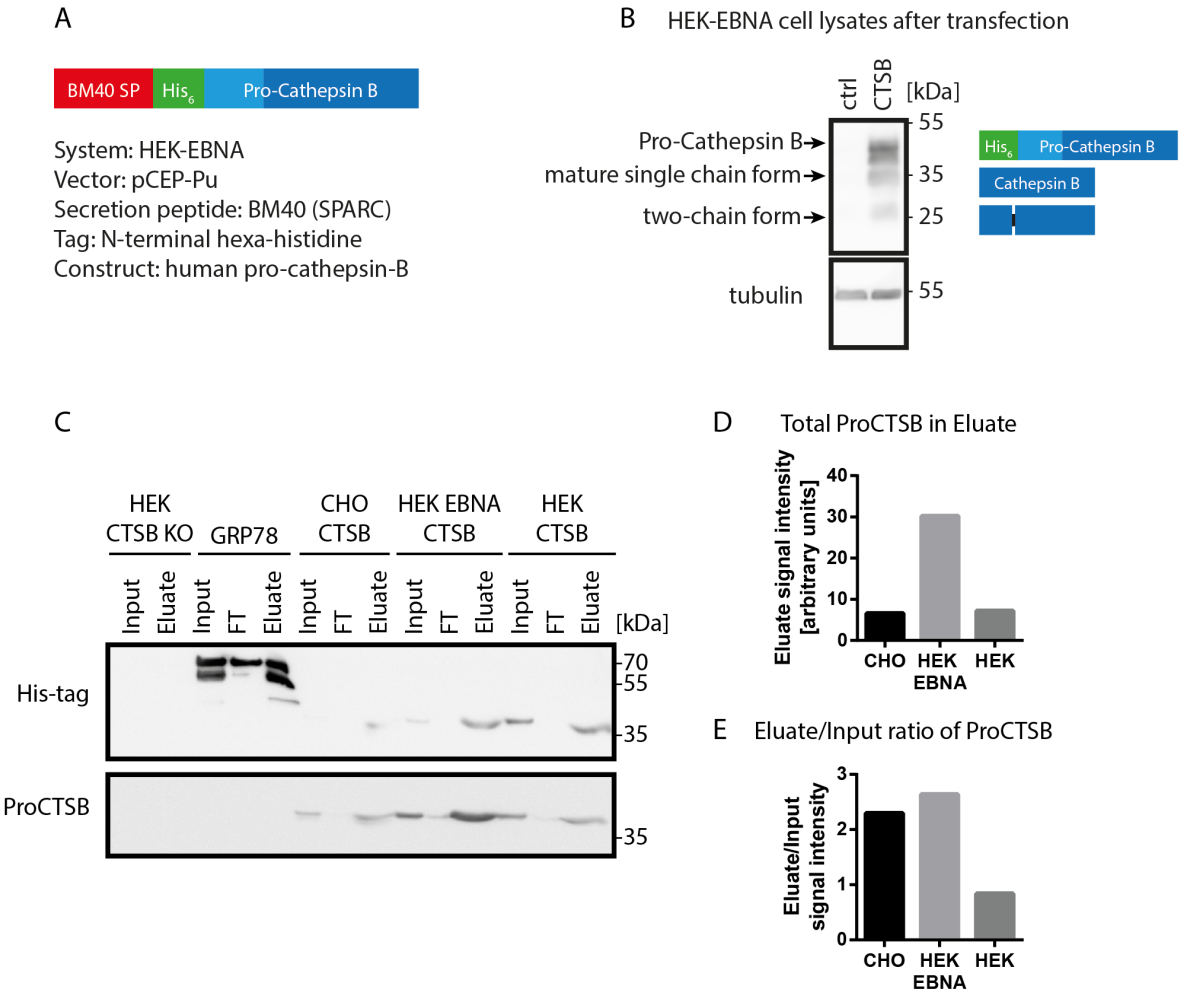

figure 4.A Graphic representation of the construct used for the transfection of HEK-EBNA cells. **B** HEK-EBNA cell lysates obtained after transient transfection with CTSB expression construct ("CTSB") in comparison to untransfected control cells ("ctrl"). 40 µg of protein lysates were loaded and separated onto 12.5 % polyacrylamide gel. Subsequently, the immunoblot was analysed with an anti-Cathepsin B antibody **C** HisPur™ Ni-NTA Magnetic Beads were used in a pulldown assay in order to collect the his-tagged protein fraction. GRP78, a protein involved in protein transport within the ER was used as positive control for the his-tag. $CTSB^{-/-}$ HEK cells' medium was used as negative control. Transfected CHO, HEK-293T and HEK-EBNA cells' media were analysed via immunoblotting. rhCTSB was detected in the media of all expression systems in input and eluate. **D** Quantification of ProCTSB signal intensity in the eluate fractions **E** Ratio of eluate signal intensity of ProCTSB versus input fraction as indicator of purifiable fraction.

The presence of all three forms of rhCTSB was detected in transfected HEK-EBNA cells (**figure 4.B**). Furthermore, a pulldown assay (3.2.3.12 Pulldown assay) revealed that HEK-EBNA cells exhibited the highest fraction of his-tagged and thus purifiable rhCTSB in comparison to transfected CHO-K1 or HEK-293T cells and were hence chosen for the establishment of a production pipeline (**figure 4.C**). Not only was the total amount of detected rhCTSB in the eluate highest in the HEK EBNA system (**figure 4.D**), also the ratio of eluate versus input as indicator of the purifiable in comparison to the non-purifiable fraction was

highest for HEK EBNA (**figure 4.E**). All systems showed an increase from the input to the eluate in rhCTSB levels and no trace detectable in the flow-through.
For the optimization of the production's yield, stably transfected clones overexpressing rhCTSB were isolated by serial dilution and the single clone with the highest enzyme production and secretion capabilities chosen for further experiments.

4.2 Establishment of a production pipeline

For further experiments, an abundance of highly purified rhCTSB was required, hence a production pipeline for continuous supply was established. The synthesized and subsequently secreted rhCTSB was purified from the supernatant in a series of filtration and concentration steps followed by both a nickel-affinity chromatography and a size-exclusion chromatography (**figure 5.A**). Coomassie staining, immunoblot analysis, as well as mass spectrometry performed in collaboration with Dr. Tholey at the Institute of Experimental Medicine, Kiel University, confirmed cathepsin B as the purified protein (s. 7 SUPPLEMENTAL DATA).

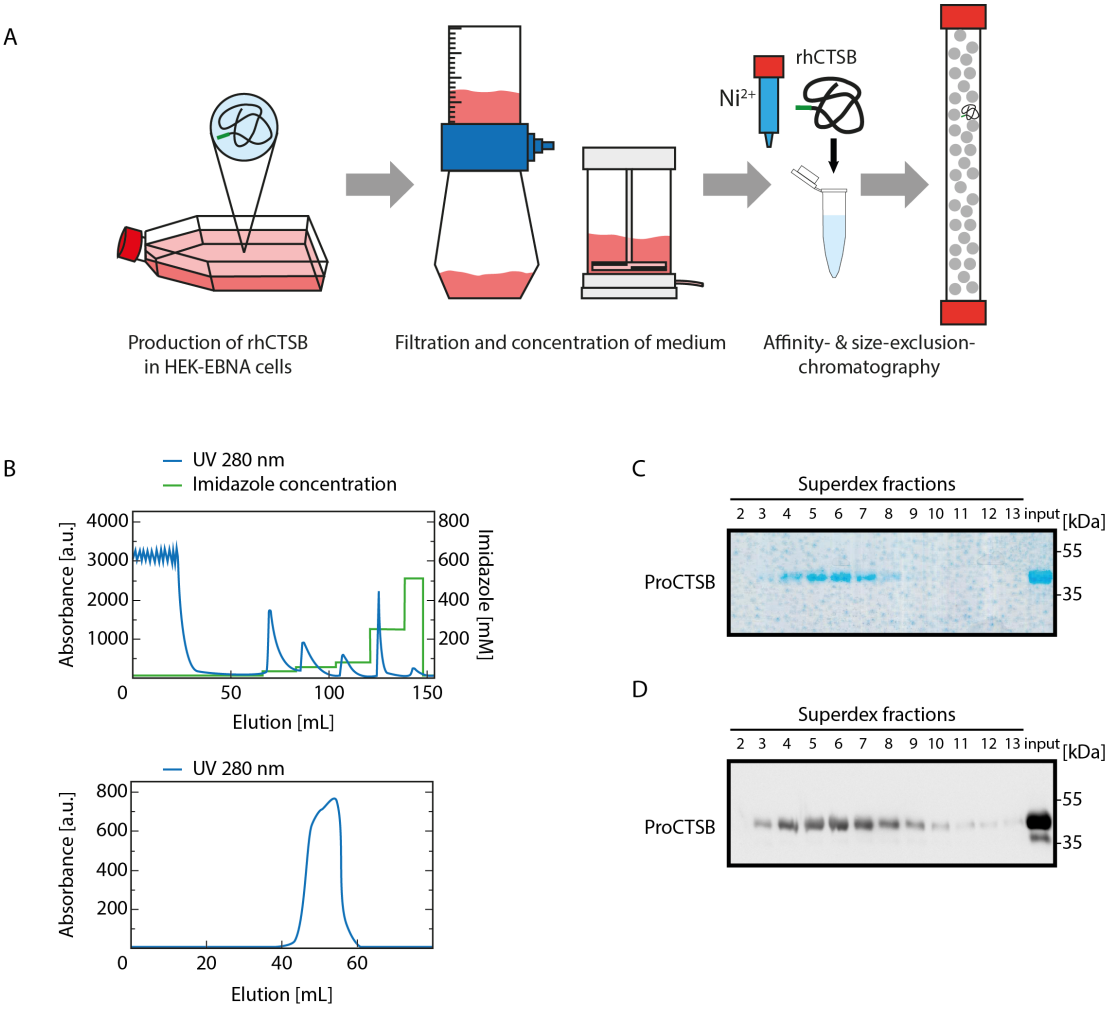

figure 5.A Schematic overview of the rhCTSB purification procedure: Medium was collected from T175 producer flasks, filtered and concentrated before it underwent a nickel-affinity-chromatography and a size exclusion chromatography. **B** Top: Representation of nickel-affinity-chromatography. rhCTSB from the media was bound to chelated Ni^{2+}-Ions through the His-Extension before it was eluted with imidazole at a concentration of 250 mM (UV 280 nm peak). Bottom: Representation of the size exclusion chromatography with samples from affinity chromatography peak in order to separate rhCTSB from Imidazole contamination. **C** Exemplarily shown fractions of Superdex purification step (2-13) as well as input solution obtained from nickel-affinity chromatography. Staining of 12.5 % polyacrylamide gel with GelCode™ Blue Stain after SDS-PAGE. **D** Subsequent analysis of Superdex fractions after 12.5 % polyacrylamide SDS-PAGE and immunoblotting on nitrocellulose membrane.

The superdex fractions showed a single band around 40 kDa matching the molecular weight of the proform of human cathepsin B (**figure 5.D**). The input for the size-exclusion chromatography is obtained as result of the previously performed nickel-affinity chromatography. This production pipeline was able to meet the demands for the following experiments described below.

4.3 *In vitro* characterization of rhCTSB

4.3.1 Stability, activation and glycosylation of rhCTSB

Before *in cellula* experiments were performed, a deeper understanding of basic enzyme kinetics was needed. One crucial requirement for the target-oriented use of rhCTSB in further experiments was its stability, as was assessed by storing equal amounts of rhCTSB under different conditions for different time intervals.

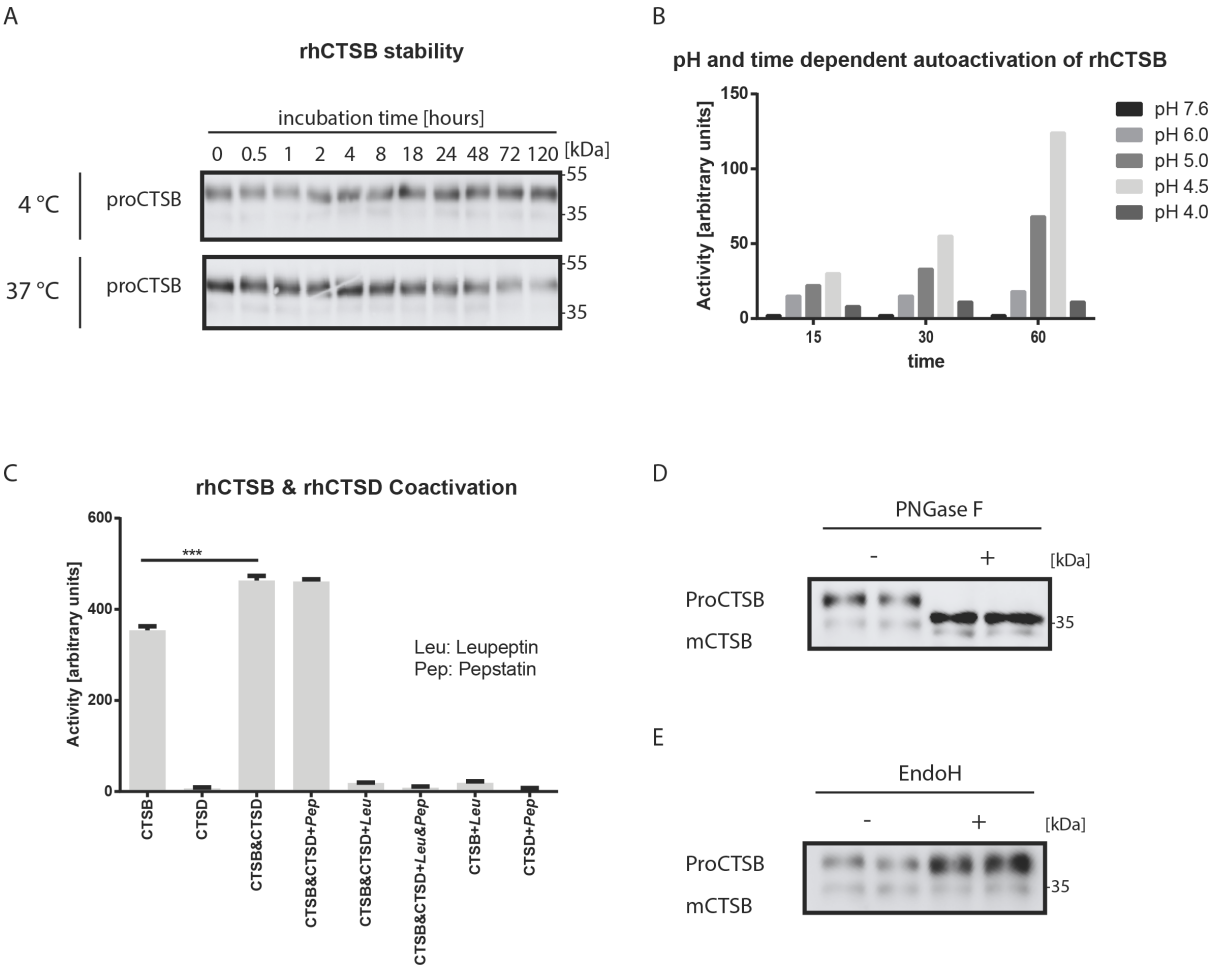

figure 6.A 0.5 µg of rhCTCB in 20 µL of PBS were incubated at either 4 °C or 37 °C and the remnant enzyme was measured by 12.5 % SDS-PAGE and immunoblotting. **B** rhCTSB was preincubated at 37 °C and different pH values for either 15, 30 or 60 minutes. The catalytic activity was measured using the Cathepsin B activity assay described previously (3.2.3.9 Cathepsin B activity assay). **C** 100 µL rhCTSB and rhCTSD at 3.14 µM in Processing Buffer were incubated for 60 minutes at 37 °C with respective inhibitors (1 µg/mL Pepstatin and 2.1 µg/mL Leupeptin). Afterwards 5 µL of processed enzyme were added to 95 µL of activity buffer. 10 µL of substrate mix were added, the mix incubated for additional 120 minutes and the Cathepsin B activity assay was performed. **D-E** 0.5 µg of rhCTSB were digested overnight with PNGase F and Endo H, respectively and compared to undigested rhCTSB undergoing the same incubation. Samples were separated via SDS-PAGE and analysed through immunoblotting **D**

Digested ProCTSB shows a different molecular weight than the undigested, indicating a complex glycan structures **E** Endo H digestion, removing core glycosylation, results in an unchanged molecular weight.

A small decrease of proCTSB signal intensity could be detected after several days at 37 °C, however, at 4 °C the proform of the enzyme was stable (**figure 6.A**).

As the activity of the produced enzyme had to be assessed prior to any further investigation its potential to self-activate, which has previously been described, was assessed using an enzyme activity assay (Rozman et al., 1999). The highest activity and thus highest potential to self-activate was recorded at a pH of 4.5, as stated before in the literature (**figure 6.B**).

Furthermore, CTSB and CTSD are thought to interact in the processing and activation of each other (Laurent-Matha et al., 2006, Aghdassi et al., 2018, Katunuma, 2010). The beneficial effect of coincubating both enzymes before performing the activity assay was investigated using the cysteine protease inhibitor leupeptin and CTSD-inhibitor pepstatin in order to suppress the processing capabilities of the two proteases. The measured CTSB activity was enhanced by coincubation of rhCTSB with rhCTSD **(figure 6.C**).

The protease was further analysed in regard to its glycosylation pattern. rhCTSB was subjected to endoglycosidase H (EndoH) and Peptide:N-glycosidase F (PNGase F) digestion and showed a band of lower mobility after SDS-PAGE, suggesting that the enzyme was purified in its glycosylated form (**figure 6.D-E**).

4.4 *In cellula* uptake studies

4.4.1 Uptake of rhCTSB in human embryonic kidney (HEK) cells

First and foremost, the uptake of the enzyme was assessed in human cells as the long-term goal was achieving a treatment for human patients. Cultured human embryonic kidney (HEK) cells were treated with rhCTSB at 20µg/mL for different periods of time, hereby allowing insights into the kinetics of the enzyme uptake and processing.

Collected cells were lysed and analysed via immunoblot and cathepsin B activity assay (**figure 7**).

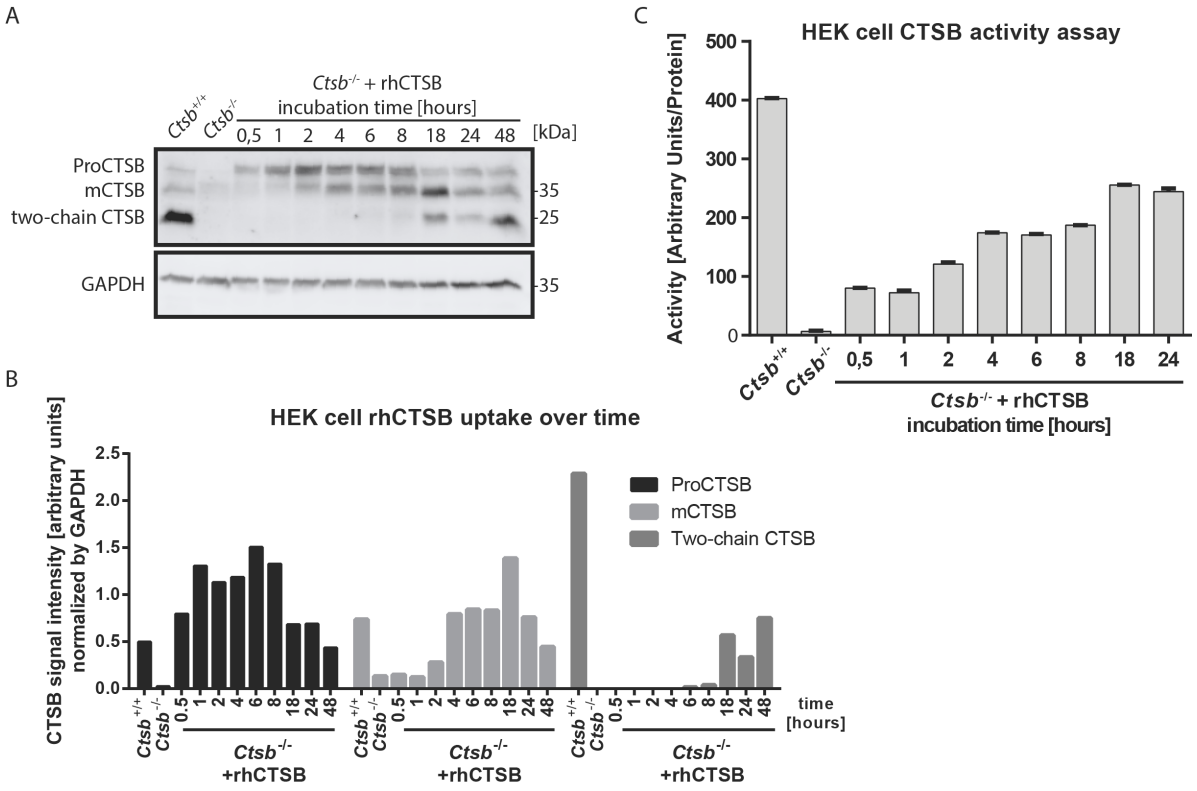

figure 7.A The proper uptake and processing was assessed incubating *Ctsb*$^{-/-}$ HEK cells with rhCTSB at 20 µg/mL for different time periods. *Ctsd*$^{+/+}$ were used as control group. Cell lysates were generated and analysed via 12.5% SDS-PAGE and subsequent immunoblotting. Pro-cathepsin B (ProCTSB), the active mature single chain cathepsin B (mCTSB) and the final two-chain cathepsin B (two-chain CTSB) were detected upon treatment. **B** Quantification of immunoblot A revealed ProCTSB and mCTSB levels comparable to endogenous *Ctsb*$^{+/+}$ levels and subendogenous two-chain CTSB levels after 48 hours. **C** Corresponding increases in enzymatic activity were measured by the Cathepsin B activity assay, reaching half of the endogenous *Ctsd*$^{+/+}$ activity at 20 µg/mL after 18 hours.

Both methods revealed a substantial increase of cathepsin B immunoblot signal and enzymatic activity, respectively. The conversion from pro-cathepsin B (ProCTSB) to mature single chain form (mCTSB) in CTSB deficient HEK cells could be detected after two hours, while further processing to the two-chain form occurred after 18 hours (**figure 7.A-B)**. The activity assay showed a gradual increase of activity with a maximum after 18 to 24 hours (**figure 7.C**).

4.4.2 Uptake of rhCTSB in murine embryonic fibroblast (MEF) cells

In parallel, the successful uptake of rhCTSB in murine cells as requirement for *in vivo* studies in the CLN10 mouse model was analysed using cathepsin-B deficient mouse embryonic fibroblast (MEF) cells. The cells were incubated with the enzyme for different time periods and generated lysates were analysed using immunoblotting.

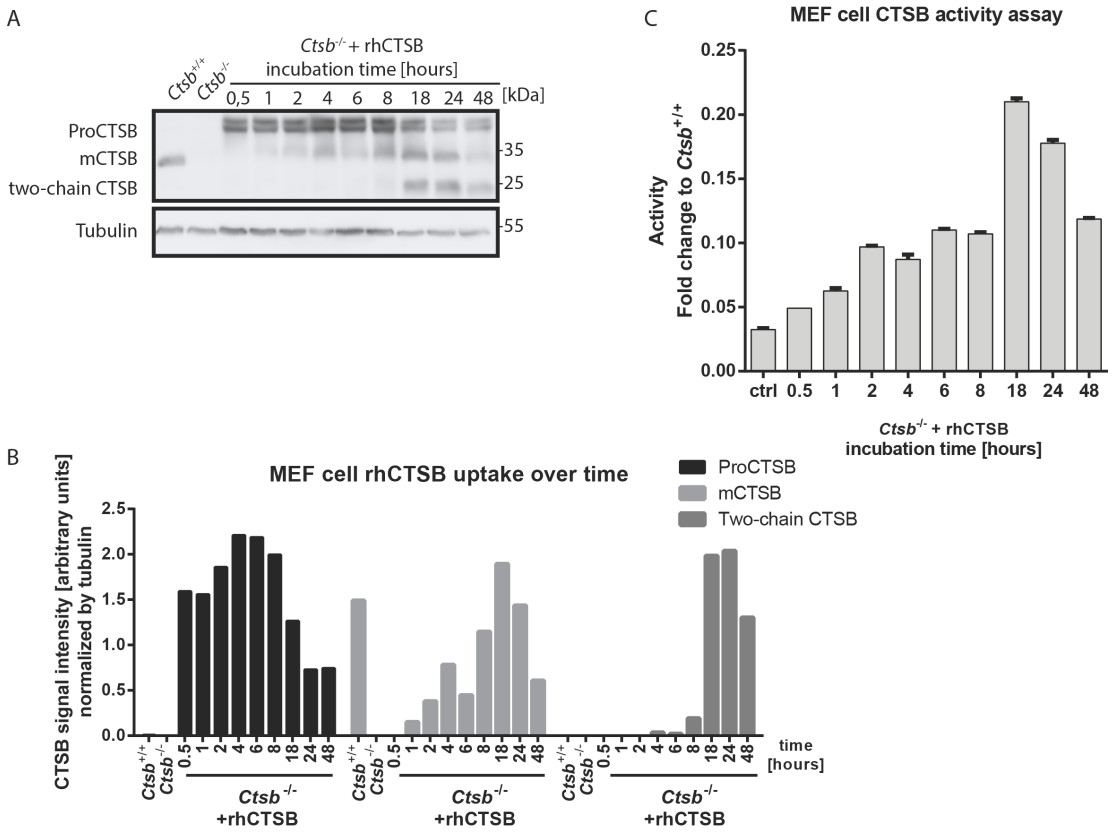

figure 8.A CTSB$^{-/-}$ MEF cells were treated with rhCTSB at 40 µg/mL and incubated for the indicated periods of time before analysis with SDS-PAGE at 12.5 % polyacrylamide and immunoblotting. **B** Quantification of CTSB signal intensity of the three enzyme forms. **C** MEF cells were treated with rhCTSB at a concentration of 20 µg/mL for different periods of time. Cells were washed collected and prepared with activity buffer for further analysis via CTSB activity assay

The successful uptake in murine cells including processing to active forms could be detected in MEF cells via immunoblot **(figure 8.A-B)** and Cathepsin B activity assay (**figure 8.C**). In *Ctsb*$^{+/+}$ MEF cells, the predominant form of endogenous CTSB was mCTSB, whereas in the *Ctsd*$^{-/-}$ cells treated with rhCTSB all three forms were detected abundantly.

4.4.3 rhCTSB uptake kinetics in MEF cells

In order to understand the uptake kinetics of rhCTSB in murine tissue, MEF cells were treated with rhCTSB at different concentration and analysed by immunoblotting. Furthermore, uptake kinetics were observed by analysing media samples of MEF cells treated with rhCTSB.

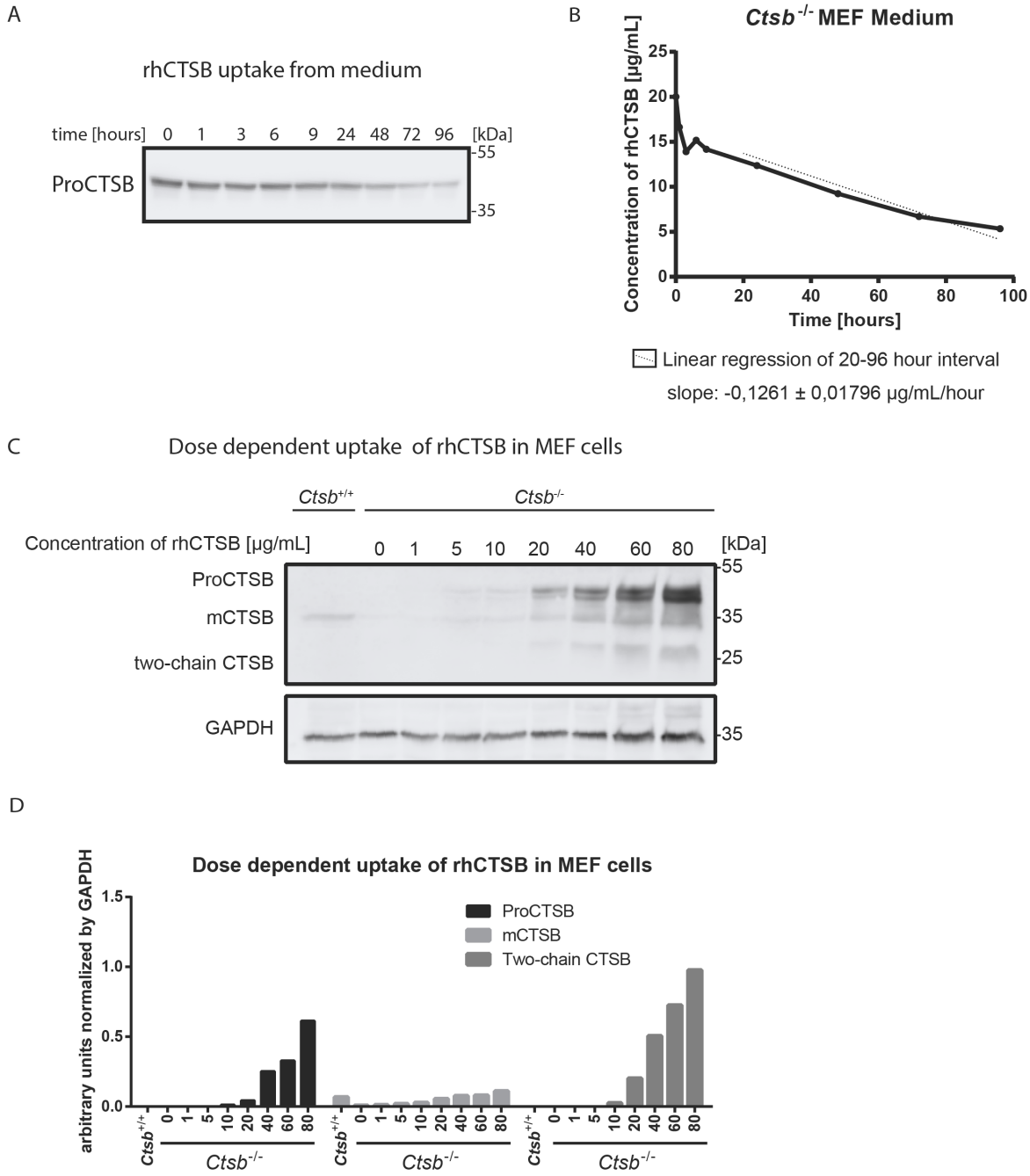

figure 9.A MEF cells deficient for CTSB were cultured and grown to confluency in 5 cm dishes before being treated with rhCTSB at a concentration of 20 µg/mL medium. At various time intervals medium samples were taken, protein fractions separated via SDS-PAGE and analysed by immunoblotting. The reduction of ProCTSB in the medium was chosen as approximation of enzyme uptake **B** Quantification of signal intensity of ProCTSB band (**A**) After an initial rapid reduction within the first hours, the decrease later on was approximated using a linear regression. **C** $CTSB^{-/-}$ and $CTSB^{+/+}$ MEF cells were treated for 48 hours with different amounts of rhCTSB. The cells were washed, lysed and protein fractions separated via SDS-PAGE before immunoblotting. **D** Signal intensity of the three forms of rhCTSB were quantified, normalized to GAPDH signal and compared to $CTSB^{+/+}$ signal.

The reduction of media concentration was used as an approximation of enzyme uptake dynamics, not taking the possible secretion of previously taken up rhCTSB and degradation of

enzyme within the medium into consideration. After an initial quick decrease, the rate of reduction was relatively stable at a speed of 0,126 µg/mL per hour after the first 20 hours (**figure 9.A-B)**. The uptake of rhCTSB in MEF cells was further analysed at different concentrations. Cells were treated for 48 hours and analysed via immunoblotting (**figure 9.C**) As observed in previous experiments with MEF cells, the predominant form in wild-type cells was mCTSB, while treatment with rhCTSB led to the detection of alle three forms of the enzyme. Quantification of band intensity did not indicate a saturation of uptake mechanisms.

4.4.4 Intracellular localization of rhCTSB in MEF cells

Even though the results of the CTSB activity assay lead to the belief that rhCTSB was routed to lysosomes, further evidence was required. The proper trafficking of rhCTSB upon uptake to its organelle of destination was assessed using immufluorescence microscopy imaging. MEF cells were incubated for 18 hours with rhCTSB at a concentration of 20 µg/mL or PBS, respectively, and fixed in methanol at -20 °C.

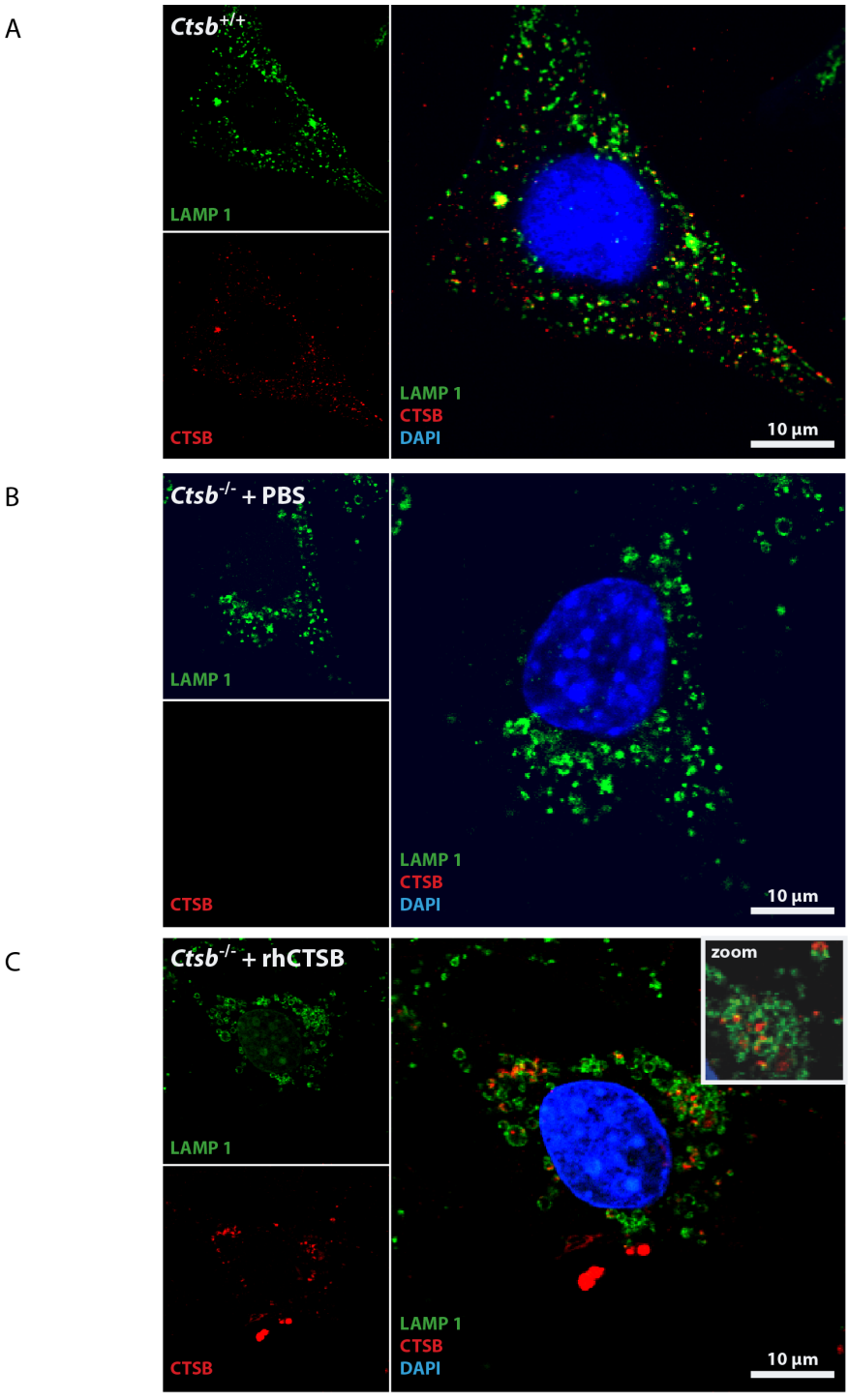

figure 10 Immunostaining of MEF wild-type cells (**A**) as well as *Ctsb*$^{-/-}$ cells treated with either PBS (**B**) or rhCTSB (**C**) at a concentration of 20 µg/mL. Cells were fixed with Methanol at -20 °C and stained with anti-LAMP1 and anti-CTSB antibodies. Nuclei were stained with DAPI. Zoom image of treated CTSB$^{-/-}$ MEF cells shows a partial localization of the two antibody signals in close vicinity. The scale bar represents 10 µm.

The confocal microscope imaging showed a very close localization of both the CTSB and the LAMP1 signal, indicating the successful trafficking of rhCTSB to the late endosome/lysosome.

However, after 18 hours of incubation rhCTSB was also located in other – not further determined – compartments (**figure 10**).

4.4.5 Half-life of rhCTSB in MEF cells

Regarding possible treatment options the enzyme would have to persist within the treated cells for extended periods. Therefore, the half-life of the enzyme was determined in pulse-chase experiments. MEF cells were incubated with rhCTSB at 20 µg/mL for 24 hours before the medium was changed to rhCTSB free medium. At different time points cells were collected, lysed and analysed to understand the kinetics of the endocytosed rhCTSB within the cells (**figure 11.A**).

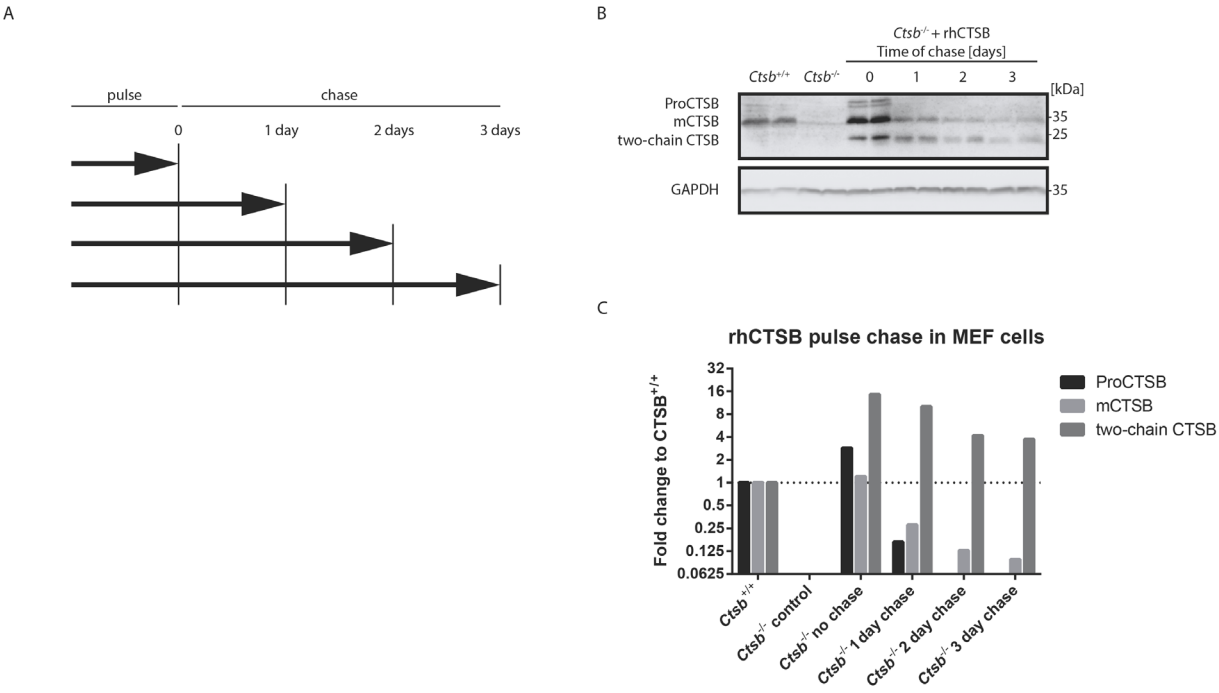

figure 11.A Schematic overview of the experiment **B** *Ctsd*$^{-/-}$MEF cells were incubated with 20 µg/mL rhCTSB for one day in order to take up rhCTSB, hereafter referred to as "pulse" period. Afterwards the media were changed to rhCTSB-free media and samples were analysed at different time points in order to assess the half-life of the enzyme within the cells', hereafter referred to as "chase period" Cells were washed, lysed, separated via SDS-PAGE and analysed via immunoblotting. **C** Quantification of the three bands of rhCTSB representing the three forms as fold change of signal intensity in comparison to endogenous wild-type CTSB.

CTSB deficient MEF cells exhibited the presence of all three forms of rhCTSB after incubation for 24 hours. The proform was not detectable once the first 24 hours had passed, however, the two active forms were present for extended periods of time (**figure 11.B**). Quantification of the CTSB immunoblot signal showed substantial amounts of rhCTSB after several days even in comparison to wild type levels (**figure 11.C**). Calculation of the half-life based on the

immunoblot quantification revealed for pro-cathepsin B $T_{1/2}$=5,83 hrs, for mature cathepsin B $T_{1/2}$= 19,98 hrs and for two-chain cathepsin B $T_{1/2}$= 33,52 hrs.

4.4.6 rhCTSB uptake mechanisms in MEF cells

The enzyme's uptake and targeting to the lysosome under physiological conditions is mediated by a set of receptors. While lysosomal enzymes are known to be directed to the lysosome directly upon synthesis through mannose-6-Phosphate dependent transport, some strongly rely on a mechanism of secretion and recapture, mediated by receptors at the cell surface. This process has been described for CTSB (Markmann et al., 2015). In order to understand if the rhCTSB is taken up by the same mechanism, CTSB-deficient MEF cells were incubated with inhibitors of such receptor mediated uptake to assess their influence on rhCTSB uptake.

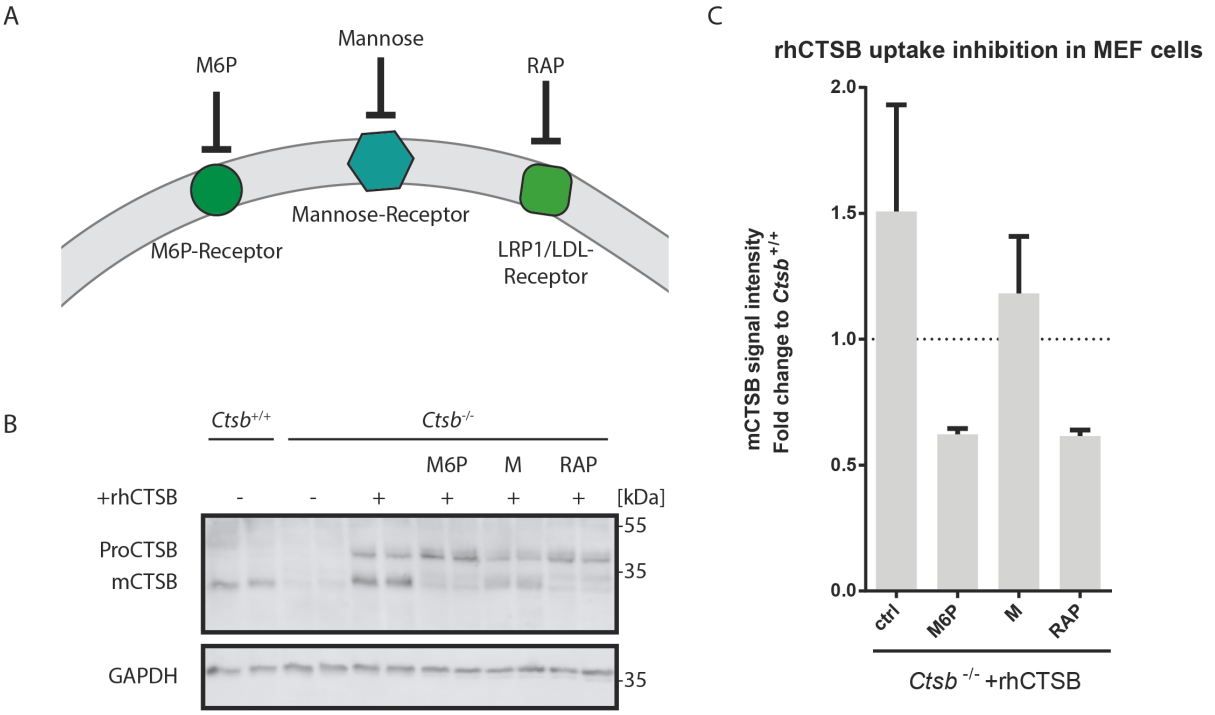

figure 12.A Schematic overview of uptake inhibitors used and their respective target structures. Mannose-6-phosphate (M6P) was used to inhibit the mannose-6-phosphate receptor (M6P-receptor), mannose (M) was used for the mannose-receptor and Ras-related protein (RAP) was used for the LRP1/LDL-receptor, respectively. **B** MEF wild-type or Ctsb$^{-/-}$ MEF cells were preincubated with respective inhibitors for one hour followed by a treatment with rhCTSB at 20 µg/mL for 6 hours. Cells were lysed and protein lysates separated by 12.5 % polyacrylamide SDS-PAGE before immunoblotting analysis. **C** Analysis of mCTSB immunoblot signal intensity displayed as fold change compared to wild-type mCTSB.

The inhibition of the mannose-6-phosphate receptor and the LRP1/LDL-receptor led to a substantial reduction of the mature form of rhCTSB, indicating a strong involvement of the LRP1/LDL-receptor in the uptake mechanism (**figure 12.C**). Even though inhibition of the

mannose-receptor did not show a comparable impact, due to the experimental setup, it does not definitively rule out the possibility of it playing a more pronounced role in the uptake of rhCTSB.

4.4.7 Processing of rhCTSB in HEK cells

The processing of CTSB can be performed by a variety of proteases. Among these are cysteine proteases like CTSB itself or CTSL and aspartyl proteases like CTSD. Both can be inhibited by specific chemical compounds as was performed in order to acquire an understanding of the processing mechanisms of the rhCTSB. HEK cells were co-incubated with the inhibitors of either the first or second processing step of ProCTSB.

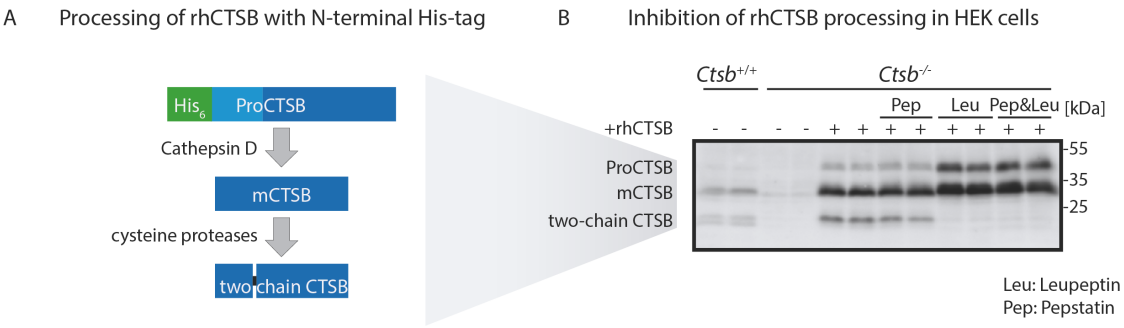

figure 13.A Schematic overview of the processing of rhCTSB. Processing of ProCTSB to mCTSB is mediated by CTSD, while the conversion from mCTSB to two-chain CTSB is managed by several cysteine proteases. **B** HEK cells were incubated with the respective inhibitor Pepstatin (Pep) and/or Leupeptin (Leu) for two hours before changing the media and treating the cells with 20 µg/mL rhCTSB for 24 hours. Cells were lysed and protein samples run on 12.5 % SDS PAGE before immunoblotting. Respective to the schematic overview (A) immunoblotting bands (B) revealed the progress of rhCTSB processing under inhibitory conditions.

The inhibition of cysteine proteases via Leupeptin stops the conversion of mature rhCTSB (mCTSB) to the final two-chain form and stresses their importance in the activation of lysosomal enzymes. Inhibition of Cathepsin D showed no effect on the processing, suggesting the existence of further candidates for the first step of cleavage (**figure 13.B**).

4.5 *In cellula* effects of rhCTSB

4.5.1 Immunoblot analysis of treated *Ctsd*$^{-/-}$ astryocytes

Before rhCTSB was applied *in vivo*, the effect of the enzyme was tested in cell-based experiments. In some forms of NCL a dysfunction of glial cells has been shown to drive the neurodegenerative decay (Takahashi et al., 2022). Hence, we tried to analyse the effect of rhCTSB on *Ctsd*$^{-/-}$ astryocytes. For this sake astrocytes were isolated from neurospheres generated from 14-day old brain cortices of either CTSD$^{+/+}$ or CTSD$^{-/-}$ mice. Hereby created astrocytes underwent lysis, samples were separated via SDS-PAGE and analysed by immunoblotting.

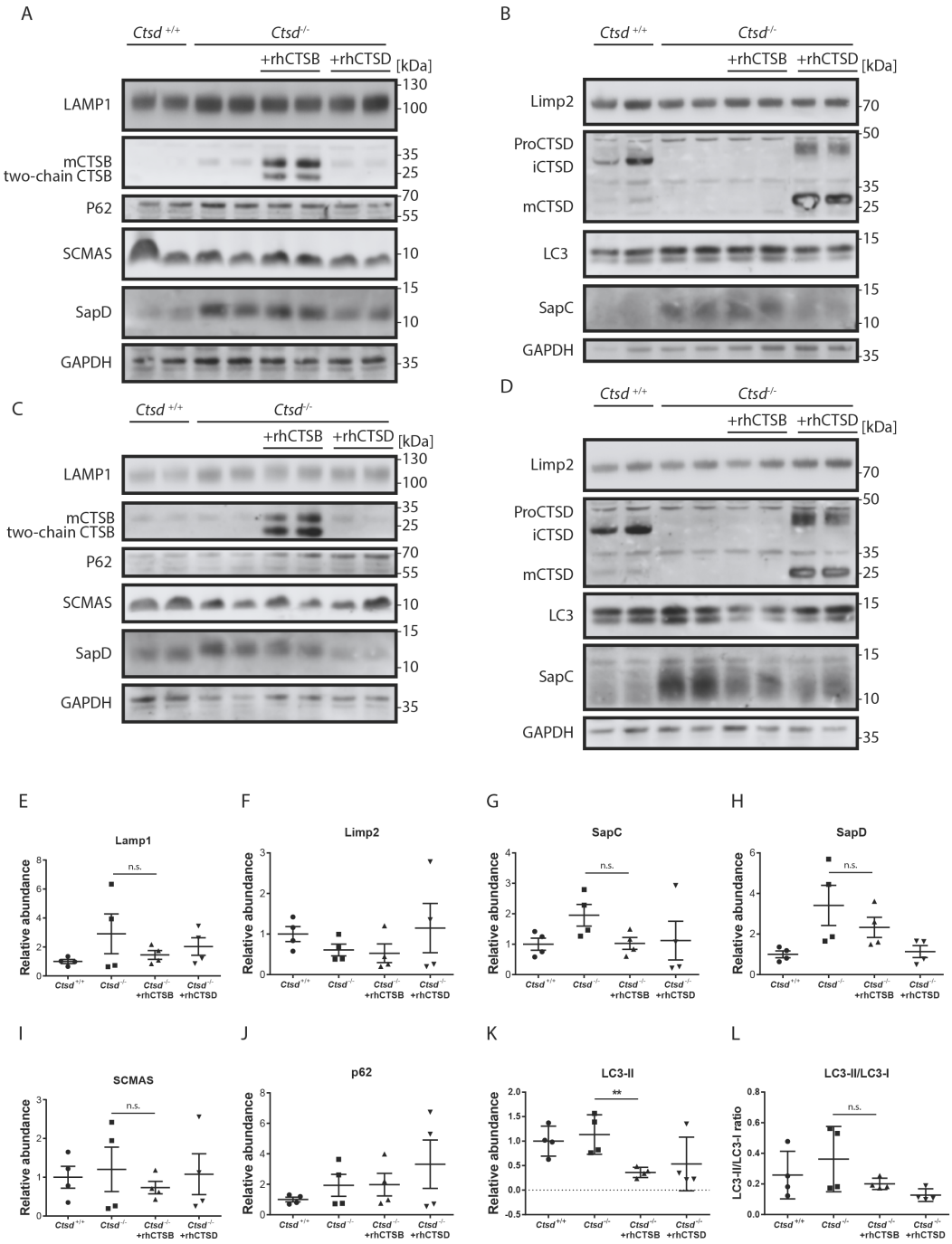

figure 14.A-D Immunoblot of generated astrocytes treated for one week with 40 µg rhCTSB or rhCTSD, respectively. **A** and **B** were loaded with the same samples, **C** and **D** likewise. Cells were treated with recombinant enzyme, lysed and 30 µg of lysate was loaded onto a NuPage gel for SDS-PAGE and subsequent immunoblotting. **E-F** Quantification of lysosomal markers Lamp1 and Limp2 was performed. **G-H** Furthermore, specific storage aggregates in NCL were quantified. **J-L** Influence of applicated enzyme on the autophagic flux was analysed by quantification of p62, LC3-II and LC3-II/LC3-I.

As a positive control the application of rhCTSD to the astrocyte cells was used (Di Spiezio et al., 2021). In this cellular model, application of rhCTSB in contrast to rhCTSD was not able to

reduce any of the analysed storage substrates like saposin C, saposin D or SCMAS to a statistically significant extent (**figure 14.G-I**).
Curiously, rhCTSB led to a significant reduction in LC3-II levels (**figure 14.K**), while p62 levels remained the same (**figure 14.J**) and LC3-II/LC3-I ratio decreased in comparison to untreated *Ctsd*$^{-/-}$ astrocytes (**figure 14.L**).
The lysosomal marker LAMP1 is increased in CTSD$^{-/-}$ astrocytes, though admittedly in this experiment with a strong variation. Lowest values were detected in the wild-type cells, stressing the desirability of low LAMP1 levels and their use as surrogate readout of lysosomal hypertrophy. The second lysosomal membrane protein Limp2 did not show any clear effect upon treatment. rhCTSB, though not statistically significant, reduced the levels of LAMP1 even further than rhCTSD did(**figure 14.A**).

In summary, in our astrocyte model rhCTSB did not exhibit an effect on storage substrate, but was shown to influence LC3-II levels indicating its influence on the autophagic machinery.

4.5.2 Immunofluorescence microscopy of treated *Ctsd*$^{-/-}$ astryocytes

Additionally, immunofluorescence staining of generated astrocytes was performed to further understand the distribution of storage aggregates within the cell. Astrocytes were stained for both lysosomal marker LAMP1 and pathological storage material SCMAS.

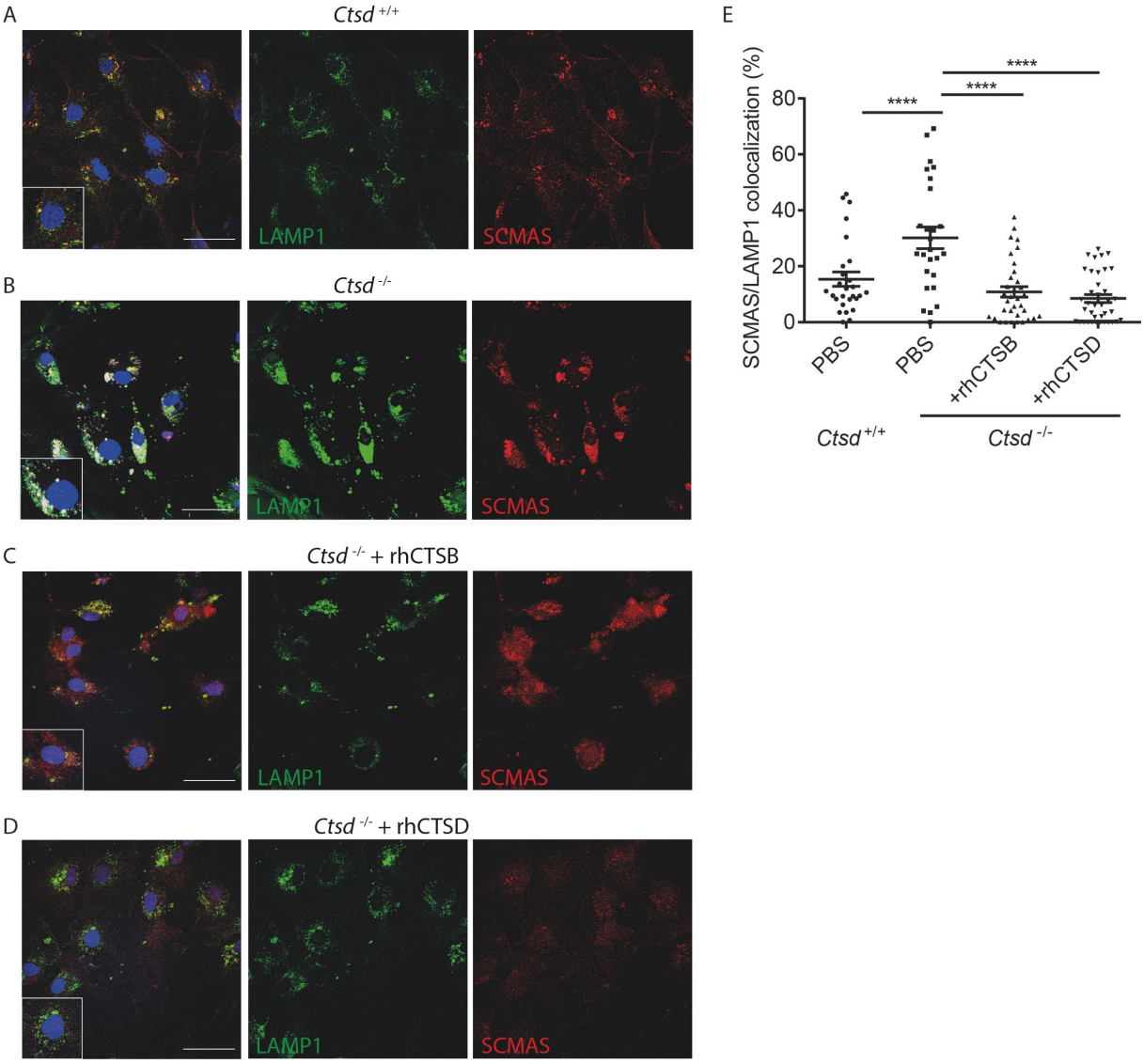

figure 15.A-D Immunofluorescence image of astrocytes generated from neuronal stem cells. Neurospheres were harvested from 14 old brain cortices of either CTSD$^{+/+}$ or CTSD$^{-/-}$ mice, stem cells isolated and further differentiated into astrocytes. Astrocytes were seeded and treated with PBS or 40 µg rhCTSB or rhCTSD, respectively, for one week before fixation and staining for immunofluorescence. Nuclei were stained with DAPI, furthermore primary antibodies directed against LAMP1 and SCMAS were used. The scale bar represents 50 µm. **E** Distribution of lysosomes marked with antibody against LAMP1 and cellular aggregate SCMAS was analysed via quantification of colocalization by a one-way ANOVA followed by Dunnett's multiple comparisons test. **** $P < 0.0001$

Ctsd$^{-/-}$ astrocytes showed a significant increase in colocalization of LAMP1 and SCMAS signal compared to CTSD$^{+/+}$ cells, indicating lysosomal accumulation (**figure 15.A-B, E**). Application of recombinant enzymes reduced lysosomal clustering and SCMAS/LAMP1 co-localization (**figure 15.C-D).** rhCTSB and the benchmark rhCTSD showed comparable effects in this experimental setup (**figure 15.E**).

4.6 *In vivo* uptake studies

4.6.1 Uptake of rhCTSB in wild-type mice

Before the therapeutic potential of rhCTSB could be tested, the uptake kinetics after intravenous or intraperitoneal injection were investigated.

In a first approach wild-type mice were injected with rhCTSB (25µg/g bodyweight) and blood samples from the facial vein were obtained immediately after the injection, after 30 minutes, two hours and six hours (figure 10 A). While in the immunoblot analysis the upper band represents the unchanged proform of CTSB, the second band seems to have already undergone partial processing, even though the molecular weight does not yet match the single chain form.

For the uptake assessment in various tissues wild-type mice were injected with 5µg rhCTSB per gram bodyweight and sacrificed at p23 or p24. SDS-PAGE with subsequent immunoblotting as well as activity assay analysis were performed in the case of brain, liver, kidney and spleen tissue.

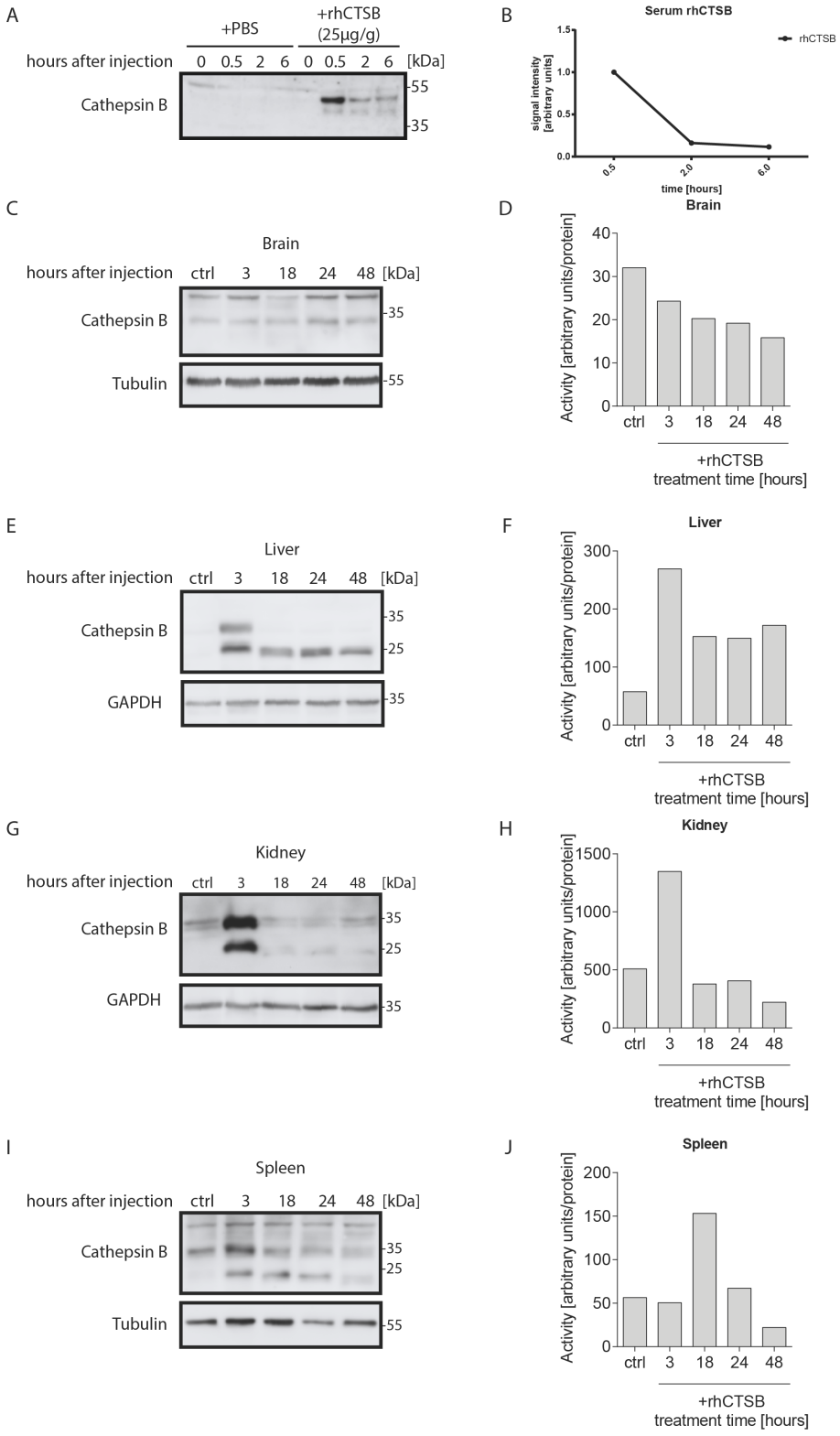

figure 16.A Serum analysis of injected wild-type mice with rhCTSB at 25 µg/g body weight. **B** Quantification of serum concentration of rhCTSB after different time intervals. **C-J** Samples of adult wild-type mice injected with 50 µg/g body weight. Each mouse was sacrificed at a specific time point and brain (**C**), liver (**E**), kidney (**G**) and spleen (**I**) tissues analysed on one hand using SDS-PAGE and subsequent immunoblotting. In parallel tissues were prepared for assessment of enzyme activity and cathepsin B activity assay (s. 3.2.3.9 Cathepsin B activity assay) was performed for brain (**D**), liver (**F**), kidney (**H**) and spleen (**J**).

In brain tissue the immunoblot intensity showed no increase of the cathepsin B signal, the activity assay displays no increase either (**figure 16.B-C**). This begs the question of whether rhCTSB is able to cross the blood brain barrier at all. The two bands detected in brain tissue represent the proform and the mature single chain form of endogenous catepsin B.
In liver tissue, an increase of the signal in western blot as well as increased activity could be detected (**figure 16.D-E**). The immunoblot analysis showed a maximum three hours after the injection with the mature single chain form still and a second band representing the two-chain form. Afterwards only one form could be detected, around 25 kDa, possibly even lighter than the form previously detected after three hours, indicating possible further cleavage and thus processing/degradation of the rhCTSB. A cell signalling technology antibody (Cathepsin B CST) could detect the endogenous enzyme better than the otherwise used R&D antibody.
In kidney tissue the immunoblot showed an increase of the mature form after three hours, in addition the presence of the two-chain form was detected, which also holds true for later timepoints (**figure 16.F-G**). However, the signal was very week and did not show any impact on the results of the activity assay, which only detected a strong increase after three hours in accordance with the immunoblot findings.
Lastly, the spleen tissue showed an increase of the mature form signal after three hours and the appearance of the two-chain form upon injection with rhCTSB, furthermore the activity showed an increase after 18 and 24 hours (**figure 16.H-I**).

4.6.2 Passage of rhCTSB through the blood brain barrier (BBB)

The absence of rhCTSB in brain tissue in immunoblot analysis as well as no detectable increase in the activity assay led to the use of CTSB deficient mice kindly provided by Thomas Reinheckel. Two CTSB $^{(-/-)}$ mice were injected intravenously with either PBS or rhCTSB. As a reference, two wild-type mice were used and equally injected with PBS. After 18 hours the mice were anesthetized, perfused to wash out remaining bloodstream based rhCTSB and organ tissues were collected. As it has proven the most sensitive method, a cathepsin B activity assay was performed on both liver and brain tissue to assess the capability of rhCTSB to cross the blood brain barrier.

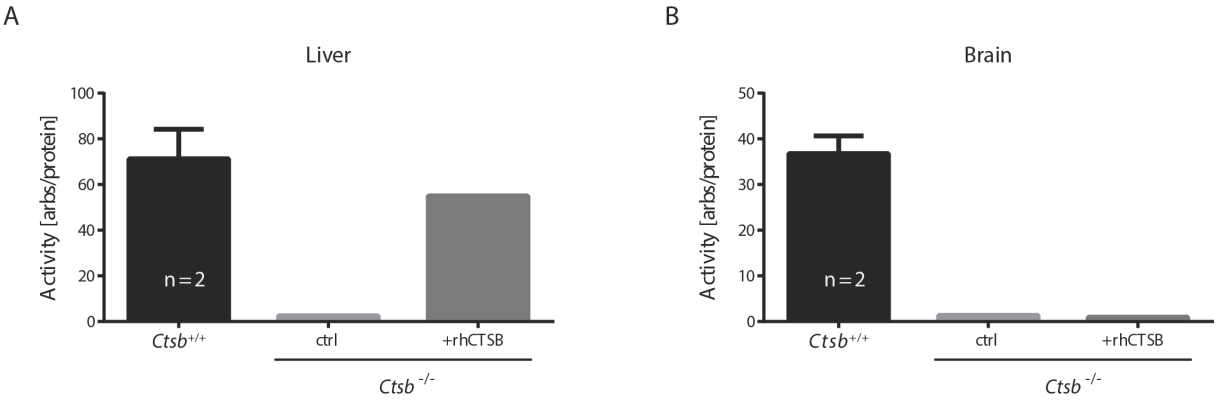

figure 17.A Two adult wild-type mice and two CTSB KO mice received an i.v. injection of PBS or rhCTSB at 50µg/g body weight, respectively. 18 hours post injection the mice were sacrificed, perfused and liver tissue samples were analysed using the Cathepsin B activity assay. **B** Two wild-type mice and two *Ctsb*$^{-/-}$ mice received an i.v. injection of PBS or rhCTSB at 50µg/g body weight, respectively. 18 hours post injection the mice were sacrificed, perfused and brain tissue samples were analysed using the Cathepsin B activity assay.

The i.v. injection of rhCTSB in a CTSB$^{-/-}$ mouse showed a strong effect in the liver, as the activity rose almost to wild-type levels (**figure 17.A**). In brain, however, there was no increase at all detected after the injection of the enzyme.

4.7 *In vivo* effect of peripheral rhCTSB application in CTSD$^{-/-}$ mice

The ultimate step of my work was to test the therapeutic potential of rhCTSB *in vivo* in the CLN10 mouse model as one of the most severe and rapidly progressing forms of NCL. To this end, one litter of mice consisting of two wild-type and five CTSD$^{-/-}$ mice were used for repetitive injections at different postnatal days.

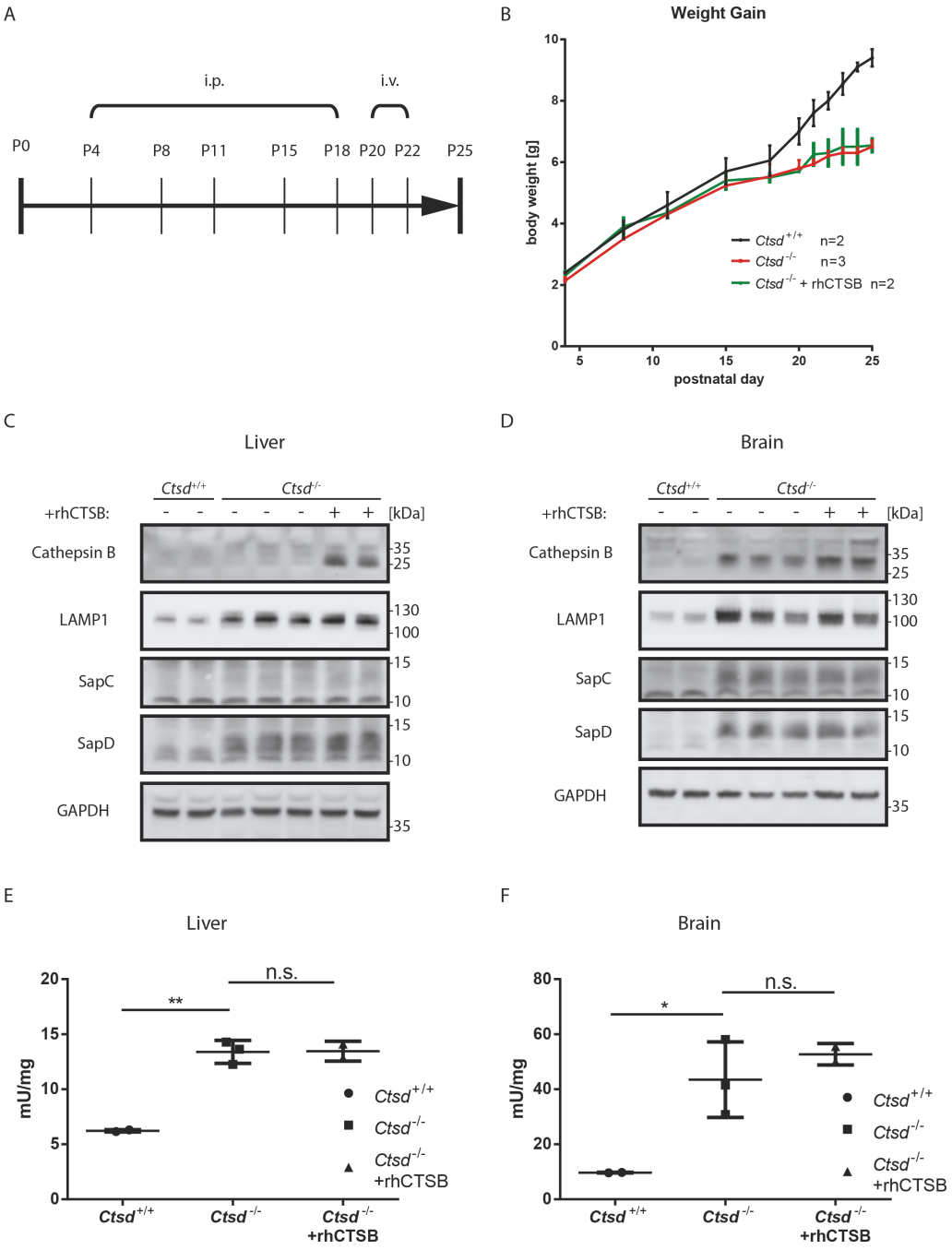

figure 18.A Schematic overview of repetitive dosing experiment in wild-type and KO mice. **B** Development of weight gain of rhCTSB injected mice in comparison to PBS injected wild-type and KO littermates from P4 until the sacrificing of the mice on P25. **C** Immunoblot analysis of liver tissue after mice were sacrificed on P25. Anti-Cathepsin B antibody was used to detect successful injection, LAMP1, SapC and SapD were used as markers for the progression of the disease. **D** Immunoblot analysis of brain tissue with focus on enzyme levels and disease markers **E** β-hexosaminidase assay performed with liver tissue. **F** β-hexosaminidase assay performed with brain tissue samples to detect lysosomal hypertrophy

The weight gain curve of wild-type mice clearly differed from both rhCTSB-treated CTSD$^{-/-}$ mice and control CTSD$^{-/-}$ mice after two weeks (**figure 18.B**). Multiple applications of rhCTSB showed no reduction of LAMP1, SapC or SapD in brain or liver tissue, respectively. (**figure 18.C-D**). The same held true for analysis of β-hexosaminidase, as a marker for lysosomal

hypertrophy and lysosomal storage in the tissues mentioned above (**figure 18.E-F**). All in all, no apparent effect of peripheral rhCTSB application on the presence of pathological of protein aggregates was observed.

4.8 *Ex vivo* assessment of the therapeutic effect in organotypic brain slices

In order to further understand the effect of rhCTSB on the brain of these mice, we devised an experiment using an *ex vivo* model. Organotypic brain slices were generated from 15 days old *Ctsd*$^{-/-}$ mice (s. 3.2.4.7 Generation of sagittal brain vibrosections). These were then treated with recombinant enzyme (rhCTSB, rhCTSD or rhCTSL, respectively) and the possible effect after such application was monitored after two weeks.

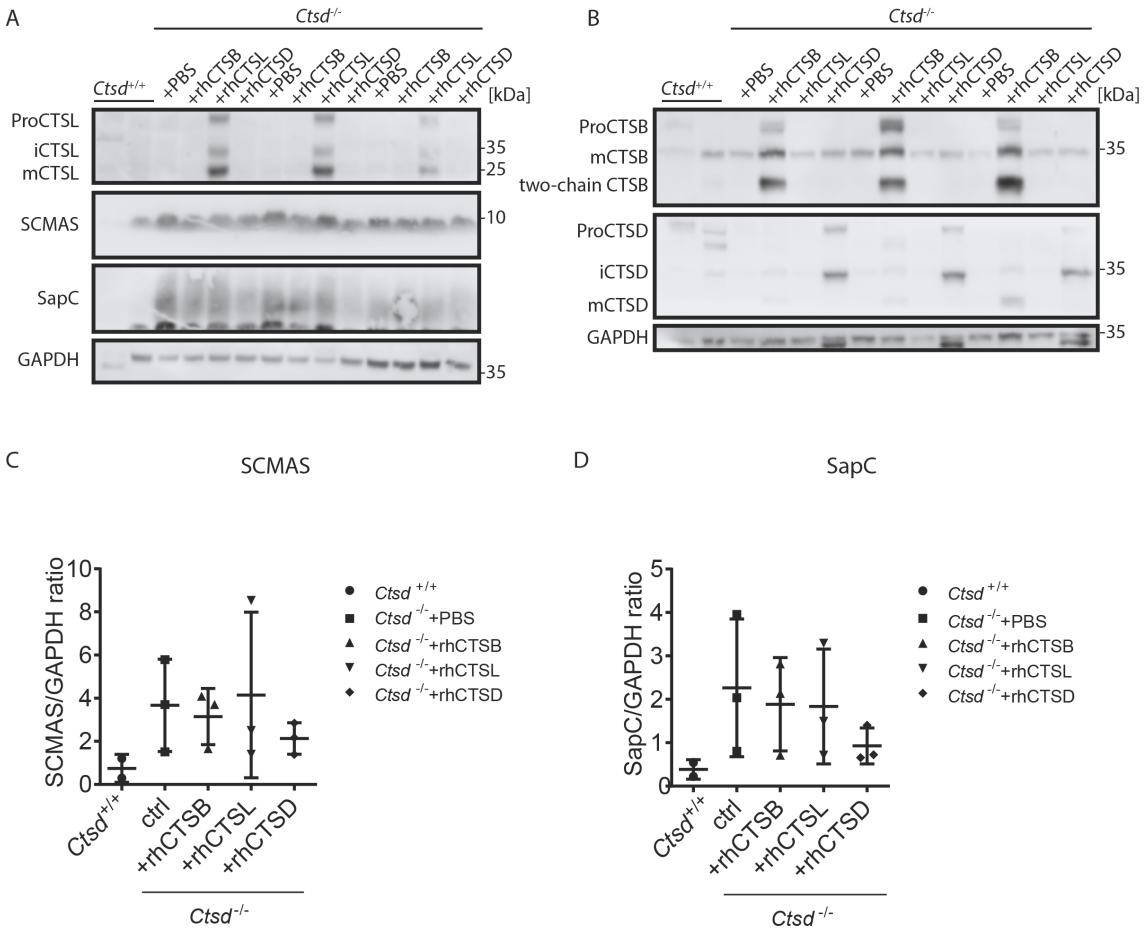

figure 19.A-B Organotypic brain slices were generated from 15 day old mice. Sagittal vibrosections were obtained and cultured for two weeks with the respective recombinant enzyme at a concentration of 40 µg/mL of medium. Cells were lysed, protein lysates separated via SDS-PAGE and analysed via immunoblotting. **C-D** Quantification of SCMAS and SapC signal intensity of immunoblot A.

Successful uptake and processing of the recombinant enzymes took place (**figure 19.A-B**). rhCTSD was used as positive control for the therapy of CTSD$^{-/-}$ brain slices. rhCTSL was used as a second representative of lysosomal cysteine proteases in order to detect differences between members of the same group of lysosomal enzymes. While quantification of SCMAS and SapC showed a substantial reduction of the signal intensity by rhCTSD, neither rhCTSB nor rhCTSL showed comparable effects. However, even if not significant, rhCTSB showed a reduction of SCMAS and SapC compared to PBS control mice.

4.9 In vivo effect of intracranial rhCTSB application in *Ctsd*$^{-/-}$ mice

4.9.1 Effect of intracranial rhCTSB injection on weight development in *Ctsd*$^{-/-}$ mice

As a last experiment the direct application of rhCTSB into the brain was devised in order to provide a treatment for the brain as location of major manifestation of NCL.
Furthermore, the impact of intracranial injection of rhCTSB on the weight gain of the CLN10 mice was assessed.

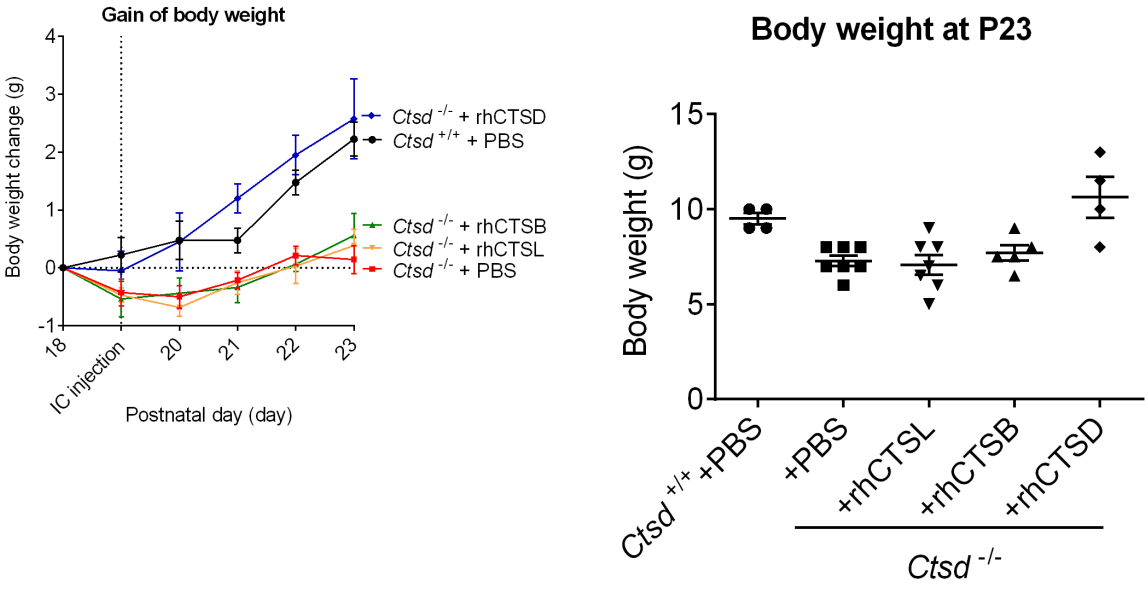

figure 20.A Development of weight gain of intracranially injected mice. As a positive control CTSD deficient mice were injected with rhCTSD. Additionally, rhCTSL, another representative of the lysosomal

cysteine-proteases, was used for comparison. All enzymes were injected at 100 µg in 10 µL at P1 and P19. **B** Weight comparison at final age of P23

Ctsd$^{-/-}$ mice and wild-type littermates were intracranially injected with the respective recombinant enzyme or PBS as control on postnatal day 1 and day 19 before being sacrificed on P23. As a first comparison, the weight gain was measured. Our previous *in vivo* experiment showed clear differences in the development of *Ctsd*$^{-/-}$ in comparison to wild-type mice (s. **figure 18**.**B)** as described in the literature **(Saftig et al., 1995)**.

While wild-type mice and rhCTSD injected mice showed a continuing weight gain after P18, injection with rhCTSB, rhCTSL and PBS stagnated around P18 levels up until P23 (**figure 20.A**). Hence, they reached a lower final weight than wild-type mice and rhCTSD injected CTSD$^{-/-}$ mice (**figure 20.B**).

4.9.2 Immunoblot analysis of intracranially injected *Ctsd*$^{-/-}$ mice

Further analysis of the mice, that were intracranially injected was undertaken in the case of rhCTSB and rhCTSD as positive control. Brain tissue of P23 mice was prepared, lysed, protein lysates separated via SDS-PAGE and analysed via immunoblotting.

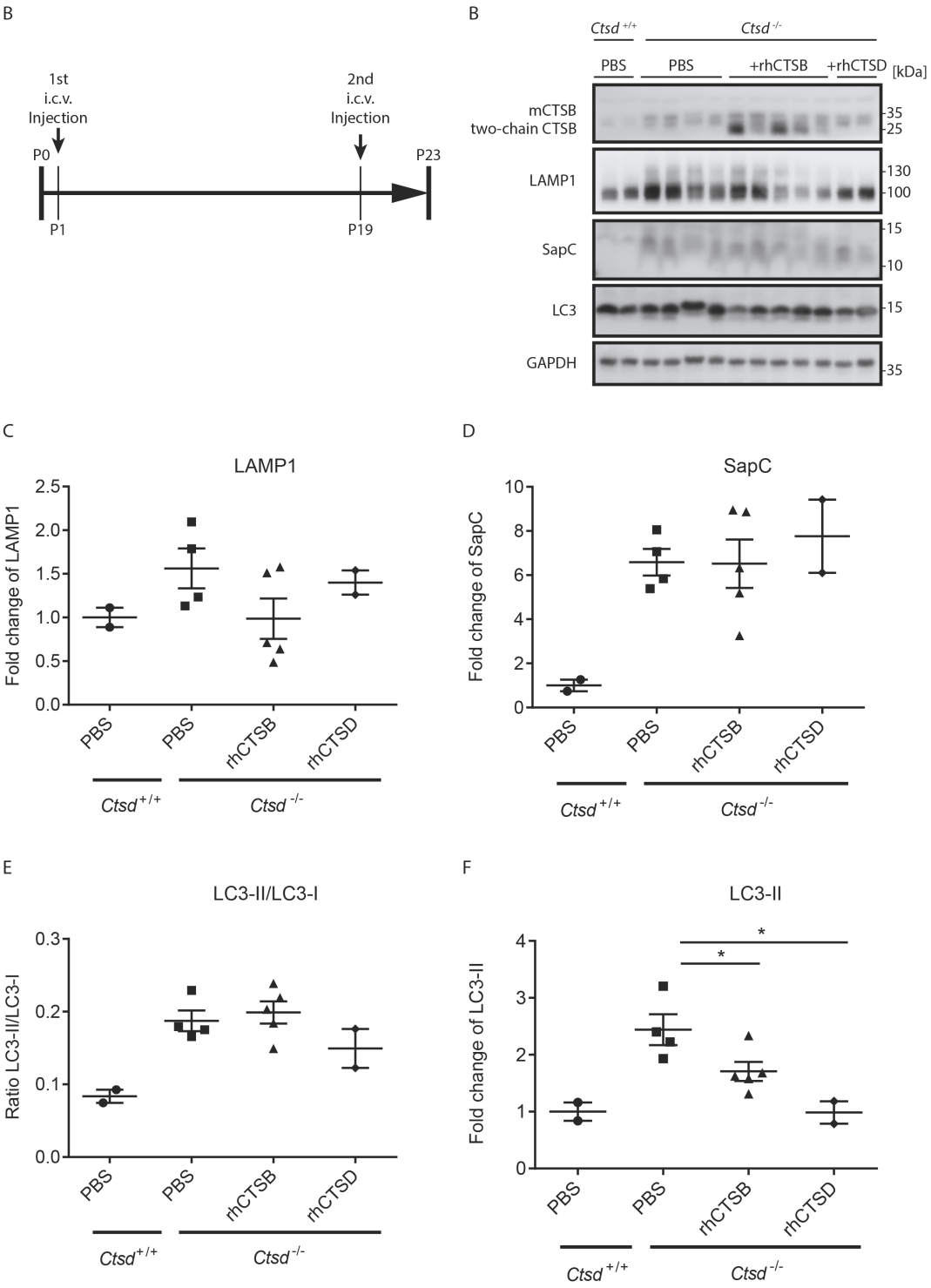

figure 21.A Immunoblot of the intracranially injected rhCTSD$^{-/-}$ and wild-type mice (**figure 15**). Injections with recombinant enzymes were performed on P1 and P19. Mice were sacrificed on day 23, brain tissue lysed, protein fractions separated via SDS-PAGE and analysed by immunoblotting. **B** Lysosomal marker Lamp1 was quantified to inspect the effect on the lysosomal biogenesis and lysosomal storage. **C** The specific storage aggregate SapC was quantified. **D-F** Quantification of markers of autophagic flux.

Successful uptake of rhCTSB after intracranial injection was demonstrated by an increased CTSB signal intensity of the immunoblot (**figure 21.A)**. Characteristic storage substrates such

as Saposin C were analysed as well as markers of autophagy (LC3) and lysosomal hypertrophy (LAMP1) (**figure 21.B**). Even though a reduction in LAMP1 levels was detected, it was not significant. However, LC3-II levels, as indicator for accumulation of autophagic vacuoles, were significantly reduced in the brain tissue of mice treated with both rhCTSB and rhCTSD.

5 DISCUSSION

5.1 Characterization of rhCTSB

5.1.1 Production of rhCTSB

Successful production of rhCTSB was achieved utilizing HEK-293-EBNA cells as a suitable expression system. This episomal system was used in our previous ERT approach with rhCTSD and proved superior to both CHO and HEK-293 systems (Marques et al., 2019). Globally, CHO cells are most commonly used for therapeutic protein production (Walsh, 2014). However, they bear the risk, of non-human post-translational modifications and thus a higher immunogenic threat (Ghaderi et al., 2010). Continuous antibiotic selection pressure ensured the stable transfection of the mammalian cells with the vector plasmid Pcep-Pu (Kohfeldt et al., 1997). Increased protein yield could be obtained by single clone selection (3.2.2.6). After successful secretion of the enzyme into the medium, isolation and purification of rhCTSB were performed. Multiple filtration steps separated floating cells from the culture medium, before isolating the rhCTSB by affinity and size exclusion chromatography. The His_6-tag used for purification in affinity chromatography is even though it was established decades ago (Hochuli et al., 1988) still one of the most widely used tags for protein purification (Arnau et al., 2006). Even though the protein function is generally not affected by the tag, a few cases of alterations due to protein-tagging are known (Wu and Filutowicz, 1999, Turkewitz et al., 2021). In the case of this project, the his-tag is cleaved off during processing and not present in the activated enzyme forms anymore.

It should be noted that the removal of any protein tag prior to administration is required for pharmaceutical application and thus further adjustments of the production procedure would be necessary (Abdullah and Chase, 2005).

Mass spectrometry confirmed human pro-cathepsin B as the purified protein. The molecular weight and sequence coverage both fit the protein. Endoglycosidase H and PNGase F digestion revealed a glycosylation of the enzyme (**figure 7**.**D-E**). Furthermore, a glycosylation in position 31 of the purified protein was only observed in a fraction of rhCTSB, thus different

glycosylation patterns exist in rhCTSB. As stated in the literature, different carbohydrate moieties of rhCTSB do not affect the activity or stability of the enzyme (Mach et al., 1992).

5.1.2 pH dependency and bifunctionality of rhCTSB

Activation of purified rhCTSB could be achieved *in vitro* by acidification (**figure 7**) as described previously. The process is most likely performed in a bimolecular between different pro-cathepsin B molecules rather than an intramolecular process (Rozman et al., 1999). Highest levels of self-activation were measured at a pH of 4.5 (**figure 7.B**) and thus under lysosome-like conditions (Pungercar et al., 2009).

It should be noted that CTSB possesses both endo- and exopeptidase activity with different optimal pH environments. The substrate Z-Arg-Arg-AMC used for the activity assays is cleaved by the endopeptidase function of CTSB (Yoon et al., 2021). The exopeptidase activity shows a pH optimum at acidic pH (pH 4-6), while the endopeptidase activity increases with pH (Almeida et al., 2001). Hence, limitations of the monitoring of enzymatic activity exist.

Cleavage specificity can be described by numbering the substrate's amino acid residue relative to the scissile peptide bond (Px') (Schechter and Berger, 1967).

The endopeptidase activity of CTSB is strongly dependent on the glycine motif in P3', shows specificity in P2' for aromatic and aliphatic residues and for glycine and phenylalanine in P1' (Biniossek et al., 2011).

In comparison to the cysteine protease CTSL and aspartyl protease CTSD, CTSB shows much weaker endopeptidase activity, presumably due to the occluding loop (Nägler et al., 1997). This feature favours the dipeptidyl carboxypeptidase activity of rhCTSB at an acidic pH.

The overall stability of rhCTSB was addressed by observing potential reduction of the pro-form under different storage conditions. At 4°C, no protein reduction over time could be detected, however, immunoblotting showed a faint band of slightly lower molecular weight beneath the original rhCTSB band. Possible partial self-activation in the process of preparing the samples for immunoblotting or unspecific binding could be taken into consideration for this observation.

5.1.3 Cellular Uptake of rhCTSB

The uptake of rhCTSB was assessed in $CTSB^{-/-}$ HEK and MEF cells. In both systems the uptake kinetics were time- and dose-dependent (**supplemental figure 4**, **supplemental figure 5**). Both human and murine cell lines require comparable time intervals in order to proceed to the mature single-chain form and the two-chain form of rhCTSB.

Curiously, the presence of double bands was observed in the western blot. This, however, could be explained by the described differing glycosylation pattern among the purified rhCTSB fractions. Similar double band effects were detected in $CTSB^{+/+}$ cells.

Even though the uptake and processing to mature forms was detected via immunoblotting, there are several limitations. First of all, the method does not allow to draw conclusions regarding the actual activity of rhCTSB. Secondly, the final two-chain form contains two domains bound by a disulfide bridge. However, while immunoblotting only detects the heavy chain of the two-chain form, the actual catalytical center resides within the smaller fragment, which is not detected. Even though the activity assay makes up for these shortcomings of immunoblotting, it only measures the endopeptidase activity, not representing the entire cleavage spectrum of rhCTSB.

Transport of rhCTSB to the lysosome could be observed via confocal microscopy. Colocalization of staining for lysosomal membrane protein LAMP1 and CTSB in MEF cells showed successful transport of the enzyme to its destination, the lysosome.

The intracellular half-life of rhCTSB was determined in MEF cells. After a pulse period in which the cells were left in rhCTSB rich medium, cells were incubated in rhCTSB free medium for different time periods. The half-life of the different forms varied greatly in our experimental setup (**figure 11**). However, one limitation is that reduction of band intensity by processing to different forms and by decay cannot be distinguished in this experimental setup, allowing only limited conclusions about the half-life of mCTSB and two-chain CTSB.

Furthermore, it should be taken into consideration, that immunoblotting with the polyclonal anti-CTSB antibody we used does not necessarily detect all forms of rhCTSB equally well and thus signal intensity does not allow comparisons of quantity among the different CTSB forms.

Uptake of rhCTSB is known to be M6P-R-dependent as holds true for most lysosomal hydrolases. However, other mechanisms of routing the endogenous enzyme to the lysosome have been described. rhCTSB depended on the uptake via M6P-R as well as Lrp1. (Markmann et al., 2015). Even though, we lack specific analysis of the glycosylation pattern of rhCTSB, the dependency of the uptake on M6P-R was shown (figure 12), indicating that at least in part the glycosylation contains M6P-moieties.

CTSB is known to undergo processing by other proteases. Use of inhibitors helped to identify important players in the processing of rhCTSB. As inhibition of CTSD by pepstatin did not prevent processing of the proform to the mature form, other proteases seem to carry out this step, including CTSB itself. The second cleavage step, however, was successfully inhibited by

Leupeptin, an inhibitor of cysteine proteases. Hence, cysteine proteases, including CTSB itself, are crucial for the processing of rhCTSB (Pungercar et al., 2009).
The lack of a positive control for the inhibitory effect of pepstatin makes it difficult to draw conclusions about the importance of CTSD in the processing of rhCTSB with absolute certainty.
In general, the question of a possible hierarchy of the cathepsins arises, as we could prove the dependence among the cathepsins in the processing of each other and the influence on the catalytic capacity.

5.1.4 Uptake of rhCTSB in murine tissue and the capability to cross the BBB

Uptake and processing of rhCTSB after intravenous injection in $CTSB^{+/+}$ mice was detectable in various tissues, especially in liver, kidney and spleen. Liver was the only one to show elevated levels even after 48 hours.
However, no increase in the immunoblot CTSB signal was detected in brain tissue. In $CTSB^{-/-}$ mice no increase in the Cathepsin B activity assay in brain tissue after i.v. injection was measured, in contrast to liver tissue, indicating that the rhCTSB is not able to cross the BBB upon peripheral i.v. injection.
It is possible to reach the CNS in LSDs in cases of a disrupted BBB (Lachmann, 2011). This effect was described for CLN10 (Okada et al., 2015). In our experiments peripheral i.v. or i.p. treatment did not lead to passage of rhCTSB through the BBB (figure 16B-C).
As forms of LSDs with minor residual enzyme activity, but mild phenotypes exist (Desnick and Schuchman, 2012), it can be postulated, that only a fraction of endogenous enzyme can be sufficient for treating the disease, given that the enzyme manages to reach the critical tissue.
In fact, most ERTs do not lead to endogenous enzyme levels (Damme et al., 2015).
It is known that upon i.v. administration most enzyme is taken up by the visceral tissues, such as liver and spleen (Concolino et al., 2018).
Regarding the uptake experiments with rhCTSB, it should be noted that neither western blotting nor the activity assay allowed for an absolute quantification of the tissue-specific enzyme uptake.
Murine endogenous CTSB and rhCTSB might show differences in antibody binding, even though the amino acid residue sequence of both forms shows only minor differences (Caglic et al., 2009). Since the successful uptake and processing in various tissues could be demonstrated, high enzyme levels were detected in peripheral tissues, e.g. liver and even sub-endogenous

enzyme levels have proven effective in the treatment of LSDs, we proceeded to experiments addressing the therapeutic potential in our preclinical CLN10 model.

5.2 rhCTSB as a therapeutic approach in CLN10

As ERT is a well-established and widely used therapy in LSDs in general, our aim was to analyse if rhCTSB application poses a comparable or subsidiary therapeutic approach in comparison to rhCTSD the benchmark for CLN10.
We tried to address all of the three biochemical hallmarks of CLN10, the impairment of the autophagic flux, the lysosomal hypertrophy and the accumulation of storage proteins.

5.2.1 *In cellula* treatment of astrocytes

The rapid progression of CLN10 makes in the study of the disease progression difficult. Lack of established cell-based models led us to creating our own model.
In our attempt to understand the role of CTSB in the pathology of CLN10, generated astrocytes deficient for CTSD were studied. Treatment of these cells with rhCTSD was used as a positive control, as its effectiveness in the treatment of CLN10 has already been proven (Marques et al., 2019).
Under rhCTSB treatment there was no significant reduction of storage material, however, a reduction of the lysosomal marker LAMP1, was observed. This finding was not statistically significant, as there was a strong biological variability.
Curiously, rhCTSB led to a significant reduction in LC3-II levels, while p62 levels remained the same and LC3-II/LC3-I ratio decreased in comparison to untreated $CTSD^{-/-}$ astrocytes. rhCTSB was not able to correct any of the three markers analysed for storage aggregates saposin C, saposin D or SCMAS to a statistically significant extent. However, it should be noted, that neither did rhCTSD in this specific setting, even though this effect was observed in other experimental setups (Di Spiezio et al., 2021, Marques et al., 2019).
Staining of neural stem cell-derived astrocytes exhibited evidence for a reduction of lysosomal clustering and LAMP1-SCMAS co-localization, even to a highly significant extent for both rhCTSB and the benchmark rhCTSD.
In summary, there is evidence for both a substrate reduction through the application of rhCTSB and a reduction of autophagic activity and possibly an amelioration of the autophagic flux. Perturbance of glial function has been shown for other forms of NCL (Parviainen et al., 2017, Shyng and Sands, 2014)

However, the role of glial cells in the pathomechanism of NCL is still unclear, therefore these effects might not play out in the neurons, themselves. Furthermore, this *in cellula* experiment might not reflect the *in vivo* disease progression adequately.

5.2.2 Intravenous and intraperitoneal treatment of CLN10 mice

Peripheral dosing with rhCTSB either intraperitoneally or intravenously did not lead to a change in the weight development in $CTSD^{-/-}$ mice compared to the PBS control group. No change in biochemical storage aggegrates saposin C and saposin D was measured at P25. The β-hexosaminidase assay, which had proven a reliable and sensitive marker of lysosomal hypertrophy/storage in previous experiments (Marques et al., 2019), did not show any amelioration in liver or brain tissue.

Curiously, while the endogenous levels of CTSB were not increased in the liver tissue of CLN10 mice, immunoblot analysis showed an increase of the CTSB signal compared to wild-type mice. This begs the question, if a tissue specific compensation of the missing aspartyl protease CTSD already takes place within affected mice, or if the increase in CTSB signal can rather be seen as expression of the ongoing lysosomal dysfunction and hypertrophy at play. Signs of such a hypertrophy can be detected in both brain and liver tissue as LAMP1 signal intensity is increased compared to wild-type mice. The fact, that the CTSB increase is only present in brain, hints toward the hypothesis of a compensation.

Mice deficient for CTSD die within the first 26±1 days of their lives. Analysing the tissues on P25 might be too late, meaning the rapid disease progression could end up disguising minor ameliorating effects of the applicated enzyme. Furthermore, dosing interval and the dose itself might need further optimization. As explained above, a peripheral application is not able to cross the BBB. All these points pose limitations to the conclusions that can be drawn from our experimental setup.

5.2.3 Treatment of organotypic brain slices

Treatment of organotypic brain slices helped eliminating interindividual differences of the mice treated and allowed observation of direct treatment effects without worrying about the mentioned concerns regarding rhCTSB distribution. Although not significant, a reduction of saposin C and SCMAS levels was observed after a two-week treatment with both rhCTSB and rhCTSD. rhCTSL, a different member of the cysteine cathepsins, led to a reduction in saposin C, but not SCMAS. The observed effects, however, were only minor.

However, the need of a direct treatment of brain tissue, to study these potential effects *in vivo* arose. The benefit of these organotypic brain slices is the absence of intra- and inter-litter differences, present in $CTSD^{-/-}$ mice.

5.2.4 Intracranial injection of CLN10 mice

Intracranial injection of rhCTSB did not change the weight development of the $CTSD^{-/-}$ mice. rhCTSD dosing, however, corrected the weight development (**figure 20**). This begs the question if the main reason for the slow weight gain is indeed the intestinal necrosis, described in the literature (Saftig et al., 1995) or rather the apathy, leading to less nutrient intake. In the former case, the transport of the enzyme over the blood brain barrier to the periphery would be necessary, or the transport within the nervous system to the enteric nervous system. Further investigation on the actual place of effect, is needed.

Via immunoblot, as held true for the astrocytes *in vitro*, a reduction of LC3-II levels, without changing LC3-II/LC3-I ratio, was achieved, again stressing the normalization of autophagic flux. LAMP1 levels were also reduced, displaying the normalization of lysosomal hypertrophy. After two injections however no effect on storage material was observed. The low number of mice used in this experiment might not be sufficient to detect a statistically significant treatment effect.

Of course, the experimental setup has other limitations. The most important point, the prolongation of the life-span was not addressed. The disease progresses rapidly, which makes it difficult to detect minor effects. Even treatment with rhCTSD intracranially survival was only extended by approximately one week (Marques et al., 2019).

As single and double injection did not seem to play a decisive role in that study, it can be postulated that a “hit hard and early” approach is most beneficial. In comparison with survival up to P62/63 after viral central re-expression of CTSD (Shevtsova et al., 2010), the result of intracranial injection still falls behind. In terms of enzyme dose and application there might still be room for improvement. This, of course, holds equally true for application of rhCTSB.

5.2.5 Protein aggregate clearance in CLN10

In summary, the clearance of protein aggregates through application of rhCTSB was only detected to a minor and non-significant degree. This was consistent in the different models, ranging from neural stem cell-derived astrocytes, murine sagittal brain slices and intracranially injected mice.

In comparison, the cysteine protease CTSL was able to reduce the storage burden to a greater extent in our experiments (Di Spiezio et al., 2021). As discussed earlier, both proteases have a broad substrate specificity, CTSL shows stronger catalytic activity as an endopeptidase, while CTSB acts primarily as an exopeptidase under lysosomal conditions. When it comes to the bulk degradation of storage material, the endopeptidase activity seems to play a more important role.

5.2.6 Reduction of lysosomal hypertrophy and accumulation

Lysosomal hypertrophy was observed in CLN10 mice (Marques et al., 2019). We detected a reduction of LAMP1 levels upon treatment with rhCTSB in neural stem cell-derived astrocytes and upon in brain tissue of CLN10 mice intracranially injected. Both results were statistically not significant.

Moreover, in generated astrocytes, the lysosomal localization of SCMAS localization was statistically significantly reduced upon treatment with rhCTSB.

These findings indicate that rhCTSB might be able to normalize the degradative machinery within the cell.

5.2.7 Normalization of autophagy

Lastly, rhCTSB had several effects on the autophagic machinery. We detected a decrease of LC3-II levels in generated astrocytes and in brain tissue upon intracranial injection. CTSB is known to influence the autophagic flux via cleavage of the calcium channel TRPML1, hereby preventing the release of calcineurin and subsequently inhibiting TFEB signalling, which in turn would otherwise orchestrate the expression of autophagy related genes (Qi et al., 2016).

All in all, of the three aims of this enzyme replacement therapy, two could be achieved:

- Normalization of the autophagic flux in the affected cells
- Reduction of lysosomal hypertrophy, which reflects the perturbance of the degradative cellular machinery

The last one, the reduction of the specific storage material, could not be successfully addressed in this therapeutic approach.

5.3 Conclusion

We were able to produce and purify recombinant human proCTSB and demonstrated that rhCTSB was successfully taken up by multiple cell lines and by mouse tissue *in vivo*, most

likely by M6P-R. and Lrp1/LDL-R. mediated trafficking. Proper activation and stability were verified *in vitro*. Via activity assay, immunoblotting and immunofluorescence microscopy successful uptake, activation and trafficking to the lysosome upon uptake were demonstrated. Uptake *in vivo* was demonstrated in wild-type mice as well as *Ctsd*$^{-/-}$ mice, proving uptake and activation in various tissues.

We tested the effects of rhCTSB in CLN10 *in cellula* with *Ctsd*$^{-/-}$ astrocytes, *ex vivo* with *Ctsd*$^{-/-}$ brain slices and *in vivo* with *Ctsd*$^{-/-}$ mice. All the data collected pointed out that in the CLN10 background rhCTSB was not able to compensate for the missing aspartyl protease CTSD in digesting the protein aggregates, such as SapC, SapD and SCMAS.

All in all, reduction of lysosomal hypertrophy and normalization of the autophagic flux were achieved, however, a significant reduction of storage material was not observed.

5.4 Further therapeutic implications

Both CTSB and CTSL show the capacity to address certain pathological hallmarks of CLN10 in our preclinical model (Di Spiezio et al., 2021). Mice double deficient for both of these cysteine proteases can be viewed as a phenocopy of the CTSD$^{-/-}$ CLN10 mice (Koike et al., 2005).

Further improvement of our established treatment of CLN10 might be possible by taking this knowledge into account and combining these lysosomal proteases, harnessing their cross-activation capabilities and hereby, setting free further degradative potential. CTSD could enhance the CTSB activity further via degradation of its inhibitors (Lenarčič et al., 1991) and vice versa CTSB plays a major role in the activation of CTSD (Laurent-Matha et al., 2006), thus a combination could harness this synergetic potential. Additionally we could already prove that CTSB and CTSL affect different aspects of the pathology, as CTSL showed superiority with regard to the reduction of storage burden, while CTSB was able to correct lysosomal hypertrophy and autophagic pathways (Di Spiezio et al., 2021).

This combinatory approach has yet to be addressed in further experiments.

5.5 Outlook

To this point, much concerning the pathomechanisms and progression of the various forms of NCL is still unknown. However, recent findings supply evidence of common pathological

hallmarks and, more importantly, common therapeutic targets. For example, cross-correction of CLN6 via CLN5 overexpression was observed (Best et al., 2021).

As described above, rhCTSB was able to partially rescue the biochemical hallmarks in CLN10 mice. However, no correction of phenotype, or delay in the progression of the disease could be achieved.

It should be noted, that there is still a lot of optimization potential in the ERT with rhCTSB. The dosing intervals and enzyme doses themselves were chosen in accordance with our previous experiments conducted with rhCTSD ERT in CLN10. Most likely an improvement of the overall outcome by adjusting the parameters mentioned above can be achieved.

Secondly, further improvement of the treatment through combining multiple lysosomal proteases, harnessing their cross-activation capabilities and hereby, setting free further degradative potential could be possible.

As there is similar storage composition and perturbance of the same cellular pathways among NCL forms, therapeutic strategies could also be applied to more than one form. As mentioned above, cross-correction has been described in NCL (Best et al., 2021). Our ERT should also be tested in other forms of NCL, as well.

In the end, clinical studies will be needed, in order to confirm the efficacy of such a combined therapeutic approach. We built a foundation for this with our collaboration with Orfo Neuro APS in Denmark. This cooperation has already led to the successful development of an ERT against alpha-mannosidosis with EMA approval in 2018.

However, in terms of NCL and more specifically CLN10, a combination of several therapeutic approaches might be necessary in order to address all hallmarks of this devastating and rapidly progressing disease. Our ERT approach might very well someday be one of the pillars of the treatment.

And lastly, rhCTSB is implicated to play a major role in various neurodegenerative diseases beyond NCL such as AD (Embury et al., 2017), PD (McGlinchey and Lee, 2015) and HD (Liang et al., 2011) and poses a promising target in respective therapies.

These points, however, will have to be addressed in the future.

6 SUMMARY

Neuronal ceroid lipofuscinoses are a group of lysosomal storage disorders (CLN1-CLN14), collectively constituting the most common cause of childhood neurodegeneration. Impairment of autophagy with accumulation of storage substrates is considered a disease hallmark.

The aim of this project was to assess if the lysosomal protease cathepsin B can be applied in a therapy for CLN10, the congenital form of neuronal ceroid lipofuscinosis, as its role in lysosomal degradation and multiple neurodegenerative diseases has been described numerously. CLN10 is caused by deficiency of the lysosomal aspartyl protease cathepsin D, in previous experiments we could demonstrate a treatment effect of recombinant human pro-cathepsin D (rhCTSD).

We sought to develop a production and purification pipeline of recombinant human pro-cathepsin B (rhCTSB) and analyse, if via degradation of storage substrate and normalization of the autophagic flux, rhCTSB was able to ameliorate the disease progression and reduce storage burden like rhCTSD.

Successful production and purification of rhCTSB were achieved and verified by mass spectrometry analysis. In order to assess the recombinant enzyme's feasibility for a therapeutic approach in CLN10, a set of preliminary experiments for further characterization were performed.

We were able to demonstrate the uptake by multiple cell lines and by murine tissue *in vivo*, most likely by M6P-R. and Lrp1/LDL-R. mediated trafficking. Proper activation and stability were verified *in vitro*. Via activity assay, immunoblotting and immunofluorescence microscopy successful uptake, activation and trafficking to the lysosome upon uptake were demonstrated.

Uptake *in vivo* was analysed in wild-type mice as well as *Ctsd*$^{-/-}$ mice. We observed uptake and activation in various tissues.

We tested the therapeutic effect of rhCTSB in CLN10 *in cellula* with *Ctsd*$^{-/-}$ astrocytes, *ex vivo* with *Ctsd*$^{-/-}$ brain slices and *in vivo* with *Ctsd*$^{-/-}$ mice.

In these models our findings indicated a reduction of lysosomal hypertrophy and accumulation and showed a reduction of LC3-II levels.

All the data collected pointed out that in the CLN10 background rhCTSB was not able to compensate for the missing aspartyl protease CTSD in digesting the protein aggregates, such as SapC, SapD and SCMAS.

All in all, reduction of lysosomal hypertrophy and normalization of the autophagic flux were achieved, however, a significant reduction of storage material was not observed.

Further research is needed to reach a deeper understanding of the underlying pathomechanisms and fully elucidate the interplay of the different cathepsins to pave the way for optimized treatment approaches.

8 REFERENCES

ABDULLAH, N. & CHASE, H. A. 2005. Removal of poly-histidine fusion tags from recombinant proteins purified by expanded bed adsorption. *Biotechnol Bioeng,* 92**,** 501-13.

ABU-REMAILEH, M., WYANT, G. A., KIM, C., LAQTOM, N. N., ABBASI, M., CHAN, S. H., FREINKMAN, E. & SABATINI, D. M. 2017. Lysosomal metabolomics reveals V-ATPase- and mTOR-dependent regulation of amino acid efflux from lysosomes. *Science,* 358**,** 807-813.

AGHDASSI, A. A., JOHN, D. S., SENDLER, M., WEISS, F. U., REINHECKEL, T., MAYERLE, J. & LERCH, M. M. 2018. Cathepsin D regulates cathepsin B activation and disease severity predominantly in inflammatory cells during experimental pancreatitis. *J Biol Chem,* 293**,** 1018-1029.

AITS, S. & JAATTELA, M. 2013. Lysosomal cell death at a glance. *J Cell Sci,* 126**,** 1905-12.

ALMEIDA, P. C., NANTES, I. L., CHAGAS, J. R., RIZZI, C. C., FALJONI-ALARIO, A., CARMONA, E., JULIANO, L., NADER, H. B. & TERSARIOL, I. L. 2001. Cathepsin B activity regulation. Heparin-like glycosaminogylcans protect human cathepsin B from alkaline pH-induced inactivation. *J Biol Chem,* 276**,** 944-51.

ANDERSON, G. W., GOEBEL, H. H. & SIMONATI, A. 2013. Human pathology in NCL. *Biochimica et Biophysica Acta (BBA) - Molecular Basis of Disease,* 1832**,** 1807-1826.

APPELQVIST, H., WASTER, P., KAGEDAL, K. & OLLINGER, K. 2013. The lysosome: from waste bag to potential therapeutic target. *J Mol Cell Biol,* 5**,** 214-26.

ARMSTRONG, R. A., LANTOS, P. L. & CAIRNS, N. J. 2005. Overlap between neurodegenerative disorders. *Neuropathology,* 25**,** 111-24.

ARNAU, J., LAURITZEN, C., PETERSEN, G. E. & PEDERSEN, J. 2006. Current strategies for the use of affinity tags and tag removal for the purification of recombinant proteins. *Protein Expression and Purification,* 48**,** 1-13.

BAROHN, R. J., DOWD, D. C. & KAGAN-HALLET, K. S. 1992. Congenital ceroid-lipofuscinosis. *Pediatric Neurology,* 8**,** 54-59.

BARRETT, A. J. & KIRSCHKE, H. 1981. Cathepsin B, Cathepsin H, and cathepsin L. *Methods Enzymol,* 80 Pt C**,** 535-61.

BEGLEY, D. J., PONTIKIS, C. C. & SCARPA, M. 2008. Lysosomal storage diseases and the blood-brain barrier. *Curr Pharm Des,* 14**,** 1566-80.

BEST, H. L., CLARE, A. J., MCDONALD, K. O., WICKY, H. E. & HUGHES, S. M. 2021. An altered secretome is an early marker of the pathogenesis of CLN6 Batten disease. *J Neurochem,* 157**,** 764-780.

BIFFI, A., MONTINI, E., LORIOLI, L., CESANI, M., FUMAGALLI, F., PLATI, T., BALDOLI, C., MARTINO, S., CALABRIA, A., CANALE, S., BENEDICENTI, F., VALLANTI, G., BIASCO, L., LEO, S., KABBARA, N., ZANETTI, G., RIZZO, W. B., MEHTA, N. A. L., CICALESE, M. P., CASIRAGHI, M., BOELENS, J. J., DEL CARRO, U., DOW, D. J., SCHMIDT, M., ASSANELLI, A., NEDUVA, V., DI SERIO, C., STUPKA, E., GARDNER, J., VON KALLE, C., BORDIGNON, C., CICERI, F., ROVELLI, A., RONCAROLO, M. G., AIUTI, A., SESSA, M. & NALDINI, L. 2013. Lentiviral Hematopoietic Stem Cell Gene Therapy Benefits Metachromatic Leukodystrophy. *Science,* 341**,** 1233158.

BINIOSSEK, M. L., NAGLER, D. K., BECKER-PAULY, C. & SCHILLING, O. 2011. Proteomic identification of protease cleavage sites characterizes prime and non-prime specificity of cysteine cathepsins B, L, and S. *J Proteome Res,* 10**,** 5363-73.

BRANDENSTEIN, L., SCHWEIZER, M., SEDLACIK, J., FIEHLER, J. & STORCH, S. 2016. Lysosomal dysfunction and impaired autophagy in a novel mouse model deficient for the lysosomal membrane protein Cln7. *Hum Mol Genet,* 25**,** 777-91.

BROOMFIELD, A., JONES, S. A., HUGHES, S. M. & BIGGER, B. W. 2016. The impact of the immune system on the safety and efficiency of enzyme replacement therapy in lysosomal storage disorders. *J Inherit Metab Dis,* 39**,** 499-512.

CAGLIC, D., KOSEC, G., BOJIC, L., REINHECKEL, T., TURK, V. & TURK, B. 2009. Murine and human cathepsin B exhibit similar properties: possible implications for drug discovery. *Biol Chem,* 390**,** 175-9.

CAO, Y., ESPINOLA, J. A., FOSSALE, E., MASSEY, A. C., CUERVO, A. M., MACDONALD, M. E. & COTMAN, S. L. 2006. Autophagy Is Disrupted in a Knock-in Mouse Model of Juvenile Neuronal Ceroid Lipofuscinosis. *Journal of Biological Chemistry,* 281**,** 20483-20493.

CONCOLINO, D., DEODATO, F. & PARINI, R. 2018. Enzyme replacement therapy: efficacy and limitations. *Ital J Pediatr,* 44**,** 120.

CONTI, L., POLLARD, S. M., GORBA, T., REITANO, E., TOSELLI, M., BIELLA, G., SUN, Y., SANZONE, S., YING, Q.-L., CATTANEO, E. & SMITH, A. 2005. Niche-Independent Symmetrical Self-Renewal of a Mammalian Tissue Stem Cell. *PLOS Biology,* 3**,** e283.

CUERVO, A. M., STEFANIS, L., FREDENBURG, R., LANSBURY, P. T. & SULZER, D. 2004. Impaired degradation of mutant alpha-synuclein by chaperone-mediated autophagy. *Science,* 305**,** 1292-5.

DAMME, M., STROOBANTS, S., LÜDEMANN, M., ROTHAUG, M., LÜLLMANN-RAUCH, R., BECK, H. C., ERICSSON, A., ANDERSSON, C., FOGH, J., D'HOOGE, R., SAFTIG, P. & BLANZ, J. 2015. Chronic enzyme replacement therapy ameliorates neuropathology in alpha-mannosidosis mice. *Ann Clin Transl Neurol,* 2**,** 987-1001.

DAS, A. M., LAGLER, F., BECK, M., SCARPA, M. & LAMPE, C. 2017. [Lysosomal Storage Diseases: Challenges in Multiprofessional Patient Care with Enzyme Replacement Therapy]. *Klin Padiatr,* 229**,** 168-174.

DE DUVE, C. 1964. FROM CYTASES TO LYSOSOMES. *Fed Proc,* 23**,** 1045-9.

DE DUVE, C., PRESSMAN, B. C., GIANETTO, R., WATTIAUX, R. & APPELMANS, F. 1955. Tissue fractionation studies. 6. Intracellular distribution patterns of enzymes in rat-liver tissue. *Biochem J,* 60**,** 604-17.

DESNICK, R. J. & SCHUCHMAN, E. H. 2012. Enzyme replacement therapy for lysosomal diseases: lessons from 20 years of experience and remaining challenges. *Annu Rev Genomics Hum Genet,* 13**,** 307-35.

DI SPIEZIO, A., MARQUES, A. R. A., SCHMIDT, L., THIEßEN, N., GALLWITZ, L., FOGH, J., BARTSCH, U. & SAFTIG, P. 2021. Analysis of cathepsin B and cathepsin L treatment to clear toxic lysosomal protein aggregates in neuronal ceroid lipofuscinosis. *Biochim Biophys Acta Mol Basis Dis,* 1867**,** 166205.

DIKIC, I. & ELAZAR, Z. 2018. Mechanism and medical implications of mammalian autophagy. *Nature Reviews Molecular Cell Biology,* 19**,** 349-364.

EMBURY, C. M., DYAVARSHETTY, B., LU, Y., WIEDERIN, J. L., CIBOROWSKI, P., GENDELMAN, H. E. & KIYOTA, T. 2017. Cathepsin B Improves ß-Amyloidosis and Learning and Memory in Models of Alzheimer's Disease. *Journal of Neuroimmune Pharmacology,* 12**,** 340-352.

FELBOR, U., KESSLER, B., MOTHES, W., GOEBEL, H. H., PLOEGH, H. L., BRONSON, R. T. & OLSEN, B. R. 2002. Neuronal loss and brain atrophy in mice lacking cathepsins B and L. *Proc Natl Acad Sci U S A,* 99**,** 7883-8.

FONG, D., MAN-YING CHAN, M., HSIEH, W.-T., MENNINGER, J. C. & WARD, D. C. 1992. Confirmation of the human cathepsin B gene (CTSB) assignment to chromosome 8. *Human Genetics,* 89**,** 10-12.

FRITCHIE, K., SIINTOLA, E., ARMAO, D., LEHESJOKI, A. E., MARINO, T., POWELL, C., TENNISON, M., BOOKER, J. M., KOCH, S., PARTANEN, S., SUZUKI, K., TYYNELÄ, J. & THORNE, L. B. 2009. Novel mutation and the first prenatal screening of cathepsin D deficiency (CLN10). *Acta Neuropathol,* 117**,** 201-8.

GEORGES, J., MILLER, O. & BINTENER, C. 2020. *Estimating the prevalence of dementia in Europe*.

GHADERI, D., TAYLOR, R. E., PADLER-KARAVANI, V., DIAZ, S. & VARKI, A. 2010. Implications of the presence of N-glycolylneuraminic acid in recombinant therapeutic glycoproteins. *Nature Biotechnology,* 28**,** 863-867.

GLICK, D., BARTH, S. & MACLEOD, K. F. 2010. Autophagy: cellular and molecular mechanisms. *The Journal of pathology,* 221**,** 3-12.

GUINEC, N., DALET-FUMERON, V. & PAGANO, M. 1993. "In vitro" study of basement membrane degradation by the cysteine proteinases, cathepsins B, B-like and L. Digestion of collagen IV, laminin, fibronectin, and release of gelatinase activities from basement membrane fibronectin. *Biol Chem Hoppe Seyler,* 374**,** 1135-46.

HARA, T., NAKAMURA, K., MATSUI, M., YAMAMOTO, A., NAKAHARA, Y., SUZUKI-MIGISHIMA, R., YOKOYAMA, M., MISHIMA, K., SAITO, I., OKANO, H. & MIZUSHIMA, N. 2006. Suppression of basal autophagy in neural cells causes neurodegenerative disease in mice. *Nature,* 441**,** 885-9.

HE, Y., XU, Y., ZHANG, C., GAO, X., DYKEMA, K. J., MARTIN, K. R., KE, J., HUDSON, E. A., KHOO, S. K., RESAU, J. H., ALBERTS, A. S., MACKEIGAN, J. P., FURGE, K. A. & XU, H. E. 2011. Identification of a lysosomal pathway that modulates glucocorticoid signaling and the inflammatory response. *Sci Signal,* 4**,** ra44.

HERSHESON, J., BURKE, D., CLAYTON, R., ANDERSON, G., JACQUES, T. S., MILLS, P., WOOD, N. W., GISSEN, P., CLAYTON, P., FEARNLEY, J., MOLE, S. E. & HOULDEN, H. 2014. Cathepsin D deficiency causes juvenile-onset ataxia and distinctive muscle pathology. *Neurology,* 83**,** 1873-1875.

HOBBS, J. R., HUGH-JONES, K., BARRETT, A. J., BYROM, N., CHAMBERS, D., HENRY, K., JAMES, D. C., LUCAS, C. F., ROGERS, T. R., BENSON, P. F., TANSLEY, L. R., PATRICK, A. D., MOSSMAN, J. & YOUNG, E. P. 1981. Reversal of clinical features of Hurler's disease and biochemical improvement after treatment by bone-marrow transplantation. *Lancet,* 2**,** 709-12.

HOCHULI, E., BANNWARTH, W., DÖBELI, H., GENTZ, R. & STÜBER, D. 1988. Genetic Approach to Facilitate Purification of Recombinant Proteins with a Novel Metal Chelate Adsorbent. *Bio/Technology,* 6**,** 1321-1325.

HOLSTEIN, M., MESA-NUÑEZ, C., MISKEY, C., ALMARZA, E., POLETTI, V., SCHMEER, M., GRUESO, E., ORDÓÑEZ FLORES, J. C., KOBELT, D., WALTHER, W., ANEJA, M. K., GEIGER, J., BONIG, H. B., IZSVÁK, Z., SCHLEEF, M., RUDOLPH, C., MAVILIO, F., BUEREN, J. A., GUENECHEA, G. & IVICS, Z. 2018. Efficient Non-viral Gene Delivery into Human Hematopoietic Stem Cells by Minicircle Sleeping Beauty Transposon Vectors. *Molecular Therapy,* 26**,** 1137-1153.

HOOK, V., TONEFF, T., BOGYO, M., GREENBAUM, D., MEDZIHRADSZKY, K. F., NEVEU, J., LANE, W., HOOK, G. & REISINE, T. 2005. Inhibition of cathepsin B reduces beta-amyloid production in regulated secretory vesicles of neuronal chromaffin cells: evidence for cathepsin B as a candidate beta-secretase of Alzheimer's disease. *Biol Chem,* 386**,** 931-40.

ILLY, C., QURAISHI, O., WANG, J., PURISIMA, E., VERNET, T. & MORT, J. S. 1997. Role of the occluding loop in cathepsin B activity. *J Biol Chem,* 272**,** 1197-202.

IVY, G. O., KANAI, S., OHTA, M., SMITH, G., SATO, Y., KOBAYASHI, M. & KITANI, K. 1989. Lipofuscin-like substances accumulate rapidly in brain, retina and internal organs with cysteine protease inhibition. *Adv Exp Med Biol,* 266**,** 31-45; discussion 45-7.

IVY, G. O., SCHOTTLER, F., WENZEL, J., BAUDRY, M. & LYNCH, G. 1984. Inhibitors of lysosomal enzymes: accumulation of lipofuscin-like dense bodies in the brain. *Science,* 226**,** 985-7.

JALANKO, A. & BRAULKE, T. 2009. Neuronal ceroid lipofuscinoses. *Biochimica et Biophysica Acta (BBA) - Molecular Cell Research,* 1793**,** 697-709.

KATUNUMA, N. 2010. Posttranslational processing and modification of cathepsins and cystatins. *J Signal Transduct,* 2010**,** 375345.

KAUR, J. & DEBNATH, J. 2015. Autophagy at the crossroads of catabolism and anabolism. *Nature Reviews Molecular Cell Biology,* 16**,** 461-472.

KETSCHER, A., KETTERER, S., DOLLWET-MACK, S., REIF, U. & REINHECKEL, T. 2016. Neuroectoderm-specific deletion of cathepsin D in mice models human inherited neuronal ceroid lipofuscinosis type 10. *Biochimie,* 122**,** 219-26.

KOGA, H., YAMADA, H., NISHIMURA, Y., KATO, K. & IMOTO, T. 1991. Multiple Proteolytic Action of Rat Liver Cathepsin B: Specificities and pH-Dependences of the Endo- and Exopeptidase Activities1. *The Journal of Biochemistry,* 110**,** 179-188.

KOHFELDT, E., MAURER, P., VANNAHME, C. & TIMPL, R. 1997. Properties of the extracellular calcium binding module of the proteoglycan testican. *FEBS Lett,* 414**,** 557-61.
KOHLSCHÜTTER, A., SCHULZ, A., BARTSCH, U. & STORCH, S. 2019. Current and Emerging Treatment Strategies for Neuronal Ceroid Lipofuscinoses. *CNS Drugs,* 33**,** 315-325.
KOIKE, M., NAKANISHI, H., SAFTIG, P., EZAKI, J., ISAHARA, K., OHSAWA, Y., SCHULZ-SCHAEFFER, W., WATANABE, T., WAGURI, S., KAMETAKA, S., SHIBATA, M., YAMAMOTO, K., KOMINAMI, E., PETERS, C., VON FIGURA, K. & UCHIYAMA, Y. 2000. Cathepsin D deficiency induces lysosomal storage with ceroid lipofuscin in mouse CNS neurons. *J Neurosci,* 20**,** 6898-906.
KOIKE, M., SHIBATA, M., WAGURI, S., YOSHIMURA, K., TANIDA, I., KOMINAMI, E., GOTOW, T., PETERS, C., VON FIGURA, K., MIZUSHIMA, N., SAFTIG, P. & UCHIYAMA, Y. 2005. Participation of autophagy in storage of lysosomes in neurons from mouse models of neuronal ceroid-lipofuscinoses (Batten disease). *Am J Pathol,* 167**,** 1713-28.
KOMATSU, M., WAGURI, S., CHIBA, T., MURATA, S., IWATA, J., TANIDA, I., UENO, T., KOIKE, M., UCHIYAMA, Y., KOMINAMI, E. & TANAKA, K. 2006. Loss of autophagy in the central nervous system causes neurodegeneration in mice. *Nature,* 441**,** 880-4.
KUMA, A., KOMATSU, M. & MIZUSHIMA, N. 2017. Autophagy-monitoring and autophagy-deficient mice. *Autophagy,* 13**,** 1619-1628.
LACHMANN, R. H. 2011. Enzyme replacement therapy for lysosomal storage diseases. *Curr Opin Pediatr,* 23**,** 588-93.
LAMBETH, T. R., DAI, Z., ZHANG, Y. & JULIAN, R. R. 2021. A two-trick pony: lysosomal protease cathepsin B possesses surprising ligase activity. *RSC Chemical Biology,* 2**,** 606-611.
LAURENT-MATHA, V., DEROCQ, D., PRÉBOIS, C., KATUNUMA, N. & LIAUDET-COOPMAN, E. 2006. Processing of human cathepsin D is independent of its catalytic function and auto-activation: involvement of cathepsins L and B. *Journal of biochemistry,* 139**,** 363-371.
LENARČIČ, B., KRAŠOVEC, M., RITONJA, A., OLAFSSON, I. & TURK, V. 1991. Inactivation of human cystatin C and kininogen by human cathepsin D. *FEBS Letters,* 280**,** 211-215.
LEVINE, B. & KLIONSKY, D. J. 2004. Development by self-digestion: molecular mechanisms and biological functions of autophagy. *Dev Cell,* 6**,** 463-77.
LIANG, Q., OUYANG, X., SCHNEIDER, L. & ZHANG, J. 2011. Reduction of mutant huntingtin accumulation and toxicity by lysosomal cathepsins D and B in neurons. *Molecular Neurodegeneration,* 6**,** 37-37.
LIU, W., KLEINE-HOLTHAUS, S.-M., HERRANZ-MARTIN, S., ARISTORENA, M., MOLE, S. E., SMITH, A. J., ALI, R. R. & RAHIM, A. A. 2020. Experimental gene therapies for the NCLs. *Biochimica et Biophysica Acta (BBA) - Molecular Basis of Disease***,** 165772.
MACH, L., STÜWE, K., HAGEN, A., BALLAUN, C. & GLÖSSL, J. 1992. Proteolytic processing and glycosylation of cathepsin B. The role of the primary structure of the latent precursor and of the carbohydrate moiety for cell-type-specific molecular forms of the enzyme. *The Biochemical journal,* 282 (Pt 2)**,** 577-582.
MARKHAM, A. 2017. Cerliponase Alfa: First Global Approval. *Drugs,* 77**,** 1247-1249.
MARKMANN, S., THELEN, M., CORNILS, K., SCHWEIZER, M., BROCKE-AHMADINEJAD, N., WILLNOW, T., HEEREN, J., GIESELMANN, V., BRAULKE, T. & KOLLMANN, K. 2015. Lrp1/LDL Receptor Play Critical Roles in Mannose 6-Phosphate-Independent Lysosomal Enzyme Targeting. *Traffic,* 16**,** 743-59.
MARQUES, A. R. A., DI SPIEZIO, A., THIEßEN, N., SCHMIDT, L., GRÖTZINGER, J., LÜLLMANN-RAUCH, R., DAMME, M., STORCK, S. E., PIETRZIK, C. U., FOGH, J., BÄR, J., MIKHAYLOVA, M., GLATZEL, M., BASSAL, M., BARTSCH, U. & SAFTIG, P. 2019. Enzyme replacement therapy with recombinant pro-CTSD (cathepsin D) corrects defective proteolysis and autophagy in neuronal ceroid lipofuscinosis. *Autophagy***,** 1-15.
MARQUES, A. R. A. & SAFTIG, P. 2019. Lysosomal storage disorders - challenges, concepts and avenues for therapy: beyond rare diseases. *J Cell Sci,* 132.
MCGLINCHEY, R. P. & LEE, J. C. 2015. Cysteine cathepsins are essential in lysosomal degradation of α-synuclein. *Proceedings of the National Academy of Sciences of the United States of America,* 112**,** 9322-9327.

MOHAMED, F. E., AL-GAZALI, L., AL-JASMI, F. & ALI, B. R. 2017. Pharmaceutical Chaperones and Proteostasis Regulators in the Therapy of Lysosomal Storage Disorders: Current Perspective and Future Promises. *Frontiers in Pharmacology,* 8.

MOLE, S. E., ANDERSON, G., BAND, H. A., BERKOVIC, S. F., COOPER, J. D., KLEINE HOLTHAUS, S.-M., MCKAY, T. R., MEDINA, D. L., RAHIM, A. A., SCHULZ, A. & SMITH, A. J. 2019. Clinical challenges and future therapeutic approaches for neuronal ceroid lipofuscinosis. *The Lancet Neurology,* 18**,** 107-116.

MORT, J. S. 2013. Chapter 406 - Cathepsin B. *In:* RAWLINGS, N. D. & SALVESEN, G. (eds.) *Handbook of Proteolytic Enzymes (Third Edition).* Academic Press.

MUELLER-STEINER, S., ZHOU, Y., ARAI, H., ROBERSON, E. D., SUN, B., CHEN, J., WANG, X., YU, G., ESPOSITO, L., MUCKE, L. & GAN, L. 2006. Antiamyloidogenic and neuroprotective functions of cathepsin B: implications for Alzheimer's disease. *Neuron,* 51**,** 703-14.

MUSIL, D., ZUCIC, D., TURK, D., ENGH, R. A., MAYR, I., HUBER, R., POPOVIC, T., TURK, V., TOWATARI, T., KATUNUMA, N. & ET AL. 1991. The refined 2.15 A X-ray crystal structure of human liver cathepsin B: the structural basis for its specificity. *Embo j,* 10**,** 2321-30.

NÄGLER, D. K., STORER, A. C., PORTARO, F. C., CARMONA, E., JULIANO, L. & MÉNARD, R. 1997. Major increase in endopeptidase activity of human cathepsin B upon removal of occluding loop contacts. *Biochemistry,* 36**,** 12608-15.

NAGREE, M. S., SCALIA, S., MCKILLOP, W. M. & MEDIN, J. A. 2019. An update on gene therapy for lysosomal storage disorders. *Expert Opin Biol Ther,* 19**,** 655-670.

NUNOMURA, A. & MIYAGISHI, T. 1993. Ultrastructural observations on neuronal lipofuscin (age pigment) and dense bodies induced by a proteinase inhibitor, leupeptin, in rat hippocampus. *Acta Neuropathologica,* 86**,** 319-328.

OKADA, R., WU, Z., ZHU, A., NI, J., ZHANG, J., YOSHIMINE, Y., PETERS, C., SAFTIG, P. & NAKANISHI, H. 2015. Cathepsin D deficiency induces oxidative damage in brain pericytes and impairs the blood-brain barrier. *Mol Cell Neurosci,* 64**,** 51-60.

PALMER, D. N., MARTINUS, R. D., COOPER, S. M., MIDWINTER, G. G., REID, J. C. & JOLLY, R. D. 1989. Ovine ceroid lipofuscinosis. The major lipopigment protein and the lipid-binding subunit of mitochondrial ATP synthase have the same NH2-terminal sequence. *J Biol Chem,* 264**,** 5736-40.

PARENTI, G., ANDRIA, G. & BALLABIO, A. 2015. Lysosomal Storage Diseases: From Pathophysiology to Therapy. *Annual Review of Medicine,* 66**,** 471-486.

PARVIAINEN, L., DIHANICH, S., ANDERSON, G. W., WONG, A. M., BROOKS, H. R., ABETI, R., REZAIE, P., LALLI, G., POPE, S., HEALES, S. J., MITCHISON, H. M., WILLIAMS, B. P. & COOPER, J. D. 2017. Glial cells are functionally impaired in juvenile neuronal ceroid lipofuscinosis and detrimental to neurons. *Acta neuropathologica communications,* 5**,** 74-74.

PLATT, F. M. 2018. Emptying the stores: lysosomal diseases and therapeutic strategies. *Nature Reviews Drug Discovery,* 17**,** 133-150.

PLATT, F. M., D'AZZO, A., DAVIDSON, B. L., NEUFELD, E. F. & TIFFT, C. J. 2018. Lysosomal storage diseases. *Nature Reviews Disease Primers,* 4**,** 27.

PORTA, E. A. 1991. Advances in age pigment research. *Archives of Gerontology and Geriatrics,* 12**,** 303-320.

PUERTOLLANO, R., FERGUSON, S. M., BRUGAROLAS, J. & BALLABIO, A. 2018. The complex relationship between TFEB transcription factor phosphorylation and subcellular localization. *The EMBO Journal,* 37**,** e98804.

PUNGERCAR, J. R., CAGLIC, D., SAJID, M., DOLINAR, M., VASILJEVA, O., POZGAN, U., TURK, D., BOGYO, M., TURK, V. & TURK, B. 2009. Autocatalytic processing of procathepsin B is triggered by proenzyme activity. *The FEBS journal,* 276**,** 660-668.

QI, X., MAN, S. M., MALIREDDI, R. K. S., KARKI, R., LUPFER, C., GURUNG, P., NEALE, G., GUY, C. S., LAMKANFI, M. & KANNEGANTI, T.-D. 2016. Cathepsin B modulates lysosomal biogenesis and host defense against Francisella novicida infection. *Journal of Experimental Medicine,* 213**,** 2081-2097.

RABANAL-RUIZ, Y. & KOROLCHUK, V. I. 2018. mTORC1 and Nutrient Homeostasis: The Central Role of the Lysosome. *International Journal of Molecular Sciences,* 19**,** 818.

RAVIKUMAR, B., VACHER, C., BERGER, Z., DAVIES, J. E., LUO, S., OROZ, L. G., SCARAVILLI, F., EASTON, D. F., DUDEN, R., O'KANE, C. J. & RUBINSZTEIN, D. C. 2004. Inhibition of mTOR induces autophagy and reduces toxicity of polyglutamine expansions in fly and mouse models of Huntington disease. *Nat Genet,* 36**,** 585-95.

ROZMAN, J., STOJAN, J., KUHELJ, R., TURK, V. & TURK, B. 1999. Autocatalytic processing of recombinant human procathepsin B is a bimolecular process. *FEBS Lett,* 459**,** 358-62.

RUSSELL, R. C., YUAN, H.-X. & GUAN, K.-L. 2014. Autophagy regulation by nutrient signaling. *Cell Research,* 24**,** 42-57.

SAFTIG, P. 2006. Physiology of the lysosome. *In:* MEHTA, A., BECK, M. & SUNDER-PLASSMANN, G. (eds.) *Fabry Disease: Perspectives from 5 Years of FOS.* Oxford: Oxford PharmaGenesis

Copyright © 2006, Oxford PharmaGenesis™.

SAFTIG, P., HETMAN, M., SCHMAHL, W., WEBER, K., HEINE, L., MOSSMANN, H., KÖSTER, A., HESS, B., EVERS, M., VON FIGURA, K. & ET AL. 1995. Mice deficient for the lysosomal proteinase cathepsin D exhibit progressive atrophy of the intestinal mucosa and profound destruction of lymphoid cells. *Embo j,* 14**,** 3599-608.

SAFTIG, P. & KLUMPERMAN, J. 2009. Lysosome biogenesis and lysosomal membrane proteins: trafficking meets function. *Nature Reviews Molecular Cell Biology,* 10**,** 623-635.

SARKAR, S. & RUBINSZTEIN, D. C. 2008. Huntington's disease: degradation of mutant huntingtin by autophagy. *FEBS Journal,* 275**,** 4263-4270.

SCHECHTER, I. & BERGER, A. 1967. On the size of the active site in proteases. I. Papain. *Biochem Biophys Res Commun,* 27**,** 157-62.

SCHULZ, A., KOHLSCHÜTTER, A., MINK, J., SIMONATI, A. & WILLIAMS, R. 2013. NCL diseases — clinical perspectives(). *Biochimica et biophysica acta,* 1832**,** 1801-1806.

SCHULZ, A. & NICKEL, M. 2018. Neurodegenerative Erkrankungen des Kindesalters. *medizinische genetik,* 30**,** 231-237.

SCHULZ, A., SPECCHIO, N., GISSEN, P., DE LOS REYES, E., CAHAN, H., SLASOR, P., AJAYI, T. & JACOBY, D. 2017. Intracerebroventricular cerliponase alfa for children with CLN2 disease: Interim results from an ongoing phase 2 extension study. *European Journal of Paediatric Neurology,* 21**,** e21.

SCHWAKE, M., SCHRÖDER, B. & SAFTIG, P. 2013. Lysosomal membrane proteins and their central role in physiology. *Traffic,* 14**,** 739-48.

SERANOVA, E., CONNOLLY, K. J., ZATYKA, M., ROSENSTOCK, T. R., BARRETT, T., TUXWORTH, R. I. & SARKAR, S. 2017. Dysregulation of autophagy as a common mechanism in lysosomal storage diseases. *Essays Biochem,* 61**,** 733-749.

SHEN, H. M. & MIZUSHIMA, N. 2014. At the end of the autophagic road: an emerging understanding of lysosomal functions in autophagy. *Trends Biochem Sci,* 39**,** 61-71.

SHEVTSOVA, Z., GARRIDO, M., WEISHAUPT, J., SAFTIG, P., BÄHR, M., LÜHDER, F. & KÜGLER, S. 2010. CNS-expressed cathepsin D prevents lymphopenia in a murine model of congenital neuronal ceroid lipofuscinosis. *The American journal of pathology,* 177**,** 271-279.

SHI, C.-S., SHENDEROV, K., HUANG, N.-N., KABAT, J., ABU-ASAB, M., FITZGERALD, K. A., SHER, A. & KEHRL, J. H. 2012. Activation of autophagy by inflammatory signals limits IL-1β production by targeting ubiquitinated inflammasomes for destruction. *Nature Immunology,* 13**,** 255.

SHYNG, C. & SANDS, M. S. 2014. Astrocytosis in infantile neuronal ceroid lipofuscinosis: friend or foe? *Biochem Soc Trans,* 42**,** 1282-5.

SIINTOLA, E., PARTANEN, S., STRÖMME, P., HAAPANEN, A., HALTIA, M., MAEHLEN, J., LEHESJOKI, A. E. & TYYNELÄ, J. 2006. Cathepsin D deficiency underlies congenital human neuronal ceroid-lipofuscinosis. *Brain,* 129**,** 1438-45.

SLOANE, B. F., MOIN, K., KREPELA, E. & ROZHIN, J. 1990. Cathepsin B and its endogenous inhibitors: the role in tumor malignancy. *Cancer and Metastasis Reviews,* 9**,** 333-352.

SPECCHIO, N., FERRETTI, A., TRIVISANO, M., PIETRAFUSA, N., PEPI, C., CALABRESE, C., LIVADIOTTI, S., SIMONETTI, A., ROSSI, P., CURATOLO, P. & VIGEVANO, F. 2021. Neuronal Ceroid Lipofuscinosis: Potential for Targeted Therapy. *Drugs,* 81**,** 101-123.

STAHL, S., REINDERS, Y., ASAN, E., MOTHES, W., CONZELMANN, E., SICKMANN, A. & FELBOR, U. 2007. Proteomic analysis of cathepsin B- and L-deficient mouse brain lysosomes. *Biochimica et biophysica acta,* 1774**,** 1237-1246.

STEFANIS, L., LARSEN, K. E., RIDEOUT, H. J., SULZER, D. & GREENE, L. A. 2001. Expression of A53T mutant but not wild-type alpha-synuclein in PC12 cells induces alterations of the ubiquitin-dependent degradation system, loss of dopamine release, and autophagic cell death. *J Neurosci,* 21**,** 9549-60.

STEINFELD, R., REINHARDT, K., SCHREIBER, K., HILLEBRAND, M., KRAETZNER, R., BRÜCK, W., SAFTIG, P. & GÄRTNER, J. 2006. Cathepsin D Deficiency Is Associated with a Human Neurodegenerative Disorder. *The American Journal of Human Genetics,* 78**,** 988-998.

TAKAHASHI, K., NELVAGAL, H. R., LANGE, J. & COOPER, J. D. 2022. Glial Dysfunction and Its Contribution to the Pathogenesis of the Neuronal Ceroid Lipofuscinoses. *Front Neurol,* 13**,** 886567.

TANAKA, K. & MATSUDA, N. 2014. Proteostasis and neurodegeneration: The roles of proteasomal degradation and autophagy. *Biochimica et Biophysica Acta (BBA) - Molecular Cell Research,* 1843**,** 197-204.

THELEN, M., DAMME, M., SCHWEIZER, M., HAGEL, C., WONG, A. M. S., COOPER, J. D., BRAULKE, T. & GALLICIOTTI, G. 2012. Disruption of the Autophagy-Lysosome Pathway Is Involved in Neuropathology of the nclf Mouse Model of Neuronal Ceroid Lipofuscinosis. *PLOS ONE,* 7**,** e35493.

TURKEWITZ, D. R., MOGHADDASI, S., ALGHALAYINI, A., D'AMARIO, C., ALI, H. M., WALLACH, M. & VALENZUELA, S. M. 2021. Comparative study of His- and Non-His-tagged CLIC proteins, reveals changes in their enzymatic activity. *Biochemistry and Biophysics Reports,* 26**,** 101015.

TYYNELÄ, J., PALMER, D. N., BAUMANN, M. & HALTIA, M. 1993. Storage of saposins A and D in infantile neuronal ceroid-lipofuscinosis. *FEBS Lett,* 330**,** 8-12.

VARVAGIANNIS, K., HANQUINET, S., BILLIEUX, M. H., DE LUCA, R., RIMENSBERGER, P., LIDGREN, M., GUIPPONI, M., MAKRYTHANASIS, P., BLOUIN, J. L., ANTONARAKIS, S. E., STEINFELD, R., KERN, I., PORETTI, A., FLUSS, J. & FOKSTUEN, S. 2018. Congenital Neuronal Ceroid Lipofuscinosis with a Novel CTSD Gene Mutation: A Rare Cause of Neonatal-Onset Neurodegenerative Disorder. *Neuropediatrics,* 49**,** 150-153.

WALSH, G. 2014. Biopharmaceutical benchmarks 2014. *Nature Biotechnology,* 32**,** 992-1000.

WANG, Y., MARTINEZ-VICENTE, M., KRUGER, U., KAUSHIK, S., WONG, E., MANDELKOW, E. M., CUERVO, A. M. & MANDELKOW, E. 2009. Tau fragmentation, aggregation and clearance: the dual role of lysosomal processing. *Hum Mol Genet,* 18**,** 4153-70.

WRAITH, J. E. 2002. Lysosomal disorders. *Semin Neonatol,* 7**,** 75-83.

WU, J. & FILUTOWICZ, M. 1999. Hexahistidine (His6)-tag dependent protein dimerization: a cautionary tale. *Acta Biochim Pol,* 46**,** 591-9.

YADATI, T., HOUBEN, T., BITORINA, A. & SHIRI-SVERDLOV, R. 2020. The Ins and Outs of Cathepsins: Physiological Function and Role in Disease Management. *Cells,* 9.

YOON, M. C., SOLANIA, A., JIANG, Z., CHRISTY, M. P., PODVIN, S., MOSIER, C., LIETZ, C. B., ITO, G., GERWICK, W. H., WOLAN, D. W., HOOK, G., O'DONOGHUE, A. J. & HOOK, V. 2021. Selective Neutral pH Inhibitor of Cathepsin B Designed Based on Cleavage Preferences at Cytosolic and Lysosomal pH Conditions. *ACS Chemical Biology,* 16**,** 1628-1643.

YOSHII, S. R., KUMA, A., AKASHI, T., HARA, T., YAMAMOTO, A., KURIKAWA, Y., ITAKURA, E., TSUKAMOTO, S., SHITARA, H., EISHI, Y. & MIZUSHIMA, N. 2016. Systemic Analysis of Atg5-Null Mice Rescued from Neonatal Lethality by Transgenic ATG5 Expression in Neurons. *Dev Cell,* 39**,** 116-130.

YU, W. H., CUERVO, A. M., KUMAR, A., PETERHOFF, C. M., SCHMIDT, S. D., LEE, J.-H., MOHAN, P. S., MERCKEN, M., FARMERY, M. R., TJERNBERG, L. O., JIANG, Y., DUFF, K., UCHIYAMA, Y., NÄSLUND, J., MATHEWS, P. M., CATALDO, A. M. & NIXON, R. A. 2005. Macroautophagy—a novel β-amyloid peptide-generating pathway activated in Alzheimer's disease. *The Journal of Cell Biology,* 171**,** 87-98.

ZHOU, R., LU, Y., HAN, Y., LI, X., LOU, H., ZHU, L., ZHEN, X. & DUAN, S. 2015. Mice heterozygous for cathepsin D deficiency exhibit mania-related behavior and stress-induced depression. *Prog Neuropsychopharmacol Biol Psychiatry,* 63**,** 110-8.

9 SUPPLEMENTAL DATA

Sequencing Results of production construct

Alignment of Sequence_1: UniProt Sequence (access number: AAC37547.1) with restriction sites NheI and NotI

with Sequence_2: Sequence obtained from DNA sequencing

```
Seq_1  1     GCGCTAGCACGGAGCAGGCCCTCTTTCCATCCCCTGTCGGATGAGCTGGTCAACTATGTC   60
             ||||||||||||||||||||||||||||||||||||||||||||||||||||||||||||
Seq_2  1     GCGCTAGCACGGAGCAGGCCCTCTTTCCATCCCCTGTCGGATGAGCTGGTCAACTATGTC   60

Seq_1  61    AACAAACGGAATACCACGTGGCAGGCCGGGCACAACTTCTACAACGTGGACATGAGCTAC   120
             ||||||||||||||||||||||||||||||||||||||||||||||||||||||||||||
Seq_2  61    AACAAACGGAATACCACGTGGCAGGCCGGGCACAACTTCTACAACGTGGACATGAGCTAC   120

Seq_1  121   TTGAAGAGGCTATGTGGTACCTTCCTGGGTGGGCCCAAGCCACCCCAGAGAGTTATGTTT   180
             ||||||||||||||||||||||||||||||||||||||||||||||||||||||||||||
Seq_2  121   TTGAAGAGGCTATGTGGTACCTTCCTGGGTGGGCCCAAGCCACCCCAGAGAGTTATGTTT   180

Seq_1  181   ACCGAGGACCTGAAGCTGCCTGCAAGCTTCGATGCACGGGAACAATGGCCACAGTGTCCC   240
             ||||||||||||||||||||||||||||||||||||||||||||||||||||||||||||
Seq_2  181   ACCGAGGACCTGAAGCTGCCTGCAAGCTTCGATGCACGGGAACAATGGCCACAGTGTCCC   240

Seq_1  241   ACCATCAAAGAGATCAGAGACCAGGGCTCCTGTGGCTCCTGCTGGGCCTTCGGGGCTGTG   300
             ||||||||||||||||||||||||||||||||||||||||||||||||||||||||||||
Seq_2  241   ACCATCAAAGAGATCAGAGACCAGGGCTCCTGTGGCTCCTGCTGGGCCTTCGGGGCTGTG   300

Seq_1  301   GAAGCCATCTCTGACCGGATCTGCATCCACACCAATGCGCACGTCAGCGTGGAGGTGTCG   360
             ||||||||||||||||||||||||||||||||||||||||||||||||||||||||||||
Seq_2  301   GAAGCCATCTCTGACCGGATCTGCATCCACACCAATGCGCACGTCAGCGTGGAGGTGTCG   360

Seq_1  361   GCGGAGGACCTGCTCACATGCTGTGGCAGCATGTGTGGGGACGGCTGTAATGGTGGCTAT   420
             ||||||||||||||||||||||||||||||||||||||||||||||||||||||||||||
Seq_2  361   GCGGAGGACCTGCTCACATGCTGTGGCAGCATGTGTGGGGACGGCTGTAATGGTGGCTAT   420

Seq_1  421   CCTGCTGAAGCTTGGAACTTCTGGACAAGAAAAGGCCTGGTTTCTGGTGGCCTCTATGAA   480
             ||||||||||||||||||||||||||||||||||||||||||||||||||||||||||||
Seq_2  421   CCTGCTGAAGCTTGGAACTTCTGGACAAGAAAAGGCCTGGTTTCTGGTGGCCTCTATGAA   480

Seq_1  481   TCCCATGTAGGGTGCAGACCGTACTCCATCCCTCCCTGTGAGCACCACGTCAACGGCTCC   540
             ||||||||||||||||||||||||||||||||||||||||||||||||||||||||||||
Seq_2  481   TCCCATGTAGGGTGCAGACCGTACTCCATCCCTCCCTGTGAGCACCACGTCAACGGCTCC   540

Seq_1  541   CGGCCCCCATGCACGGGGGAGGGAGATACCCCCAAGTGTAGCAAGATCTGTGAGCCTGGC   600
             ||||||||||||||||||||||||||||||||||||||||||||||||||||||||||||
Seq_2  541   CGGCCCCCATGCACGGGGgAGGGAGATACCCCCAAGTGTAGCAAGATCTGTGAGCCTGGC   600

Seq_1  601   TACAGCCCGACCTACAAACAGGACAAGCACTACGGATACAATTCCTACAGCGTCTCCAAT   660
             ||||||||||||||||||||||||||||||||||||||||||||||||||||||||||||
Seq_2  601   TACAGCCCGACCTACAAACAGGACAAGCACTACGGATACAATTCCTACAGCGTCTCCAAT   660

Seq_1  661   AGCGAGAAGGACATCATGGCCGAGATCTACAAAAACGGCCCCGTGGAGGGAGCTTTCTCT   720
             ||||||||||||||||||||||||||||||||||||||||||||||||||||||||||||
Seq_2  661   AGCGAGAAGGACATCATGGCCGagaTCTACAAAAACGGCCCCGTGGAGGGAGCTTTCTCT   720

Seq_1  721   GTGTATTCGGACTTCCTGCTCTACAAGTCAGGAGTGTACCAACACGTCACCGGAGAGATG   780
             ||||||||||||||||||||||||||||||||||||||||||||||||||||||||||||
Seq_2  721   GTGTATTCGGACTTCCTGCTCTACAAGTCAGGAGTGTACCAACACGTCACCGGAgagaTG   780

Seq_1  781   ATGGGTGGCCATGCCATCCGCATCCTGGGCTGGGGAGTGGAGAATGGCACACCCTACTGG   840
             ||||||||||||||||||||||||||||||||||||||||||||||||||||||||||||
```

```
Seq_2  781   ATGGGTGGCCATGCCATCCGCATCCTGGgCTGGGGAGTGGAGAATGGCACACCCTACTGG   840

Seq_1  841   CTGGTTGCCAACTCCTGGAACACTGACTGGGGTGACAATGGCTTCTTTAAAATACTCAGA   900
              ||||||||||||||||||||||||||||||||||||||||||||||||||||||||||||
Seq_2  841   CTGGTTGCCAACTCCTGGAACACTGACTGGGGTGACAATGGCTTCTTTAAAATACTCAGA   900

Seq_1  901   GGACAGGATCACTGTGGAATCGAATCAGAAGTGGTGGCTGGAATTCCACGCACCGATCAG   960
              ||||||||||||||||||||||||||||||||||||||||||||||||||||||||||||
Seq_2  901   GGACAGGATCACTGTGGAATCGAATCAGAAGTGGTGGCTGGAATTCCACGCACCGATCAG   960

Seq_1  961   TACTGGGAAAAGATCTAAGCGGCCGC   986
              |||||||||||||||||||||||||
Seq_2  961   TACTGGGAAAAGATCTAAGCGGCCGC   986


Similarity : 986/986 (100,00 %)
```

Mass Spectrometry analysis of rhCTSB

(Kindly provided by Prof. A. Tholey, Institute of Experimental Medicine, Kiel University)

In the MaxQuant-search (MQ-search) using the *human* fasta file the major protein identified (major in respect to identified peptides spectral matches) was cathepsin B. Cathepsin B was identified with a sequence coverage of 79.9% and 381 MS/MS counts for the sample CathepsinB_6 and a sequence coverage of 79.1% and 345 MS/MS counts for he sample CathepsinB_4 (See Excel table values labeled in yellow and sequence 1 and 2). On the other hand, a few other proteins were identified as contaminants, e.g. keratins.

>sp|P07858|CATB_HUMAN Cathepsin B OS=Homo sapiens OX=9606 GN=CTSB PE=1 SV=3 [**CathepsinB_4**]

MWQLWASLCCLLVLANARSRPSFHPLSDELVNYVNKRNTTWQAGHNFYNVDMSYLKRLCG
TFLGGPKPPQRVMFTEDLKLPASFDAREQWPQCPTIKEIRDQGSCGSCWAFGAVEAISDR
ICIHTNAHVSVEVSAEDLLTCCGSMCGDGCNGGYPAEAWNFWTRKGLVSGGLYESHVGCR
PYSIPPCEHHVNGSRPPCTGEGDTPKCSKICEPGYSPTYKQDKHYGYNSYSVSNSEKDIM
AEIYKNGPVEGAFSVYSDFLLYKSGVYQHVTGEMMGGHAIRILGWGVENGTPYWLVANSW
NTDWGDNGFFKILRGQDHCGIESEVVAGIPRTDQYWEKI

Sequence 1. Sequence coverage for gel band 4 of human cathepsin B [CathepsinB_4]. The highlighted sequences indicates the peptides found using LC MS analysis for the gel band line 4 [CathepsinB_4]. 79,9 % Sequence covergage.

>sp|P07858|CATB_HUMAN Cathepsin B OS=Homo sapiens OX=9606 GN=CTSB PE=1 SV=3 [**CathepsinB_6**]

MWQLWASLCCLLVLANARSRPSFHPLSDELV**N**YVNKRNTTWQAGHNFYNVDMSYLKRLCG
TFLGGPKPPQRVMFTEDLKLPASFDAREQWPQCPTIKEIRDQGSCGSCWAFGAVEAISDR
ICIHTNAHVSVEVSAEDLLTCCGSMCGDGCNGGYPAEAWNFWTRKGLVSGGLYESHVGCR
PYSIPPCEHHVNGSRPPCTGEGDTPKCSKICEPGYSPTYKQDKHYGYNSYSVSNSEKDIM
AEIYKNGPVEGAFSVYSDFLLYKSGVYQHVTGEMMGGHAIRILGWGVENGTPYWLVANSW
NTDWGDNGFFKILRGQDHCGIESEVVAGIPRTDQYWEKI

Sequence 2. Sequence coverage for gel band 6 of human cathepsin B [CathepsinB_6].
The highlighted sequences indicates the peptides found using LC MS analysis for the gel band line 6

[CathepsinB_6]. 79,1 % Sequence coverage.

The peptide SRPSFHPLSDELVNYVNK was identified in both samples. However, in this peptide an O18 deamidation at the asparigine residue was observed in the sample CathepsinB_6 but not in the sample CathepsinB_4 (See figure 2 and 3). The O18 deamidation suggests a glycosylation in the position 31 in the protein.

10 ACKNOLEDGEMENTS

On the long and oftentimes rocky road towards finishing my thesis, I encountered many obstacles and was lucky I could rely on the support of numerous people, whom I want to thank for their support. Without you this work would not exist.

First of all, I want to thank Prof. Paul Saftig for letting me work under his guidance in his group and on such an interesting project. I am really thankful for this experience.

Secondly, I want to express gratitude to André R. A. Marques, PhD, for his great support and even greater patience. When I started, I was new to every single technique and the very basics of working experimentally. With unmatched forbearance, he guided me, helped me overcome setbacks and answered even my most ridiculous questions without making me feel bad.

This great support was continued by Dr. Alessandro Di Spiezio, who helped me a great deal with finishing my experiments and with the writing of the thesis. I could always count on an open ear and immediate support, even after his return to Italy.

I am really grateful and feel privileged to have had them as my supervisors.

While working on the project was stressful and exhausting at times, my co-workers never failed to make my days at the Biochemical Institute a pleasant experience, be it chats or coffee breaks with my lovely office mates David, Marlies and Jessica or my group members Saskia and Sönke, who even visited me during my Erasmus semester. Especially Moritz, who started on his project at the same time, never failed to lift my spirits.

My friends and especially my roommates in the best flat share in the world were a great support throughout the years of working on my thesis. Sharing troubles and concerns as well as joys and laughter were a great remedy for the exhaustion of long working hours.

I would not have been able to finish this without the constant support of my girlfriend Johanna. In believing in me, enduring listening to me going on and on about lab topics and motivating me when I had already half forgotten about the thesis, she made this very work possible, while at the same time helping me to not get lost in all the lab work. Additionally, I want to thank her family for their great support.

And ultimately I want to thank my parents and my sister for always helping, looking out for me and supporting me in any means possible in whatever I do. I am truly thankful to have you always by my side.

11 DECLARATION OF AUTHORSHIP

I hereby declare that apart from my supervisors' guidance I wrote this doctor thesis on my own with no outside assistance and that information taken from other sources is marked as such.

Kiel, 27.09.2022

_____
Niklas Thießen

12 PUBLICATIONS

12.1 Poster Abstract:

Niklas Thießen, Jens Fogh, André R. A. Marques, Paul Saftig (2018) Analysis of Cathepsin replacement as a therapeutic approach to clear protein accumulations in Neuronal Ceroid Lipofuscinosis, NCL 2018 London Conference, Royal Holloway, University of London

12.2 Journal co-authorships:

André R. A. Marques, Alessandro Di Spiezio, Niklas Thießen, Lina Schmidt, Joachim Grötzinger, Renate Lüllmann-Rauch, Markus Damme, Steffen E. Storck, Claus U. Pietrzik, Jens Fogh, Julia Bär, Marina Mikhaylova, Markus Glatzel, Mahmoud Bassal, Udo Bartsch & Paul Saftig (2020) Enzyme replacement therapy with recombinant pro-CTSD (cathepsin D) corrects defective proteolysis and autophagy in neuronal ceroid lipofuscinosis, Autophagy, 16:5, 811-825, DOI: 10.1080/15548627.2019.1637200

Di Spiezio A, Marques ARA, Schmidt L, Thießen N, Gallwitz L, Fogh J, Bartsch U, Saftig P. Analysis of cathepsin B and cathepsin L treatment to clear toxic lysosomal protein aggregates in neuronal ceroid lipofuscinosis. Biochim Biophys Acta Mol Basis Dis. 2021 Oct 1;1867(10):166205. doi: 10.1016/j.bbadis.2021.166205. Epub 2021 Jun 30. PMID: 34214607.